

MSc Program Earth Sciences and Environment
Specialization: Mineral Resources- Petrology and Environmental Management

**Geochemistry and oral bioaccessibility of potentially toxic
elements in soil and house dust:
Comparison of urban and abandoned Cu-mine areas of Cyprus**

MSc Dissertation

Avgerinos Pitsillis

R.N 22007

Athens

October 2023

Τμήμα Γεωλογίας και Γεωπεριβάλλοντος
Πρόγραμμα Μεταπτυχιακών Σπουδών Επιστήμες Γης και Περιβάλλον:
Ειδίκευση Ορυκτοί Πόροι - Πετρολογία και Διαχείριση Περιβάλλοντος

**Γεωχημεία και στομαχική βιοπροσβασιμότητα δυνητικά τοξικών στοιχείων
στο έδαφος και την οικιακή σκόνη: Σύγκριση οικιστικών περιοχών και
περιοχής εγκαταλελειμμένου μεταλλείου χαλκού της Κύπρου.**

Διπλωματική Εργασία

Αυγερινός Πιτσιλλής

AM 22007

Επιβλέπουσα Αριάδνη Αργυράκη, Καθηγήτρια

Τριμελής Εξεταστική Επιτροπή:

Αριάδνη Αργυράκη, Καθηγήτρια ΕΚΠΑ

Ευστράτιος Κελεπερτζής, Επίκουρος Καθηγητής ΕΚΠΑ

Φωτεινή Μπότσου, ΕΔΙΠ Τμ. Χημείας ΕΚΠΑ

Αθήνα

Οκτώβριος 2023

Ευχαριστίες

Αρχικά, θα ήθελα να ευχαριστήσω τη καθηγήτρια μου Αριάδνη Αργυράκη για τη βοήθεια σε όλοι αυτή την πορεία μέχρι την ολοκλήρωση της διπλωματικής μου εργασίας. Επιπλέον, τα άτομα της ομάδας του Dustsafe project για τις δωρεάν αναλύσεις των οικιακών σκονών για ολικές συγκεντρώσεις. Ακόμη, θα ήθελα να ευχαριστήσω τη Φωτεινή Μπότσου για την βοήθεια της στις διορθώσεις και στις αναλύσεις της μαγνητικής επιδεκτικότητας σε όλα τα δείγματα, όπως επίσης και τον Ευστράτιο Κελεπερτζή για την βοήθεια κατά τη συγγραφή της διπλωματικής μου έρευνας. Ακόμη την Χαρά Κυπριτίδου για την βοήθεια της στην ατομική απορρόφηση και στη διαδικασία βιοπροσβασιμότητας.

Περαιτέρω, θα ήθελα να αφιερώσω αυτή τη διπλωματική στους χορηγούς μου, Χαράλαμπο Πιτσιλλή και Άντρη Πιτσιλλή, στην υπόλοιπη οικογένεια μου και στους φίλους μου που με στήριξαν σε όλοι αυτή την διαδικασία σε όλους του τομείς.

Περίληψη

Ο προσδιορισμός των δυνητικά τοξικών στοιχείων στο έδαφος και στην οικιακή σκόνη είναι απαραίτητη για την αξιολόγηση των κινδύνων για την ανθρώπινη υγεία. Στην παρούσα εργασία εξετάστηκε η περίπτωση αστικών και μεταλλευτικών περιοχών της Κύπρου με στόχους α) την εκτίμηση περιεχομένων δυνητικά τοξικών στοιχείων (ΔΤΣ) στο έδαφος γύρω από το εγκαταλελειμμένο μεταλλείο χαλκού της Κοκκινοπεζούλας στην περιοχή του Μιτσερού, β) τη μελέτη για πρώτη φορά της σύστασης της οικιακής σκόνης στις περιοχές του Μιτσερού, της Λευκωσίας και της Λεμεσού, και γ) τη διερεύνηση της βιοπροσβασιμότητας των ΔΤΣ δια της στοματικής οδού στο έδαφος του Μιτσερού και στη σκόνη των τριών περιοχών μελέτης. Έγινε επίσης εκτίμηση της επικινδυνότητας για την υγεία παιδιών ηλικίας <2 έτη με βάση την προτεινόμενη μεθοδολογία του διεθνούς έργου DUST SAFE. Οι μετρήσεις συγκεντρώσεων στοιχείων στα δείγματα που συλλέχθηκαν (22 δείγματα εδάφους και 38 δείγματα οικιακής σκόνης) πλαισιώθηκαν με μετρήσεις μαγνητικής επιδεκτικότητας σε δύο συχνότητες ώστε να διερευνηθεί η σχέση μεταξύ περιεχομένων στοιχείων και μαγνητικών κόκκων. Ελέγχθηκε επίσης η ορυκτολογία των δειγμάτων με χρήση περιθλασιμετρίας ακτίνων Χ και μετρήθηκε το pH όπου υπήρχε αρκετό δείγμα.

Οι διάμεσες τιμές των συγκεντρώσεων στοιχείων μετά από διαλυτοποίηση με βασιλικό ύδωρ στα εδαφικά δείγματα από το Μιτσερό βρέθηκαν ίσες με 4, 26, 85, 960, 20, 6, 75 mg/kg για τα As, Cr, Cu, Mn, Ni, Pb, Zn αντίστοιχα οι οποίες είναι συγκρίσιμες με αυτές από προηγούμενες έρευνες σε εδάφη της Κύπρου. Αντίστοιχα στα δείγματα σκόνης οι διάμεσες τιμές μετά από ανάλυση φθορισμομετρίας ακτίνων Χ βρέθηκαν 4, 120, 114, 302, 57, 21, 516 mg/kg για τα As, Cr, Cu, Mn, Ni, Pb, Zn. Η στατιστική συσχέτιση των παραμέτρων που μελετήθηκαν στη σκόνη κατέδειξε τρεις διακριτές ομάδες στοιχείων: Pb-As, Zn-Cu και Mn-Fe-Ni-Cr και οι οποίες παραπέμπουν σε διαφορετικές ανθρωπογενείς και γεωγενείς πηγές προέλευσης των στοιχείων. Η στατιστική ομαδοποίηση στο έδαφος διαφέρει και πιθανά σχετίζεται με το μετάλλευμα που φιλοξενεί η περιοχή, τη γεωλογία της περιοχής του Μιτσερού αλλά και την ανθρώπινη δραστηριότητα στην περιοχή. Τα υψηλότερα επίπεδα βιοπροσβασιμότητας, ως ποσοστό του ψευδοσολικού περιεχομένου στο έδαφος, προσδιορίστηκαν για τα Zn (59%), Cr (35%), Ni (30%). Στην οικιακή σκόνη υψηλά ποσοστά βιοπροσβασιμότητας προσδιορίστηκαν για τα Zn (98%), Ni (52%), Cu (42%). Τα αποτελέσματα έδειξαν ότι η οικιακή σκόνη που μελετήθηκε βρίσκεται εντός των επιτρεπτών επιπέδων κινδύνου εμφάνισης καρκίνου για όλα τα στοιχεία, ενώ, ως προς το μη-καρκινογόνο επίπεδο κινδύνου βρέθηκε ότι το χρώμιο έχει τις υψηλότερες τιμές πιθανά λόγω του γεωλογικού υποβάθρου, αλλά δεν υπερβαίνει το επιτρεπτό όριο.

Τα ευρήματα της εργασίας είναι χρήσιμα για τη διαχείριση και τη μείωση των πιθανών κινδύνων που προκύπτουν από έκθεση σε σκόνη εσωτερικού χώρου, αλλά και από τα εδάφη, ενώ τοποθετεί την Κύπρο στον παγκόσμιο χάρτη δεδομένων σύστασης της οικιακής σκόνης ο οποίος είναι διαθέσιμος στο διαδίκτυο μέσω του έργου DUST SAFE.

Λέξεις κλειδιά: περιβαλλοντική γεωχημεία, εκτίμηση επικινδυνότητας για την υγεία, ανθρωπογενής ρύπανση, γεωγενής ρύπανση

Abstract

The determination of potentially toxic elements in soil and household dust is crucial for assessing risks to human health. This study examines urban and mining areas in Cyprus with the objectives of a) assessing the levels of potentially toxic elements (PTEs) in the soil around the abandoned copper mine in Kokkinopezoula in the Mitsero region, b) studying the composition of household dust in Mitsero, Nicosia, and Limassol for the first time, and c) investigating the bioaccessibility of PTEs through oral ingestion in Mitsero's soil and dust in the three study areas. Health risk assessment for children under 2 years old was also conducted based on the proposed methodology of the international project DUST SAFE. The data set of elemental contents was accompanied by magnetic susceptibility measurements, mineralogical analysis and pH measurements.

The median concentrations of elements after aqua regia dissolution in soil samples from Mitsero were found to be 4, 26, 85, 960, 20, 6, 75 mg/kg for As, Cr, Cu, Mn, Ni, Pb, Zn, respectively. Similarly, in dust samples, the median values after X-ray fluorescence analysis were 4, 120, 114, 302, 57, 21, 516 mg/kg for As, Cr, Cu, Mn, Ni, Pb, Zn. Statistical correlation of the studied parameters in dust revealed three distinct element groups: Pb-As, Zn-Cu, and Mn-Fe-Ni-Cr, suggesting different anthropogenic and geogenic sources. Soil grouping differs, possibly related to mining activities, the region's geology, and human activities. The highest bioaccessibility percentages of pseudo-total content in the soil, were determined for Zn (59%), Cr (35%), Ni (30%). In household dust, high bioaccessibility percentages were found for Zn (98%), Ni (52%), Cu (42%). Health risk assessment for children indicated that the studied household dust is within acceptable risk levels for all elements, while chromium for non-carcinogenic risk, had the highest value for all elements, possibly due to the geological substrate, but it did not exceed the limit.

The findings of this study are valuable for managing and reducing potential risks arising from indoor dust and soil exposure. Moreover, it positions Cyprus on the global map of household dust composition data, which is available online through the DUST SAFE project.

Key words: environmental geochemistry, health risk assessment, anthropogenic contamination, geogenic contamination

Contents

Περίληψη.....	3
Abstract	4
1. Introduction.....	8
1.1. Research background	8
1.2 Research rational and objectives.....	9
2. Literature review	11
2.1 Contaminated soil and dust as exposure media affecting human health.	11
2.1 Previous Studies on Soil geochemistry in Cyprus.....	14
2.1.1 Mine legacy in Cyprus and Mitseros area	15
3. Materials and Methods.....	20
3.1 Sample collection and preparation for analysis.....	20
3.1.1 Soils.....	20
3.1.2 House dust.....	22
3.2 Analytical methods.....	22
3.3 Magnetic Susceptibility Measurement procedure.....	25
3.4 Calculation of Enrichment Factor (EF) and Combined Pollution Index (CPI).....	26
3.5 Statistical data analysis methods	26
3.6 Exposure dose calculations	27
4. Results and Discussion	31
4.1 Soil geochemistry	31
4.1.1 Soil pH and mineralogy	31
4.1.2 Magnetic susceptibility of soil samples.....	32
4.1.3 Chemical composition of soil samples.....	35
4.1.4 Enrichment factor & Principal Component Analysis of soil	40
4.1.5 Oral Bioaccessibility and Human Health Risk Assessment	41
4.2 House Dust.....	44
4.2.1 Mineralogy and natural properties of house dust samples.....	44
4.2.2 Magnetic Susceptibility of house dust samples	45
4.2.3 Total elemental content in house dust samples	47
4.2.4 Enrichment Factor	50
4.2.4 Metadata Analysis.....	50
4.2.5 Principal Component Analysis of household dust.	53
4.2.6 Human Health Risk Assessment and Oral Bioaccessibility.	54

4.2.7 Comparison with other studies	60
5.0 Conclusion	65
References	66
Appendix I – Basic statistical summary for Mitsero Soil Samples.	70
Appendix II- XRD patterns of the studied samples	79
Appendix III –Enrichment factor for soil, as reference element AL, Fe, and Mn	74
Appendix IV –Principal Component Analysis	78
Appendix IIV- XRD patterns of the studied samples	71
Appendix V – Pearson correlation test of elements for household dust.	81
Appendix VI –Metadata	84
Appendix VII- Principal component analysis of house dust	100
Appendix VIII – Scatter plots for magnetic susceptibility and elements for household dust.	101

1. Introduction

1.1. Research background

Potentially toxic elements (PTEs) such as Pb, Cd, As, Cr, Ni, Cu, Mn, Fe, and Zn have been the subject of various environmental geochemistry studies (Charlesworth et al. 2011; Harb et al., 2015; Kelepertzis et al., 2021; Kelepertzis et al., 2020; Kelepertzis et al., 2019; Kelepertzis et al., 2016; Kelepertzis & Argyraki, 2015; Wong et al., 2011) and they are common contaminants of concern in soil and dust. Some PTEs, such as Zn, Cu, Mn, Cr, and Ni are required in trace amounts by biological functions, whereas others, such as Pb, As, and Cd, are harmful for health even at low concentrations. Pollution and degradation of various environmental matrices, including soil and dust, are caused by PTEs originating from geological or anthropogenic sources. PTEs are released into the environment because of human activities, and some of them are harmful to humans, plants, and animals, so their environmental behaviour and fate is a major global environmental and public health challenge ((Kelepertzis et al., 2021; Wong et al., 2011). For example, when PTEs are released into the atmosphere by combustion processes, they have a high solubility and reactivity, particularly at low pH (Andonovska et al. 2015; Yoshinaga et al.,2014). They are quite mobile and migrate from one reservoir to another as gases or as species adsorbed on suspended particulate matter (Charlesworth et al. 2011; Harb et al.2015; Kelepertzis et al., 2021; Kelepertzis et al., 2020; Kelepertzis et al., 2019; Kelepertzis et al., 2016; Wong et al., 2011).

PTEs, such as metals and metalloids, are among the most common chemical constituents in soil that are associated with human activities (Martin et al., 2015; Wong et al., 2011). Metal(loids) are continuously accumulating in urban soil from both localized and diffuse sources, resulting in significant geographical variation (Wong et al., 2011). The soil plays an important role for agricultural, environmental, land preservation, perspective architecture, and urban activities. Urban soils are particularly affected by long-term or immediate intense concentration of human activities in an area or in a natural landscape (Andonovska et al. 2015; Cohen et al., 2021; Wragg et al., 2011).

In comparison to natural and agricultural soils, urban soil inherits some of the parent rock's features, but it is also influenced by the surrounding microenvironment and the formation process. Furthermore, PTE contaminated soils are typically found around mining

areas, posing major environmental and public health risks. The environmental risks refer to the acute and chronic toxicity caused by high PTE concentrations in plants, animals, aquatic creatures, and microbes (Hadjipanagiotou et al., 2020). Mine wastes, which include ore, gangue, industrial minerals, loose sediment, mill tailings, metallurgical slag and wastes, ash, processing chemicals and fluids, usually carry high levels of PTEs (Cohen et al., 2021; Hadjipanagiotou et al., 2020; Hudson-Edwards, 2016). The spread of PTE-containing soil particles is attributed to several processes such as plant uptake, groundwater leaching, and wind erosion. PTEs in soil are dispersed among diverse fractions and forms with varying solubility and reactivity (Rodrigues et al., 2010), especially on sites near mine wastes (Hadjipanagiotou et al., 2020).

House dust is another urban environmental compartment that typically includes outside and interior sources. House dust is a heterogeneous collection of organic and inorganic particles that serves as a reservoir for a variety of contaminants. The contaminants that may be encountered in a living space include PTEs, plastic additives, semivolatile and nonvolatile pesticides, flame retardants, and persistent organic pollutants, such as polycyclic aromatic hydrocarbons and polychlorinated biphenyls (KurtKarakus, 2012; Turner et al., 2011). Those particles may enter the interior environment via soil and road dust particulates remaining on footwear and by wind diffusion (Kelepertzis et al., 2021), but also may originate from indoor activities. Research interest concerning the composition of house dust has been on a rise during recent years, especially because of the noted health risks from exposure to PTEs laden finely grained material globally as reported in the recent worldwide Dust Safe study (Isley et al., 2021).

1.2 Research rational and objectives

Cyprus presents an interesting case study to examine PTEs content and their distribution in soil and house dust. The geochemical atlas of Cyprus soil has demonstrated that areas of elevated PTEs content are spatially correlated with the abandoned copper mines at Kalavassos and Kokkinopezoula, near Mitseros village (Cohen et al., 2012). Furthermore, recent urban geochemistry studies at Nicosia and Limassol have resulted in the detailed soil geochemical mapping of major Cyprus cities (Zissimos et al. 2018, Zissimos et al. 2021). The availability of these data sets, combined with the extensive exposure of ophiolite rocks of

Troodos Mountain (Figure 1.1) provide the rationale of research to answer questions related to potential effects of geology and mining legacy to soil and house dust PTEs content. Also, this study provides the opportunity to compare house dust concentrations from Cyprus with the global dataset of DustSafe (Isley et al., 2021).

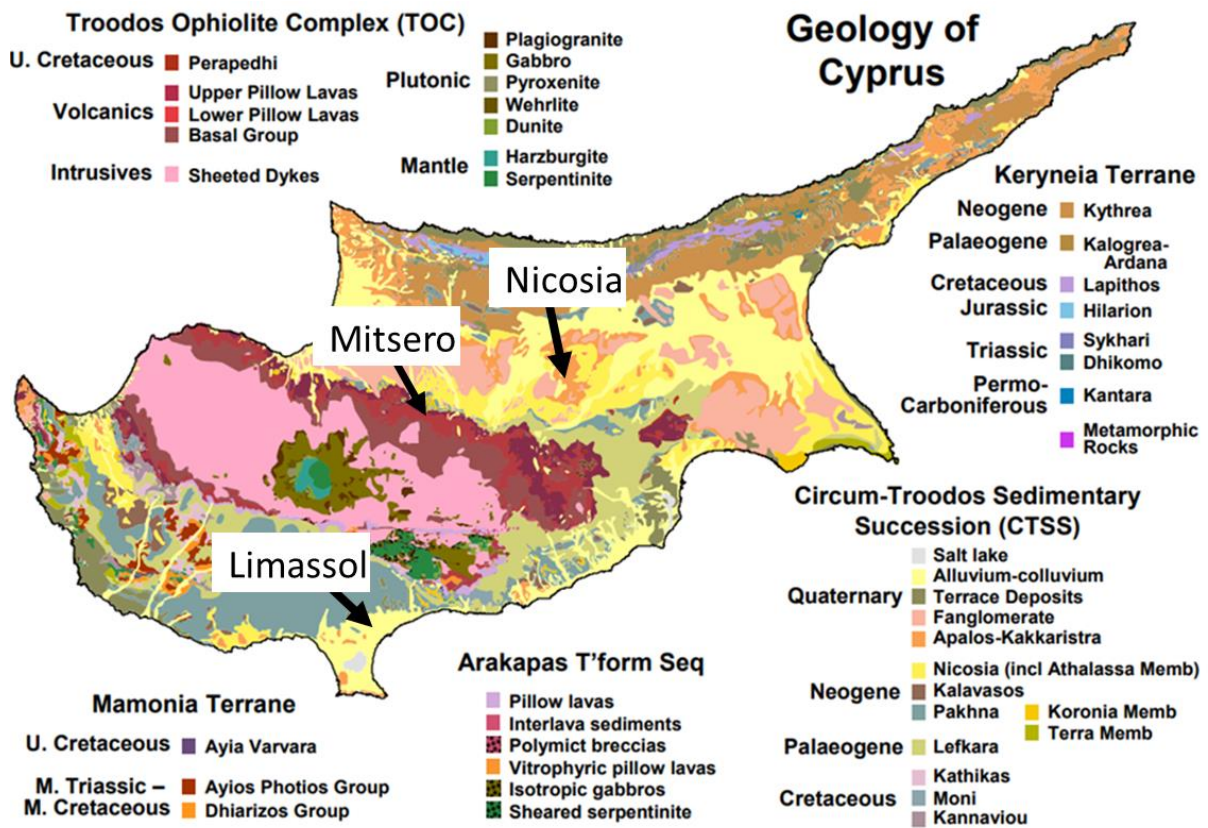


Figure 1.1. Geological map of Cyprus Island (Cohen et al., 2011) and study areas of the present research.

Within this frame, the specific objectives of the research were:

- To perform a focused soil geochemical survey in the Mitsero area, near the Kokkinopezoula abandoned copper mine and compare PTEs soil content with concentration levels of the Cyprus Geochemical Atlas,
- To study for the first time the composition of house dust in Mitseros, Nicosia and Limassol and compare the PTEs contents with those in soils of Cyprus and other datasets worldwide,
- To explore the factors affecting the oral bioaccessibility of PTEs in house dust and soil samples and estimate the health hazards from potential exposure to PTEs.

2. Literature review

2.1 Contaminated soil and dust as exposure media affecting human health.

Soil and street dust particles are the most common sources of interior house dust. Studies have discovered a general positive relationship between the content of Cr, Cu, Ni, Pb, and Zn in indoor and outdoor dusts, indicating automobile emissions and attritions as their source from worn car motors and metal-plated car parts, which can then transfer them into the living space on shoes or clothes (Charlesworth et al. 2011; Harb et al., 2015; Lisiewicz et al., 2000; Mercier et al 2011; Sabzevari & Sobhanardakani, 2018). When external particles enter the house, they mingle with the internal component to generate a complicated mixture of house dust. Wind, vehicular and pedestrian traffic, and street-sweeping operations in urban areas can easily mobilize a complex mixture of deposited airborne particles, displaced urban soil particles, and biogenic materials (such as weathered rock fragments and plant fragments) (Charlesworth et al. 2011; Shi et al. 2008). Furthermore, emissions from manmade materials can all contribute to the composition of urban dust (Charlesworth et al. 2011; Harb et al., 2015; Kelepertzis et al., 2021; Kelepertzis et al., 2020; Kelepertzis et al., 2019; Kelepertzis et al., 2016; Kelepertzis & Argyraki, 2015; Lisiewicz et al., 2000; Mercier et al 2011; Sabzevari & Sobhanardakani, 2018).

Indoor sources of harmful elements in household dusts include cigarette smoking, cosmetics, paint chips, municipal waste incineration, construction and building renovations, all of which result in higher Cd, Zn, and Cr levels (Charlesworth et al. 2011; Harb et al., 2015; Lisiewicz et al.,2000; Mercier et al 2011). As a result, worn building, furnishing and carpet materials, as well as tenant activities, might result in an increase in PTEs content. All of the above-mentioned media are likely to be found in dust that accumulates over time on surfaces in homes (Harb et al., 2015; Lisiewicz et al.,2000).

PTEs pollution is now affecting public health in the air and ground environment (Charlesworth et al., 2011; Hadjipanagiotou et al., 2020; Kelepertzis et al., 2019; Kurt-Karakus, 2012; Sabzevari & Sobhanardakani, 2018). The persistence of these contaminants in the urban environment for an extended period of time, as well as their proximity to people, may increase the urban population's exposure to certain elements. Trace elements related with fine particulates and of toxicological concern have been linked to sinusitis, asthma, chronic

bronchitis, pneumonia, lung bleeding, cancer, and brain haemorrhage in occupational settings (Charlesworth et al., 2011). Trace metal exposure is also becoming recognized as a new risk factor for neurodegeneration and neurotoxicity. Trace metal levels, such as manganese (Mn), copper (Cu), and zinc (Zn), have been linked to amyotrophic lateral sclerosis (ALS). Manganese has been linked to Parkinson's disease, while Pb has been linked to adult cognitive decline and Alzheimer's disease. As a result, the discovery of high trace metal concentrations in soils and the workplace environment is a catalyst for taking steps to regulate, limit, and mitigate exposures across a lifetime (Isley et al., 2022, Turner, 2011).

Chemical components from dust and soil can enter the human body through eating, contact with the skin, or breathing (Yoshinaga et al., 2014). Because of outdoor and indoor activities, oral ingestion is almost always the most important pathway of exposure for children, especially toddlers, who spend the majority of their time in playgrounds or on floors, mouthing hands and other objects such as toys, or eating food contaminated by hands. They can unintentionally ingest house dust and soil particles (Bo Li et al., 2015; Ljung et al., 2007; Sabzevari & Sobhanardakani, 2018; Turner, 2011; Yoshinaga et al., 2014).

Following exposure, a PTE's potential to cause harm for health is determined by its chemical speciation and ability to get mobilized in the human gastrointestinal system. For evaluating the risks associated with oral exposure to environmental pollutants, the concepts of bioaccessibility and oral bioavailability are critical. The amount of PTE that may be dissolved in human gastrointestinal fluids is known as oral bioaccessibility (Bo Li et al., 2015; Ljung et al., 2007; Sabzevari & Sobhanardakani, 2018; Turner, 2011; Wagg et al., 2011). Thus, bioaccessibility represents the maximum amount of a potential pollutant that can be absorbed through the intestine. The gut epithelium can only absorb a small percentage of these bioaccessible pollutants. Inorganic pollutants are then transferred to the liver for biotransformation via the portal vein. The bioavailable fraction is the portion of the parent chemical that reaches the systemic circulation. To test the human bioaccessibility of trace metals in soils and dusts, several *in vitro* digestive models have been applied (Luo et al., 2012; Yoshinaga et al., 2014).

Thus, bioaccessibility is an important characteristic to examine for risk assessment purposes because it is one of the primary factors determining the bioavailable fraction (Wagg et al., 2011). Single, laboratory-based extraction processes and *in vitro* digestion models have

been devised to provide a conservative evaluation of the relative threat to ecological and human receptors as scientific methods for evaluating the bioavailability of PHEs. The simplified extraction test (SBET) is used to examine human oral bioaccessibility, providing useful information about PTE solubility in a medium that is comparable to acid stomach fluids (Ibanez et al., 2015; Kelepertzis and Argyraki, 2015; Kelepertzis et al., 2019; Kelepertzis et al., 2021; Luo et al., 2012).

Lately, the possibility to use simpler methods to overcome the laborious chemical-laboratory procedures has been explored. For example, magnetometry is now being used more frequently in research on environmental contaminants. Magnetic susceptibility is affected by physicochemical properties, temperature, biological and human activities (Murthuza et al., 2022). Anthropogenic magnetic inputs are responsible for the higher magnetic enrichment in soil and dust (Jordanova et al., 2014; Murthuza et al., 2022; Schmidt et al. 2004), whilst the mean mass specific magnetic susceptibility has been observed to have a positive correlation with population size (Jordanova et al., 2014). Besides, it is a known fact that the waste materials and pollutants from manufacturing processes and mining include a significant magnetic component along with many other ingredients (Rutkowski et al., 2020; Hanesch et al., 2007; Jordanova et al., 2012). For instance, magnetite and hematite are products of the burning of fossil fuels and they are formed via the oxidation of iron sulphides during high temperature combustion (Hanesch et al., 2007). In addition, vehicle emissions such as vehicular exhaust are sources of anthropogenic magnetic particles (Murthuza et al., 2022).

Measuring magnetic susceptibility is a quick and inexpensive technique for determining the level of environmental contamination (Hanesch et al., 2007; Petrovsky et al., 2000). The method utilizes the consequence of superior magnetic signature of the polluted sources due to the incorporation of strongly magnetic fraction from anthropogenic effects into the total magnetic signal (Jordanova et al., 2014). Furthermore, magnetic particles serve as carriers for various pollutants such as PTEs, which can be absorbed in ferro(i)magnetic phases (Jordanova et al., 2012; Petrovsky et al., 2000; Yang et al 2017), so the magnetic susceptibility could be used to identify hot spots of iron and associated heavy metal(oid)s,

such as Cu, Pb, Zn, Ni, As (Hanesch et al., 2007; Jordanova et al., 2014; Schmidt et al.2004; Yang et al 2017).

The use of household dust as a sampling medium to measure human exposure to anthropogenic metal(loids) is gaining popularity globally (Ibanez et al., 2010; Kelepertzis et al., 2019; Kelepertzis et al., 2021; Turner, 2011). In comparison to other types of dust, house dust may be more harmful to human health because individuals spend more than half of their time indoors (Ibanez et al., 2010; Isley et al., 2022; Kelepertzis et al., 2019; Kelepertzis et al., 2021; Turner, 2011). The research of indoor dust is crucial for figuring out the source, distribution, and quantity of PTE exposure because humans spend a large portion of their time indoors and PTE in the settled house dust can accumulate in humans through inhalation, ingestion, or skin contact absorption (Sabzevari & Sobhanardakani, 2018). As a result, assessments of PTEs levels in indoor environment dust are quickly expanding globally (Ibanez et al., 2010; Isley et al., 2022; Sabzevari & Sobhanardakani, 2018). In the areas where the study is conducted and in Cyprus generally, no study has been carried out on the potentially toxic elements contained in household dust.

2.1 Previous Studies on Soil geochemistry in Cyprus

A geochemical mapping program has been implemented for creating the geochemical atlas of Cyprus (Cohen et al., 2011). The influence of geology and anthropogenic effects on soil geochemistry has been determined. The results of this program provide that major, minor and trace element geochemistry in soils across Cyprus are dominated by the parent lithology (Cohen et al 2011; Cohen et al.,2012). Subsequently, in urban and industrial areas there are elevated levels of some metals, including Pb, Hg, Sn, As and Cu (Cohen et al., 2011; Cohen et al., 2012; Cohen et al., 2012; Zissimos et al., 2018; Zissimos et al., 2020). Mining activities have also contributed increased elemental concentrations in soils (Cohen et al., 2011; Cohen et al., 2012; Cohen et al., 2012). The natural concentration of elements in Cyprus soils varies by orders of magnitude depending on the parent material and the subsequent soil-forming processes. The anthropogenic geochemical influences on soils in Cyprus outside the major urban areas, industrial and mining sites are minor compared with the effects of parent lithology (Cohen et al., 2011; Cohen et al.,2012; Cohen et al., 2012).

2.1.1 Mine legacy in Cyprus and Mitseros area

The Troodos Ophiolite (TO) can be classified into basaltic pillow lavas that are overlaying, ultramafic and mafic cumulate units, the mafic sheeted dyke complex, and related ferruginous sediment units (Cohen et al., 2012). Numerous Cyprus-type Volcanogenic Massive Sulphides' (VMS) deposits, including the Kokkinopezoula deposit, are found in the basaltic pillow lavas of TO (Adamides, 2010; Galanopoulos et al., 2019). The mineralization is hosted within the extrusive volcanic sequence (Lower Pillow Lavas) of the Late Cretaceous Troodos ophiolite, being genetically related to contemporaneous submarine hydrothermal activity (Martin et al., 2019). The ore bodies are fault controlled and mushroom-shaped, comprising a lens of massive sulphide ore consisting mainly of pyrite, chalcopyrite and minor bornite and sphalerite (Galanopoulos et al., 2019). Immediately beneath the massive pyritic lens, a complex network of quartz and sulphide veins – with pyrite as the predominant sulphide mineral –exists, cutting through intensively propylitised basalts (Galanopoulos et al., 2019; Martin et al., 2019). This complex network, with sulphur content between 15 and 35 wt%, narrows downwards and becomes poorer in pyrite. This association of pyrite and quartz veins is known as stockwork-type mineralization which represents the feeder zone for the overlying massive sulphide lens. Most of the deposits are overlain by a manganese-poor, iron-rich sediment, which commonly contains sulphides (ochre) or/and manganese- and iron-rich sediment devoid of sulphides (umbers) and unmineralized Upper Pillow Lavas (Galanopoulos et al., 2019; Robertson and Hudson, 1973).

More than 30 massive sulphide ore bodies ranging in size between several thousands of tonnes to 16 million tonnes, with an average copper content between 0.5 to 4.5 wt%, have been mined in the TO and many other exploration targets have been reported. As a result of the extensive mining activity and the closure of mines, abandoned open pits are scattered around Troodos Mountain, whereas mine waste spoils surround open pits. Open pits have been flooded with acidic water, while the mine waste spoils react with the environment releasing potentially toxic metals to the surrounding soils and the open-pit lakes (Galanopoulos et al., 2019 and references therein). Twelve of these primary deposits (Adamides, 1984) have been exploited this way. These deposits, apart from Cu also contain high levels of Zn, Ag, and Au, but relatively lower levels of Pb (Constantinou and Govett, 1972,

1973). Umbers have increased Cu, Zn, Pb, Ba, V, Co, and Ni contents that are strongly connected with Fe and are frequently associated with hydrothermal venting near the VMS mineralization (Robertson and Hudson, 1973).

The Kokkinopezoula deposit is located on the northern side of TO, in the Mitseros region (Figure 2.1). It was mined until the middle of the 1960s and produced about 6Mt at 0.2 % wt. copper (Adamides,13). On the northern and southern edges of the pit, there are enormous amounts of mining waste. Intense acid leaching is visible on the pit walls and waste heaps due to the oxidation of pyrite and chalcopyrite, which transforms primary

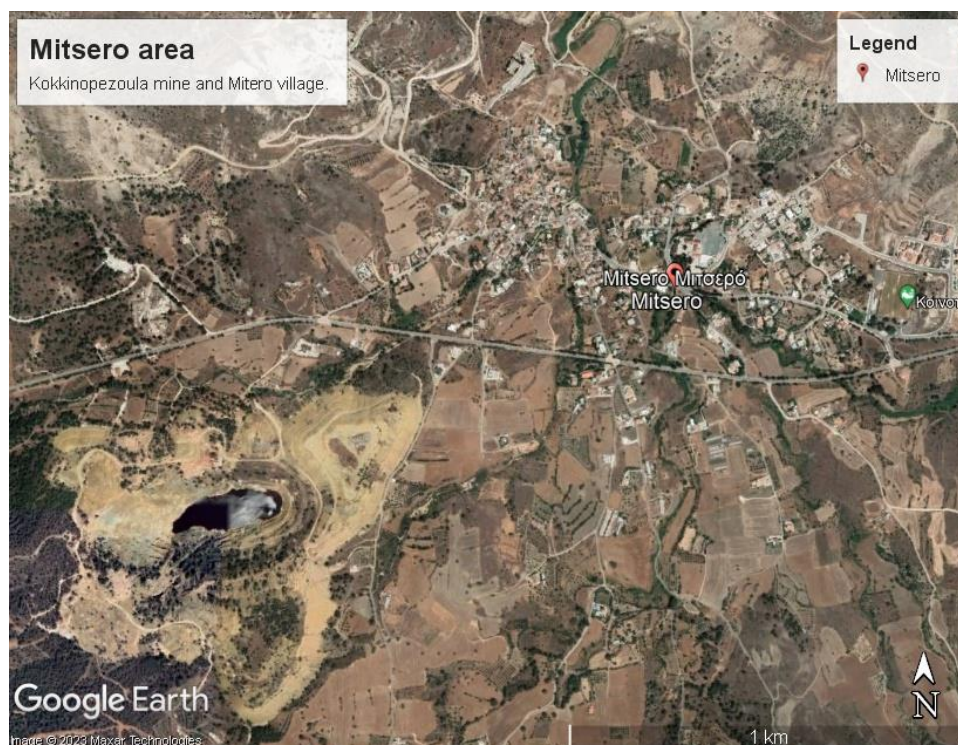


Figure 2.1. Map showing location of Mitsero and the abandoned Cu mine of Kokkinopezoula. Source Google Earth.

sulphides into secondary Fe oxyhydroxides and sulphates (Cohen et al., 2012). The mine wastes contain extremely high levels of Cu and other chalcophile elements, just as other abandoned deposits to the east of Kokkinopezoula.

According to Cohen et al. (2012), all of Cyprus' abandoned copper mines show elevated soil copper levels up to two kilometres from the exposed mineralization and the

mining operations, but there are little signs of pollution or naturally high soil copper levels beyond this point.

2.1.2 Nicosia

Nicosia (Lefkosia), the largest city of Cyprus (www.census2021.cystat.gov.cy; published 18/05/2022) is described as a discontinuous urban fabric of residential and commercial areas in the northern half, while a mixture of agriculture, forested areas and woodlands dominate to the south, with some industrial, commercial and residential areas along the main roads (Zissimos et al., 2018) (Figure 2.2).



Figure 2.2. Google Earth map showing the urban fabric of Nicosia.

The geology of the region is mainly carbonate-rich lithologies that were deposited in shallow marine environments, submarine conglomerate, subaerial terrace deposits or alluvium. The Apalos and Nicosia formations' calcarenite and siliciclastic rocks, as well as some conglomerate made up of a combination of TO-derived mafic intrusive and basaltic volcanic material, constitute the foundation of the city's eastern side (Zissimos et al., 2018). Cyprus's soil features, which generally lack the preservation of residual soil profiles, reflect the young age of the terrane (Mid-Miocene) (Cohen et al., 2011). Massive chalky soil (calcisol) is produced by the carbonate-rich units on hill slopes, while terra rossa (chromic luvisol) is

produced over exposed carbonates in places with flat topography (Cohen et al., 2011; Hadjiparaskevas, 2008).

The distribution of the major and the majority of the trace elements in the soil of Nicosia is controlled by geogenic processes. This reflects the parent lithology's makeup and the adsorption or precipitation on Fe/Mn oxides or carbonates. In different areas of the city, anthropogenic contributions to soil element levels can be seen. This is especially obvious for trace elements since their concentration in the local geological units is often quite low. When compared to parklands, forests, and agricultural areas, industrial, commercial, and residential districts in cities have varying higher levels of environmental concern (Cohen et al., 2012; Zissimos et al., 2018). In Cyprus, Ni and Cr are tightly correlated with one another in the soil and are connected to ultramafic lithologies. While Pb is obviously higher in residential areas, Zn values tend to be moderately elevated in industrial, commercial, and, to a lower extent, residential regions. Additionally, there are significant concentrations of As in the material used to fill some school yards and playgrounds (Zissimos et al., 2018; Zissimos et al., 2020).

2.1.3 Limassol

Limassol (Lemesos), which is one of the island's major economic, real estate, commercial, tourism, and shipping hubs, is situated on Cyprus' southern coast and stretches from the Troodos Mountains' edge to the water (Zissimos et al., 2020) (Figure 2.3). Marine carbonates of the Pakhna and Lefkara formations, as well as younger carbonate-rich strata on the northern slope and alluvium-colluvium cover on the coastal plains, make up the majority of the region's geology.

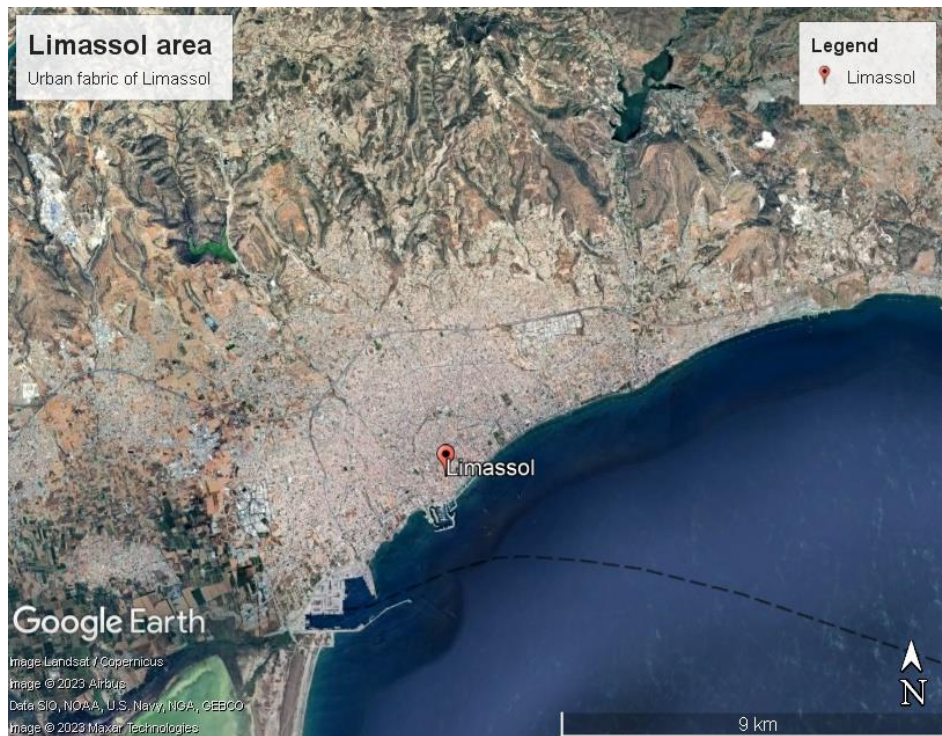


Figure 2.3. Google Earth map showing the urban fabric of Limassol.

The geochemistry of soils formed from the carbonates and the TO units is very different (Ren et al., 2015). Although the underlying primary material may have been transported as alluvium and colluvium, the soils of the Limassol region are primarily residual. Recognizable A and C horizons (calcaric regosols) are frequently produced by soil profile development, with rare exposures of somewhat ferruginous B horizons (calcaric cambisols). Carbonate-rich units are related to chalky soil characteristics (Hadjiparaskevas, 2008). Industrial sectors, which include industries for processing various raw materials and light engineering work are located within the urban net of Limassol. Lead, Sn, Zn, and Hg are all noticeably higher at the industrial zone locations, while Cr and Ni are also somewhat raised (Zissimos et al., 2020). The As and Sb levels in the Limassol soils are low and consistent across lithologies and varied land uses. The playgrounds for kids are the exception, having much higher values and a peak of 47 mg/kg As (Zissimos et al., 2020). Due to the use of materials from basalt or basaltic soil quarries, with traces of the Cyprus-style base metal mineralisation element suite, school grounds have a very distinct chemistry with higher Cu, Fe, Ti, Al, Mn, Zn and S, but lower Ba and Ca contents than most other land use areas (Zissimos et al., 2020). Near vehicle repair shops or firms that sell replacement components, Pb levels are at their highest.

3. Materials and Methods

3.1 Sample collection and preparation for analysis

3.1.1 Soils

Soil sampling was carried out in an area of 2 km², near the abandoned copper mine of Mitseros in Cyprus. The sampling area of Mitseros is located at a distance of less than one kilometre from the abandoned mine of Kokkinopezoula. The area was divided into 28 cells with dimensions 370 m x 370 m and one sample was collected in the centre of each cell (Figure 3.1). If the sampling spot was inaccessible, the sampling location was shifted to the nearest available space of soil material. A total of 28 composite topsoil samples were collected in the summer of 2021. Stainless steel sampling equipment was used in order to collect the soil samples. Each soil sample was made up of four 250 g sub-samples collected from the four corners of a 5 m square.

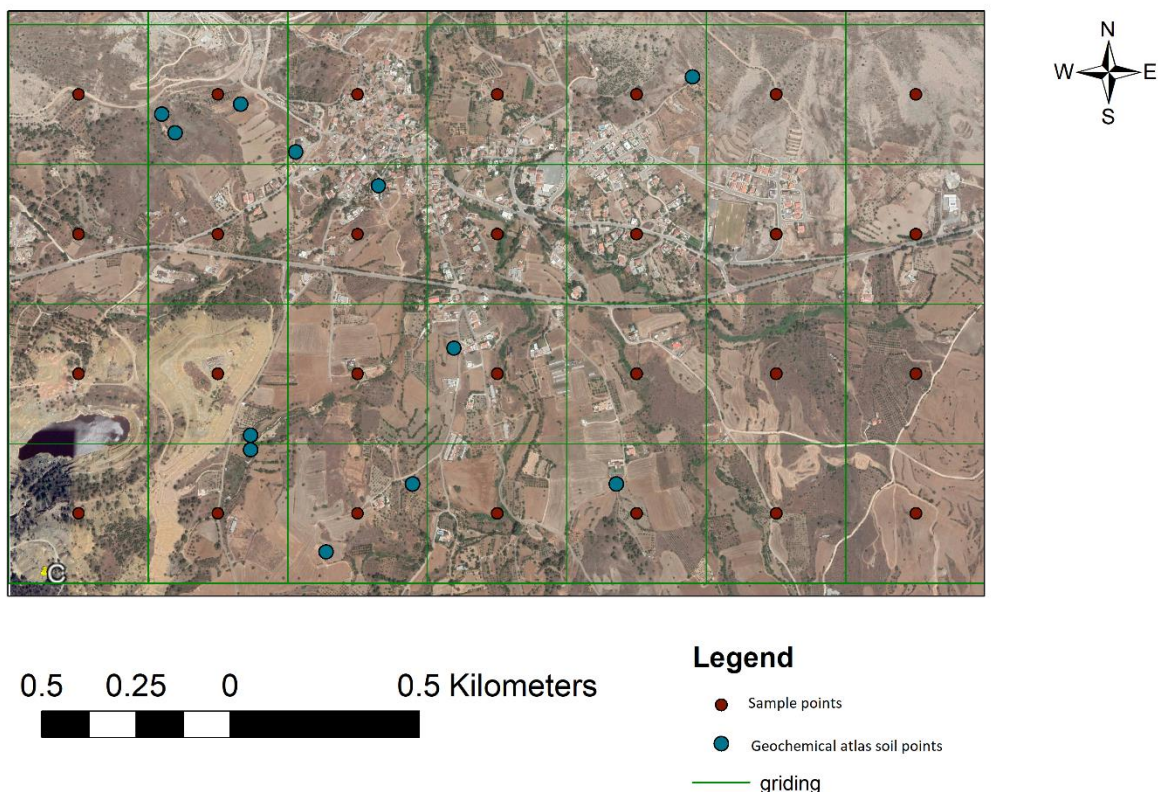


Figure 3.1 Map of the soil sampling in Mitsero area. Blue dots represent previously collected soil sample locations for the Cyprus geochemical map.

In the field, samples were sieved to <math><2\text{ mm}</math>. The coordinates, sampler, soil colour, and complete site descriptions, including land use, were all recorded, and snapshots were captured at each sampling site. Duplicate sampling took place at 9 randomly selected sites, roughly 5 meters away from the initial sampling location while keeping the same 370×370 m sampling cell. To eliminate cross contamination, all the equipment was carefully cleaned between the samples and Google map was used to record the exact geographical coordinates for each soil sample, as well as the field observations. Additionally, for the sake of reference, sampling sites were photographed (Figure 3.2).

After collection, the samples were transported to the Laboratory of Economic Geology and Geochemistry (LEGG), NKUA for the pre-analysis procedures. In a laboratory TEMA mill, the samples were ground to $<75\ \mu\text{m}</math>. The $<2\text{ mm}</math> fraction was kept for the physiochemical tests while the fine powder fraction was used for chemical analysis and mineralogical investigation.$$

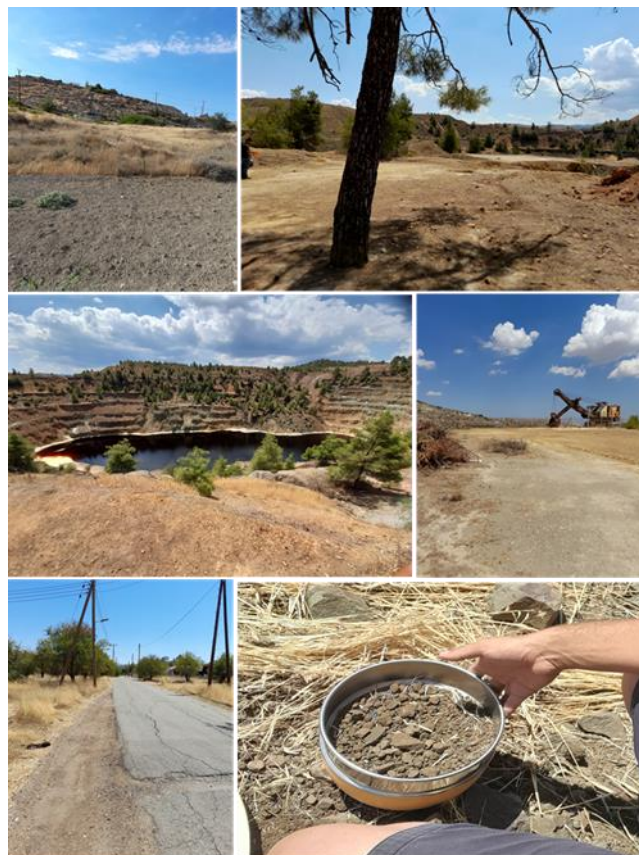


Figure 3.2. Photographs from the sampling procedure

3.1.2 House dust

Within the urban net, dust samples were collected from 42 homes in the areas of Nicosia (n=10), Limassol (n=23), and Mitsero (n=9) (see map https://iupui-earth-science.shinyapps.io/MME_Global/). Participants were selected through an open call for volunteer citizen scientists. They filled in an online survey (<https://www.mapmyenvironment.com/homebiome/home-biome-submission/>) and handed in their vacuum cleaner bags. In the laboratory (NKUA), vacuum cleaner bags were cut-opened under a fume cupboard and the contents were sieved to < 250 µm using single-use polypropylene mesh. Subsequently, each sieved dust sample was sealed in a plastic bag and labelled. A survey was designed to gather data from the occupant to evaluate household characteristics and personal behaviours. The information included: the house's floor level, footwear within the house, the number of people (specified by the number of kids), the house's surface area, recent refurbishment activity, the existence of a pet, smoking activity, and the house's age. Furthermore, residents of the house gathered the samples by cleaning the floor surfaces of all rooms, at least once a week, within a specific period window; from May 2021 to September 2021.

3.2 Analytical methods

The different analytical methods applied to the samples are presented in Table 3.1. A selected set of samples were analysed, using X-ray powder diffraction (XRD) and XRD patterns were determined with Eva software. Furthermore, all soil and dust samples (when there was enough quantity) were measured for magnetic susceptibility (see details in 3.3). The soil pH was determined with a bench-top pH meter after mixing soil or dust with deionised water in an 8:20 solid to water extract ratio.

Table 3.1 Analytical methods applied to the samples of this research. Sample description is based on field observations.

AA	sample ID	XRD	Magnetic susceptibility	Aqua regia ICP-AES)	XRF	SBET	pH	Sample description
1	MSS01		✓	✓		✓	✓	Topsoil of Mitsero
2	MSS02	✓	✓	✓		✓	✓	Topsoil of Mitsero
3	MSS03		✓			✓	✓	Topsoil of Mitsero
4	MSS04		✓	✓		✓	✓	Topsoil of Mitsero

AA	sample ID	XRD	Magnetic susceptibility	Aqua regia ICP-AES)	XRF	SBET	pH	Sample description
5	MSS05		✓	✓		✓	✓	Topsoil of Mitsero
6	MSS06		✓	✓		✓	✓	Topsoil of Mitsero
7	MSS07		✓	✓		✓	✓	Topsoil of Mitsero
8	MSS08		✓	✓		✓	✓	Topsoil of Mitsero
9	MSS09		✓	✓		✓	✓	Topsoil of Mitsero
10	MSS10		✓			✓	✓	Topsoil of Mitsero
11	MSS11		✓			✓	✓	Topsoil of Mitsero
12	MSS12		✓	✓		✓	✓	Topsoil of Mitsero
13	MSS13		✓			✓	✓	Topsoil of Mitsero
14	MSS14		✓			✓	✓	Topsoil of Mitsero
15	MSS15		✓	✓		✓	✓	Topsoil of Mitsero
16	MSS16		✓	✓		✓	✓	Topsoil of Mitsero
17	MSS17	✓	✓			✓	✓	Topsoil of Mitsero
18	MSS18		✓	✓		✓	✓	Topsoil of Mitsero
19	MSS19		✓	✓		✓	✓	Topsoil of Mitsero
20	MSS20		✓	✓		✓	✓	Topsoil of Mitsero
21	MSS21	✓	✓			✓	✓	Topsoil of Mitsero
22	MSS22		✓	✓		✓	✓	Topsoil of Mitsero
23	MSS23		✓	✓		✓	✓	Topsoil of Mitsero
24	MSS24		✓			✓	✓	Topsoil of Mitsero
25	MSS25		✓			✓	✓	Topsoil of Mitsero
26	MSS26		✓			✓	✓	Topsoil of Mitsero
27	MSS27		✓	✓		✓	✓	Topsoil of Mitsero
28	MSS28		✓	✓		✓	✓	Topsoil of Mitsero
29	MSS29		✓			✓	✓	Topsoil of Mitsero
30	MSS30		✓			✓	✓	Topsoil of Mitsero
31	MSS31		✓	✓		✓	✓	Topsoil of Mitsero
32	MSS32		✓	✓		✓	✓	Topsoil of Mitsero
33	MSS33		✓			✓	✓	Topsoil of Mitsero
34	MSS34		✓	✓		✓	✓	Topsoil of Mitsero
35	MSS35		✓			✓	✓	Topsoil of Mitsero
36	MSS36		✓	✓		✓	✓	Topsoil of Mitsero
37	MSS37		✓			✓	✓	Topsoil of Mitsero
38	LimDS01		✓		✓	✓	✓	House dust of Limassol
39	LimDS02		✓		✓	✓		House dust of Limassol
40	LimDS03				✓	✓		House dust of Limassol
41	LimDS04		✓		✓	✓		House dust of Limassol
42	LimDS05	✓	✓			✓	✓	House dust of Limassol
43	LimDS06					✓		House dust of Limassol
44	LimDS07				✓	✓		House dust of Limassol
45	LimDS08		✓		✓	✓		House dust of Limassol
46	LimDS09		✓		✓	✓		House dust of Limassol
47	LimDS10		✓		✓	✓		House dust of Limassol
48	LimDS11		✓		✓	✓	✓	House dust of Limassol
49	LimDS12		✓		✓	✓	✓	House dust of Limassol
50	LimDS13		✓		✓	✓	✓	House dust of Limassol
51	LimDS14		✓		✓	✓		House dust of Limassol
52	LimDS15				✓		✓	House dust of Limassol
53	LimDS16		✓		✓	✓		House dust of Limassol
54	LimDS17		✓		✓	✓		House dust of Limassol
55	LimDS18		✓			✓		House dust of Limassol
56	LimDS19				✓	✓		House dust of Limassol
57	LimDS20				✓		✓	House dust of Limassol
58	LimDS21		✓			✓		House dust of Limassol
59	LimDS22				✓	✓		House dust of Limassol
60	LimDS23				✓			House dust of Limassol
61	MDS01		✓		✓	✓		House dust of Mitsero
62	MDS02				✓	✓		House dust of Mitsero
63	MDS03	✓	✓		✓	✓		House dust of Mitsero

AA	sample ID	XRD	Magnetic susceptibility	Aqua regia ICP-AES)	XRF	SBET	pH	Sample description
64	MDS04		✓		✓	✓		House dust of Mitsero
65	MDS05		✓		✓	✓		House dust of Mitsero
66	MDS06		✓		✓	✓		House dust of Mitsero
67	MDS07		✓		✓	✓		House dust of Mitsero
68	MDS08		✓		✓	✓		House dust of Mitsero
69	MDS09		✓		✓	✓		House dust of Mitsero
70	NicDS01		✓		✓	✓		House dust of Nicosia
71	NicDS02		✓		✓	✓		House dust of Nicosia
72	NicDS03		✓		✓	✓		House dust of Nicosia
73	NicDS04	✓	✓		✓	✓		House dust of Nicosia
74	NicDS05				✓			House dust of Nicosia
75	NicDS06		✓		✓	✓		House dust of Nicosia
76	NicDS07		✓		✓	✓		House dust of Nicosia
77	NicDS08					✓		House dust of Nicosia
78	NicDS09					✓		House dust of Nicosia
79	NicDS10				✓	✓		House dust of Nicosia
80	NicDS11				✓	✓		House dust of Nicosia

A selection of 22 soil samples based on logistical considerations (i.e. available budget) was sent to *SGS Canada Minerals Burnaby* for chemical analysis. Specifically, the pseudototal content of PTEs in soil samples after dissolution by aqua regia (HNO₃-HCl) were measured by ICP-AES at *SGS Laboratories Ltd* in Canada. The concentrations of the major elements (calcium (Ca), magnesium (Mg), aluminum (Al), iron (Fe), sulfur (S), and phosphorus (P)) were also determined. The study focused on Arsenic (As), cadmium (Cd), chromium (Cr), copper (Cu), manganese (Mn), nickel (Ni), lead (Pb), and zinc (Zn) content data. These eight trace metal(oid)s were chosen because they are known to occur at potentially hazardous amounts in soils and house dust context (Charlesworth et al., 2011; Harb et al., 2015; Ibanez et al., 2011; Isley et al., 2022; Kelepertzis et al., 2021; Kelepertzis et al., 2019; Kelepertzis & Argyraki, 2015; Li et al., 2015; Luo et al., 2012; Mercier et al., 2011; Sabzevari & Sobhanardakani, 2018; Wragg et al., 2011; Yang & Cattle, 2015; Yoshinaga et al., 2014; Zissimos et al., 2018; Zissimos et al., 2021). For quality control, duplicates, reference materials SRM (OREAS 260, 520a for Soils), and reagent blanks were used.

Total chemical analysis of house dust samples for seven trace elements (As, Cr, Cu, Mn, Ni, Pb, Zn) using energy-dispersive X-ray fluorescence spectrometry (EDXRF) has been performed in the Laboratories of Northumbria University, Department of Geography and Environmental Sciences, Engineering and Environment, Newcastle, UK according to the analytical protocol of the Dust Safe study (Isley et al., 2021).

All soil and dust samples were subjected to the Simplified Bioaccessibility Test (SBET) in the LEGG, NKUA. The SBET method, which simulates the low pH conditions of human gastric solution, was used to test the oral bioaccessibility of PTEs (USEPA, 2013: Method 1340). 0.5 g of soil/dust was weighted in 50-mL centrifuge tubes and 50 mL of the 0.4 M glycine extraction solution (adjusted to pH 1.5 with concentrated HCl) was added. The suspensions were shaken in an orbital shaker for 1 hour at 37°C. The pH of the unfiltered suspensions was determined using a pH electrode calibrated with standard solutions of pH 1 and 4, and all pH readings were within 0.5 units of the starting pH (1.5). After extraction, a 10 mL aliquot was transferred from the extraction bottle to a disposable 20 mL syringe and filtered using a Whatman® GD/X 0.22 µm cellulose acetate disk filter (13 mm diameter). A Flame Atomic Absorption Spectrophotometer (FAAS - Perkin Elmer Pinaacle 500) was used to measure the metal concentrations in the filtered solution. The pH of the extraction residual fluid was then determined to ensure that the final pH was within 0.5 pH units of the original. The experiment was carried out at the LEGG, NKUA analytical facilities.

For quality control, blank samples and analytical duplicates were added to each analytical batch. Moreover, the CRMs NIST 2710 and NIST 2709a were introduced in duplicate for analysis at random positions. For each pair of duplicates, the relative percent difference (RPD) was determined as an indicator of analytical precision.

3.3 Magnetic Susceptibility Measurement procedure

Samples were weighed, wrapped in cling film to keep them immobile, and put into 10 cm³ cylindrical plastic pots. The Laboratory of Environmental Chemistry, National and Kapodistrian University of Athens, used a dual frequency (0.465 and 4.65 kHz) Bartington sensor to assess low field mass specific magnetic susceptibility. Low frequency or initial magnetic susceptibility (χ) is typically employed as a proxy for magnetic mineral concentration and is frequently equated to magnetite content (Jordanova et al., 2014; Kelepertzis et al., 2019). When magnetite is present in a sample, it will dominate the magnetic susceptibility values. Smaller magnetic susceptibility values may arise from the presence of antiferromagnetic and paramagnetic minerals. Finally, diamagnetic minerals, having typically negative magnetic susceptibility values, will dilute the magnetic signal of the sample

(Thompson and Oldfield, 1986). The findings were presented on a mass specific basis ($10^{-6} \text{ m}^3 \text{ kg}^{-1}$). The difference between low and high frequency susceptibility (frequency dependent susceptibility χ_{fd}) was determined and expressed as a percentage of the low frequency susceptibility ($\chi_{fd}\%$), ($\chi_{fd}\% = [(\chi - \chi_{hf})/\chi] \times 100$), where χ and χ_{hf} indicate magnetic susceptibility values at 0.465 and 4.65 kHz, respectively.

3.4 Calculation of Enrichment Factor (EF) and Combined Pollution Index (CPI)

The enrichment factor (EF) and the related combined pollution index (CPI) was determined for As, Cr, Cu, Ni, Pb, and Zn in each location to determine the impact of anthropogenic activities on soil and dust concentrations (Isley et al., 2022; Kelepertzis et al., 2019; Zissimos et al., 2018; Zissimos et al., 2020). Normalizing trace metal ratios to global crustal values derived from relevant crustal evaluations in the literature for house dust and the geochemical Atlas of Cyprus for soils yielded enrichment factors.

$$EF = \frac{\left(\frac{TE}{RE}\right)_{SAMPLE}}{\left(\frac{TE}{RE}\right)_{CURST}}$$

where TE represents the trace element concentration in dust or soil and RE represents the respective concentration of a reference element.

Due to its correlation with natural soil sources and the lowest variability compared to other analysed trace metals, Mn was chosen as the most suitable reference element in house dust samples in accordance to the DUSTSAFE study (Isley et al., 2022), whereas Fe, Al and Mn was chosen for soils (Reimann & Caritat, 2000). Background concentrations were taken from geochemical map of Cyprus (Cohen et al., 2012). This choice is also consistent with previous studies. The CPI is the average EFs of the PTE (Zissimos et al., 2021).

$$CPI = \frac{\sum_{n=1}^{n} EF_x}{n}$$

3.5 Statistical data analysis methods

The IBM SPSS v.28 (2022) program was used to conduct the statistical analysis. Descriptive statistics were calculated for soil and dust analytical data. Box plots were plotted and after performing the Anderson-Darling normality test, all data were log-transformed to satisfy the normality rule for further statistical tests (e.g. Pearson correlation, factor analysis and one-way ANOVA). Pearson correlation coefficients were calculated between elemental concentrations and other parameters (pH, magnetic susceptibility). Factor analysis with varimax rotation was performed to group the elements in soil and dust and identify possible related anthropogenic or geogenic geochemical processes controlling their distribution in the samples. Regarding the house dust data provided by the questionnaires, trace element contents were compared using one way ANOVA, coupled with Tukey-Kramer multiple comparison tests (Isley et al., 2021) to appraise homes for smoking activities, recent renovation, the presence versus absence of pets, peeling paint, garden access, effects of home age, vacuuming frequency, construction material, flooring, heating fuel, and home type and hobbies such as hunting or gardening.

3.6 Exposure dose calculations

Exposure dose calculations were performed to determine the health risk via dust and soil trace element exposure in children. Thus, the estimated all-day exposure to PTEs in dust from Nicosia, Limassol and Mitsero districts and to soil trace elements in Mitsero has been calculated. The equations for Chronic Daily Intake (CDI) for non-carcinogenic risk calculations are as follows:

$$\text{Ingestion: } CDI = TEC \cdot \frac{\text{IngR} \cdot \text{EF} \cdot \text{ED}}{\text{BW} \cdot \text{AT}} \cdot CF$$

$$\text{Inhalation: } CDI = TEC \cdot \frac{\text{InhR} \cdot \text{EF} \cdot \text{ET} \cdot \text{ED}}{\text{PEF} \cdot \text{BW} \cdot \text{AT}}$$

$$\text{Dermal: } CDI = TEC \cdot \frac{\text{SA} \cdot \text{SL} \cdot \text{ABS} \cdot \text{EF} \cdot \text{ED}}{\text{BW} \cdot \text{AT}} \cdot CF$$

All exposure factors supplied for the calculation of CDIs were adopted from Isley et al. (2022) and Cao et al. (2020) as follows:

Table 3.2 Exposure factors for calculation of non-carcinogenic

IngR	dust ingestion rate	60 mg/d for children <2 years of age
EF	Exposure Frequency	350 days/year
ED	Exposure duration	2 years.
BW	body weight	11.4 kg
AT	Averaging time	ED*365 days
CF	conversion factor	1×10^{-6} kg/mg.
InhR	inhalation rate	6.7 mg/day
PEF	dust-to-air particulate emission factor	1.36×10^9 m ³ /kg
ABS	Absorption factor for dermal	0.03
SA	Skin surface area	5300 cm ²
SL	Solid to skin adherence factor	0.03 mg/cm ²
TEC	total element concentration	-

Carcinogenic health risk assessment was estimated for As, Cr, Ni, and Pb. Given that Cu, Mn, and Zn are not recognized as human carcinogens, carcinogenic assessment was evaluated only for As, Cr, Ni, and Pb. The chronic daily intake (CDI) for ingestion, inhalation, and dermal exposure pathways was estimated using the equations:

$$\text{Ingestion: } CDI = TEC \cdot \frac{IR \cdot EF}{AT} \cdot CF$$

$$\text{Inhalation: } CDI = TEC \cdot \frac{EF \cdot ET \cdot ED}{PEF \cdot 24 \cdot AT} \cdot 10^3$$

$$\text{Dermal: } CDI = TEC \cdot \frac{ABS \cdot EF \cdot DFS}{AT} \cdot CF$$

All exposure factors supplied for the calculation of CDIs were adopted from Isley et al. (2022) and Cao et al. (2020) as follows:

Table 3.3 Exposure factors for calculation of carcinogenic

IR	Intake rate	113 mg*year/kg/day
DFS	Age adjusted soil dermal factor	362.4 mg*year/kg/day

EF	Exposure Frequency	350 days/year
ED	Exposure duration	2 years.
CF	conversion factor	1×10^{-6} kg/mg.
PEF	dust-to-air particulate emission factor	1.36×10^9 m ³ /kg
AT	Average Time	28470 days
ET	Exposure time	24 hours/day
LT	lifetime	78 years
ABS	Absorption factor for dermal	0.03

Following the calculation of the CDI for each exposure pathway, the hazard quotient (HQ) and carcinogenic risk (Risk) were determined using the reference dose (RfD; ingestion; noncarcinogenic), reference concentration (RfC; inhalation; noncarcinogenic), dermal reference dose (DRfD; dermal; noncarcinogenic), oral slope factor (OSF; ingestion; carcinogenic), inhalation unit risk (IUR; inhalation; carcinogenic), and dermal slope factor (DSF; dermal; carcinogenic) (Table 3.2) using the equations:

Non-carcinogenic:

$$HQ = CDI / \text{Reference- non carcinogenic (Table 3.4)}$$

$$HI = \sum HQ$$

Carcinogenic:

$$\text{Risk} = CDI / \text{Reference- carcinogenic (Table 3.4)}$$

$$TR = \sum \text{Risk}$$

The hazard index (HI) for each element is the sum of HQs (Cao et al., 2020). The sum of risk estimates for each exposure factor for each elements provided the Target Risk (TR). A HI or TR < 1 and 1×10^{-6} indicates no significant risk of non-carcinogenic and carcinogenic effects respectively. A HI or TR > 1 and 1×10^{-6} indicates a significant risk of non-carcinogenic and carcinogenic effects, respectively and a probability that tends to increase as the HI or TR increases (Cao et al., 2020; Isley et al., 2022).

Table 3.4 Reference doses (RfD), reference concentrations (RfC), dermal reference doses (DRfD), oral slope factors (OSF), inhalation unit risks (IUR) and dermal slope factors (DSF)

applied for each trace metal. Carcinogenic risk modelling was not conducted for Cu, Mn or Zn as they are not classified as human carcinogens (Isley et al., 2022).

Trace Elements	Non-Carcinogenic			Carcinogenic		
	RfD (mg/Kg)	RfC (mg/Kg)	DRfD (mg/Kg)	OSF (mg/Kg)	IUR (mg/Kg)	DSF (mg/Kg)
As	3.00E ⁻⁴	1.50E ⁻⁵	1.23E ⁻⁴	1.50	4.30E ⁻³	1.50
Cr	3.00E ⁻³	1.00E ⁻⁴	6.00E ⁻⁵	5.00E ⁻¹	1.20E ⁻²	5.00E ⁻¹
Cu	1.00E ⁻²	6.90E ⁻⁴	1.20E ⁻²	-		
Mn	2.40E ⁻²	5.00E ⁻⁵	1.84E ⁻³	-		
Ni	2.00E ⁻²	2.00E ⁻³	5.40E ⁻³	1.54E ⁻¹	2.60E ⁻⁴	9.10E ⁻¹
Pb	3.50E ⁻³	3.52E ⁻³	5.25E ⁻⁴	8.50E ⁻³	1.20E ⁻⁵	2.10E ⁻¹
Zn	3.00E ⁻¹	3.00E ⁻¹	6.00E ⁻²	-		

4. Results and Discussion

4.1 Soil geochemistry

4.1.1 Soil pH and mineralogy

The soil samples from Mitsero were predominantly alkaline (8.23 average pH value) and calcareous (average Ca 7.38 %). The pH of the soil ranges from 4.37 to 9.91, with most values being around 8 (Appendix I). Based on Pearson correlation test (log-transformed data) the pH values had been associated with Ca, Fe, Cu and S (Table 4.0). The negative correlation of pH with Fe, Cu, and S is indicative of the weathering of primary sulfides (chalcopyrite) under low pH conditions (4.37-4.58) around the abandoned copper mine, while the positive correlation between pH and Ca is related with the alkaline soils in the Mitsero.

Table 4.0. Pearson correlation test of pH with elements.

	Correlations	pH	Cr	Ca	Mn	Ni	Fe	Zn	Cu	S
pH	Pearson Correlation	1	0.217	.496*	0.412	0.269	-.858**	-0.386	-.781**	-.884**
	Sig. (2-tailed)		0.332	0.019	0.057	0.226	<.001	0.076	<.001	<.001
	N	22	22	22	22	22	22	22	22	21

The mineralogical composition of Mitseros' soil was determined through XRD of 4 selected samples (see XRD patterns in Appendix II; MSS02; MSS03; MSS17; MSS21). Quartz, Anorthite, Dolomite and Calcite are the common and main minerals in soils. Mitsero samples which are located next to the abandoned copper-mine also contain Chalcopyrite, Hematite, Goethite, Atacamite, and Jarosite (samples MSS02, MSS03). Chalcopyrite is one of the main minerals of the VMS Cyprus- type ore (Galanopoulos et al., 2019), while the secondary minerals are related to Acid Mine Drainage, which means that the oxidation process of sulphides continues to occur in the region. Atacamite is formed, as a primary product of supergene oxidation, after leaching of Cu sulphides by oxygenated meteoric waters that percolate through the deposits (Reich et al., 2008). Jarosite is also being formed as a solid residue through the weathering of the ore (Pappu et al., 2005). Cowlesite is a Ca-rich zeolite, and it may be one of the main constituents of the porous zones in mid-oceanic ridge basalts. It is recovered inside geodes in basaltic rocks that experienced fast cooling and hydrothermal alteration (Mugnaioli et al., 2020). In the Mitseros soil is probably originating from the pillow lavas hosting the ore. In addition, Norsethite is indicative for low-sulphate depositional environments, and it is an analogue to the mineral dolomite (Böttcher, 1999) which is found also in soils and the possible source is the overlying carbonate rocks, in Mitsero. Another

detected mineral is Caoxite which is calcium oxalate (Graustein et al., 1977) and it has a large impact on biological and geochemical processes in soils.

4.1.2 Magnetic susceptibility of soil samples

Primary anthropogenic sources such as mining or later smelting of ores that need heat produced by burning fossil fuels, are linked to the magnetic signal further through these processes (Blundell et al. 2009). Low-frequency magnetic susceptibility (xlf), which can be acquired from a variety of sources, is often comparable to the concentration of ferrimagnetic minerals in topsoil, such as magnetite and maghemite (Blundell et al. 2009). Furthermore, compared to magnetic minerals of pedogenic origin, anthropogenic particles are coarse-grained (multidomain (MD) and stable single domain (SSD)), do not display frequency dependence, but rather contribute to overall magnetic susceptibility (xlf) (Blundell et al. 2009). In this study the xlf values are relatively high with range 4.1-17.5 and median is recorded at 6.36 (Table 4.1) where it appears that the soils in Mitsero contain ferrimagnetic minerals.

Table 4.1 Descriptive statistics of magnetic susceptibility measurements in soil samples.

Magnetic Susceptibility	No. samples	Mean	SE Mean	StDev	Median	Minimum	Maximum
xlf ($10^{-6} \text{ m}^3/\text{kg}$)	37	7.28	0.65	3.92	6.36	4.1	17.49
xhf ($10^{-6} \text{ m}^3/\text{kg}$)	37	7.22	0.64	3.9	6.33	4.05	17.38
xfd ($10^{-8} \text{ m}^3/\text{kg}$)	37	6.02	0.78	4.75	5	2.76	26.27
xfd%	37	0.9	0.07	0.47	0.95	0.02	1.71

In addition, viscous superparamagnetic (VSPM) nanoscale grains with features that increase magnetic susceptibility can be created by natural soil-forming processes (Blundell et al. 2009). The frequency dependency of magnetic susceptibility (xfd%), which is used to identify VSPM, has been shown to have a significant impact on topsoil. Due to pedogenic processes, magnetically enhanced topsoil which is mostly secondary magnetite/maghemite has elevated values of xfd%, frequently > 8 (Dearing et al., 1996a). All xfd% values $< 2\%$ signifying a near absence of VSPM magnetic grains and range from 0.02 to 1.71 (table 4.1), so pedogenic processes are not carried out in the area.

Using low frequency susceptibility (xlf) and frequency dependent susceptibility (xfd%), it is possible to distinguish between soils that have been pedogenically modified and those that have increased sensitivity from a major contamination source. It is helpful to assess how magnetic signatures in topsoils differ from their "natural" background in order to identify the possible impact of anthropogenic magnetic enhancement. According to a method proposed by Blundell et al. (2009) the median of xlf and xfd% for each soil series from a whole data set serves as a representation of the expected background value for each soil type. The magnetic value of each sample is subtracted from the median value of the soil series the sample represents to provide residual values for the whole data set. Negative xfd% residuals and enhanced xlf values that are 1.4 and 1.75 times higher than the median indicate anomalous samples that are likely to represent increased input of coarse magnetic material from pollution sources (Blundell et al. 2009). In Figure 4.1 the residual values of the three anomalous samples appear in agricultural land with scattered houses but generally the soils were not affected from anthropogenic inputs. However, the high value of xlf can be rendered to the igneous rocks, when SSD and MD ferrimagnetic minerals do not show viscous behavior (Dearing, 1996a). The soil samples in Mitsero showed high xlf and low xfd% values, which indicate the influence of pillow lava weathering and provision of primary geological grains in topsoils.

Principal component analysis showed that parent material was found to be the primary control of topsoil magnetic enhancement in Mitsero. xlf has positive correlation with Mg, Mn, and negative correlation with As, Cu, Fe, S and Ca (see section 2.1.4). The elements with positive correlation are most likely related to the underlying geology, especially with pillow lavas and the elements with negative correlation related to ore and the carbonate rocks. The low xfd% nearby abandoned copper mine (Figure 4.1) exists for other reasons including domination by non-frequency dependent material such as paramagnetic (quartz, calcite), antiferromagnetic minerals (pyrite, chalcopyrite, dolomite,) and water logging causing reductive dissolution of ferrimagnetic grains.

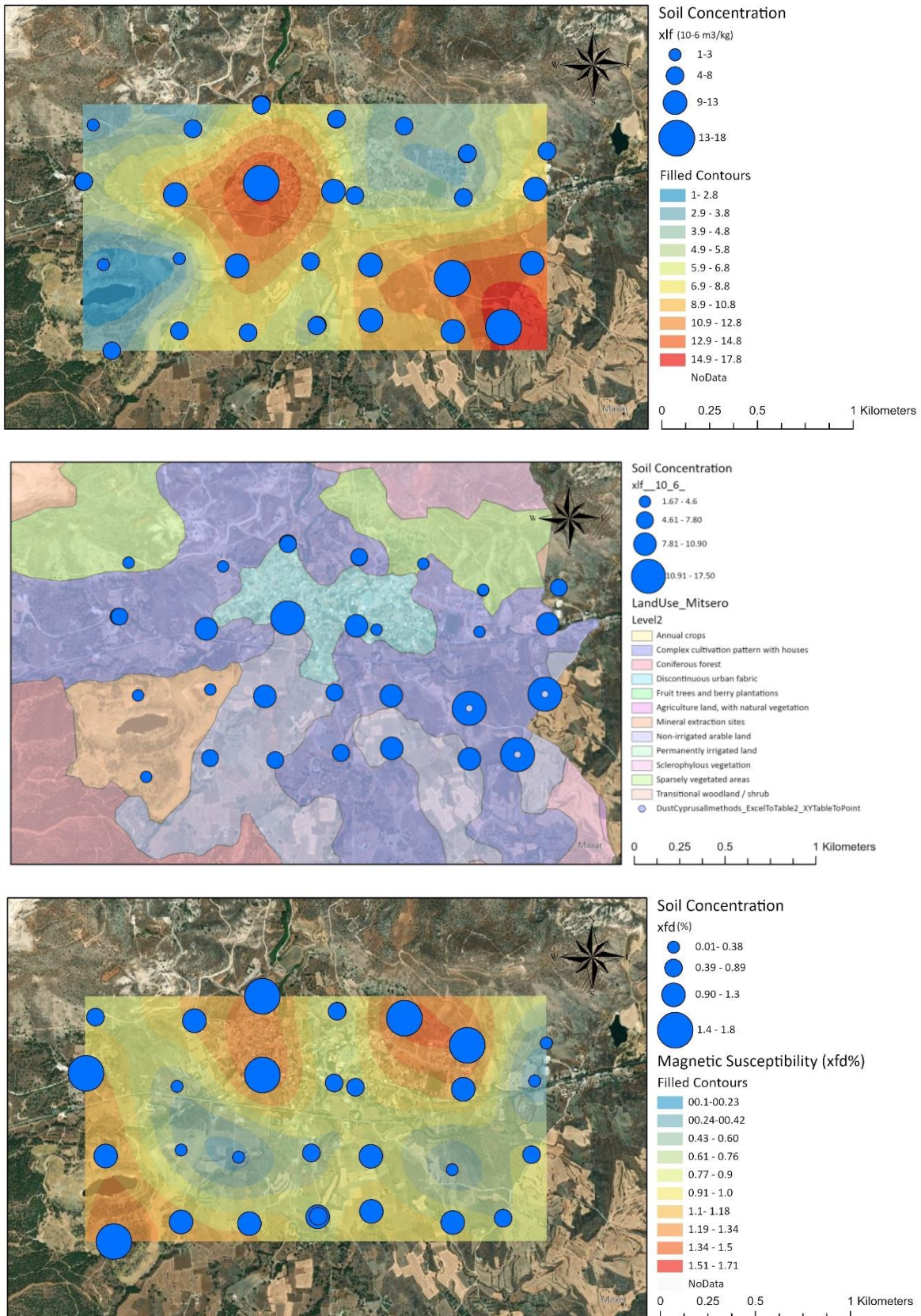


Figure4.1. The distribution maps of Magnetic Susceptibility and Frequency dependent magnetic susceptibility in the Mitsero village.

4.1.3 Chemical composition of soil samples

The quality of the analytical data, based on duplicate analysis and analysis of SRM, has been found within acceptable limits. The results of quality control are presented in Table 4.2.1. All relative percentage differences are lower than 5% and the recovery percentage there in the acceptable range of 80-120%.

Table 4.2.1 Relative Percent Difference (RPD) and recovery of chemical analysis of pseudototal in soil samples

Elements	Al	As	Ca	Cr	Cu	Fe	Mg	Mn	Na	Ni	Pb	S	Zn
RPD	0.37	0.00	1.04	0.00	0.82	0.18	0.27	1.38	6.45	2.82	0.00	0.00	3.28
Recovery% OREAS 502c	104.00	112.50	80.00	84.42	104.00	89.41	98.46	91.75	105.26	56.67	111.11	47.06	89.80
Recovery% OREAS 260	101.50	120.00	105.08	103.66	101.08	104.56	107.93	101.33	109.76	100.00	100.00	100.98	90.91

Median values of the studied elements follow the decreasing order: Ca > Fe > Al > Mg > S > P > Mn > Cu > Zn > Cr > Ni > Pb > As. The research focused on PTEs of environmental concern, including As, Cr, Cu, Fe, Mn, Ni, Pb and Zn. None of the studied elements followed the normal distribution and the data were log-transformed for normalisation.

Table 4.2.2 Soil total concentrations of studied elements of different Cyprus districts.

Region	Mitsero Soil (n=22)						Limassol soil (Zissimos et al., 2018; n=441)	Nicosia soil (Zissimos et al., 2018; n=441)	Cyprus soil (Cohen et al., 2012; n=5377)
	Mean	SE Mean	St.Dev.	Min	Max	Median	Median	Median	Mean
As (ppm)	7	2.64	9.5	3	38	4	4.5	5.5	4.9
Ca (%)	6.89	0.95	4.47	0.14	13.44	7.4	16	13.5	11.9
Cr (ppm)	43.64	9.43	44.23	6	174	25.5	55.4	36	73.7
Cu (ppm)	155	38.5	180	14.6	734	85.4	42.5	44.5	87.9
Fe (%)	15.66	0.56	2.64	2.85	13.31	5	2.3	2.7	3.6
Mn (ppm)	990.5	60.4	2.83	492	1517	960	531	617	981
Ni (ppm)	27.41	5.19	24.36	4	118	20	52.2	33.3	111
Pb (ppm)	7.8	1.88	5.94	2	19	6	8.7	7.7	11
S (%)	0.3	0.17	0.79	0.01	3.27	0.06	0.05	0.06	-
Zn (ppm)	98.6	12.8	60.2	36	253	75	49	60.5	67

Comparison of the soil composition results based on median values from this work to Limassol and Nicosia geochemical survey indicated that elemental contents of Cu, Fe, S, Zn

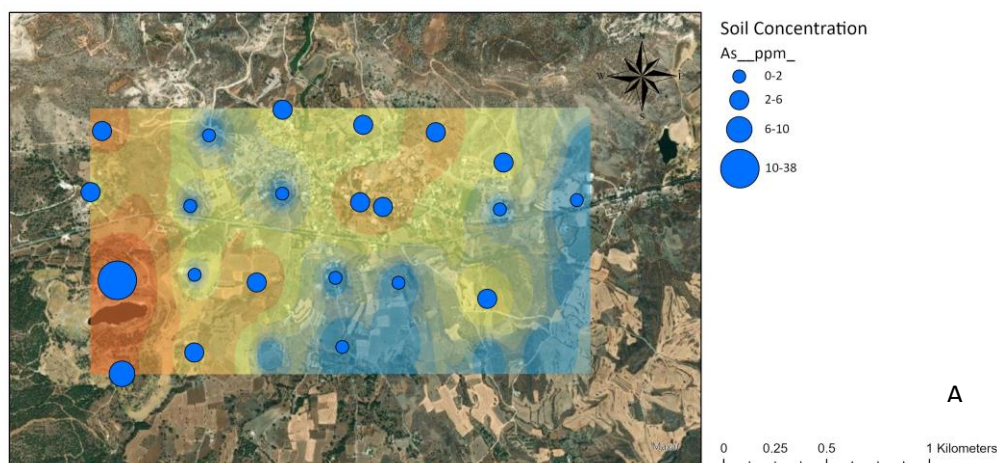
are higher in Mitsero area. Mean values at Mitsero are also higher than the Cyprus reported mean values. These elements are associated with the mineralogy of the VMS type ore of the abandoned copper mine in the Mitsero village. Specifically, typical ore minerals include FeS_2 (pyrite), CuFeS_2 (chalcopyrite) and ZnS (sphalerite) (Martin et al. 2019). In addition, Mn soil content is also higher in Mitsero due to enrichment of parent ophiolitic rocks. However, Ni, and Cr have higher concentrations in Limassol soil (Zissimos et al., 2020) and As is higher in Nicosia soil (Zissimos et al., 2018) (Table 4.2). Ephemeral streams draining the exposed ultramafic core of Troodos Ophiolite rocks (i.e., serpentinized peridotite) correspond to the source of Ni and Cr in Limassol and the coastal fringe where detrital chromite and other ferromagnesian minerals have accumulated (Zissimos et al., 2020), whilst in Mitsero the parent material consists of pillow lavas (i.e. basalt). Furthermore, Pb and As in Limassol and Nicosia is correlated with industrial urban areas (Zissimos et al., 2018; Zissimos et al., 2020). In contrast to metropolitan regions that have burden and enrichment of PTEs from anthropogenic sources, in Mitsero, Pb contents are probably related to the ore composition (geogenic source) which generally contains low concentrations of Sn and Pb (Adamides, 1984; Govett, 1972). The high As values observed in Nicosia are associated with children's playgrounds which contain As-rich transported fill (Zissimos et al., 2018). Furthermore, Nicosia had the highest values of Ca which were largely due by the Apalos and Nicosia formations (Zissimos et al., 2018).

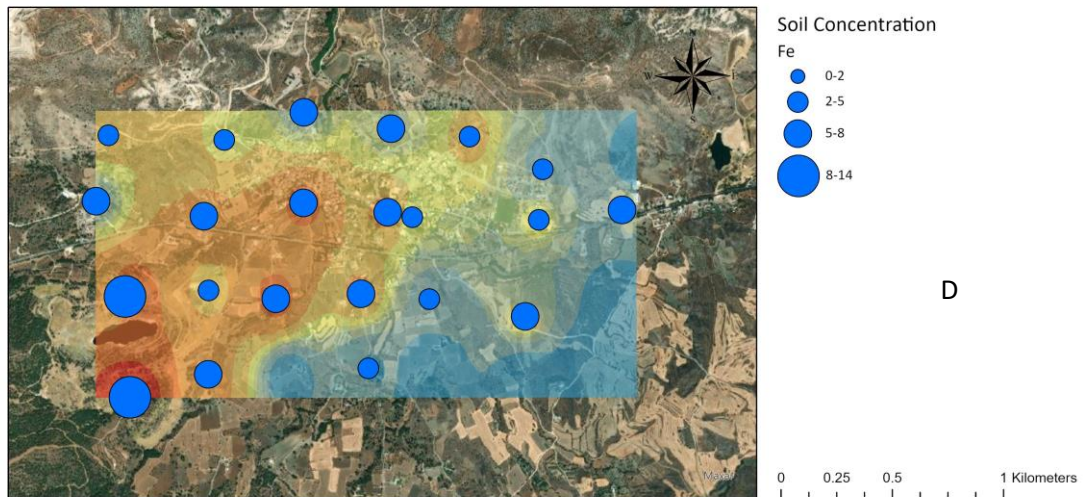
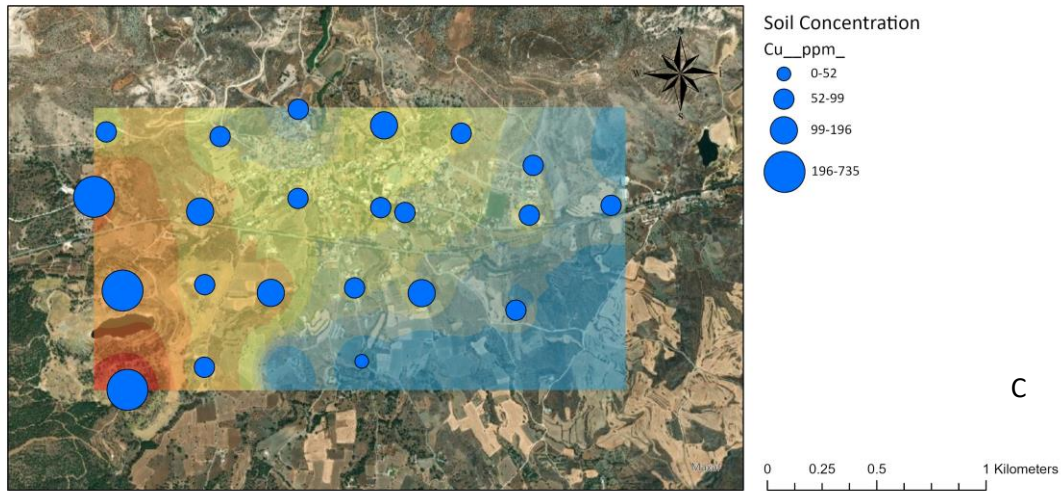
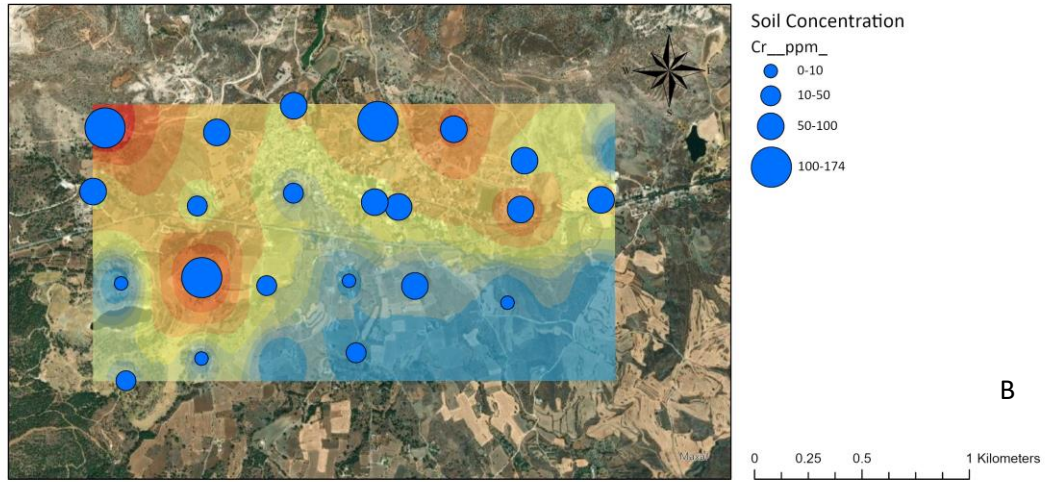
The correlation between 8 elements in the soil samples from Mitsero was evaluated with Pearson correlation test in logarithmic data (Table 4.3). Copper shows positive correlation with As, Fe and Zn for which the source is the VMS ore. This perspective is strengthened through the distribution maps of As, Cu and Zn (Figure 4.2 a, c, h), where the highest concentration of the elements appear around the mine. Furthermore, Cu and Zn may also originate from vehicle emissions (Ibanez et al., 2010; Isley et al., 2022; Kelepertzis et al., 2019; Kelepertzis et al., 2021; Turner, 2011). This is supported by their high concentration near roads and in the vehicle junkyard in the east site of the village. In addition, Fe showed a significant negative correlation with Cr and Ni which could be attributed to different geogenic source. The relationship between Cr and Ni is apparent from the positive correlation (Table 4.3) and from the distribution maps (Figure 4.2b and f), where the elements distribution is roughly the same and shows common source which is pillow lavas. Moreover, the upper

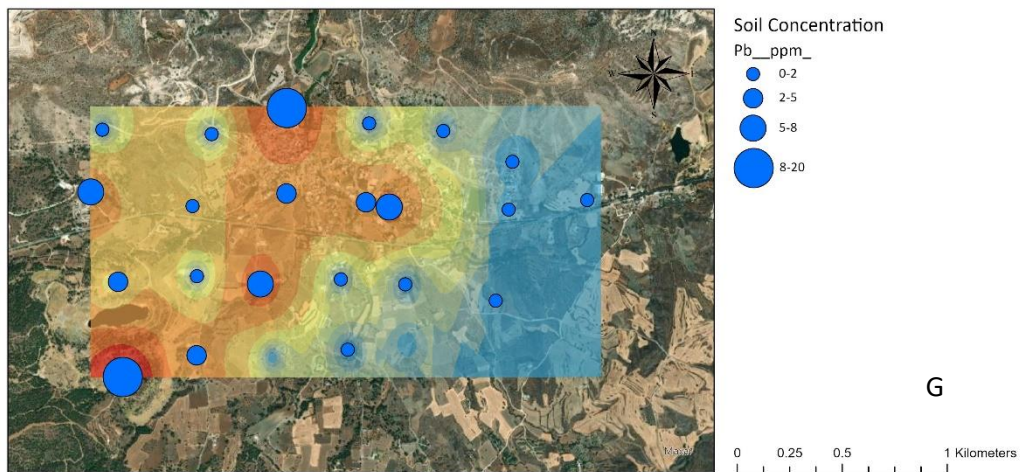
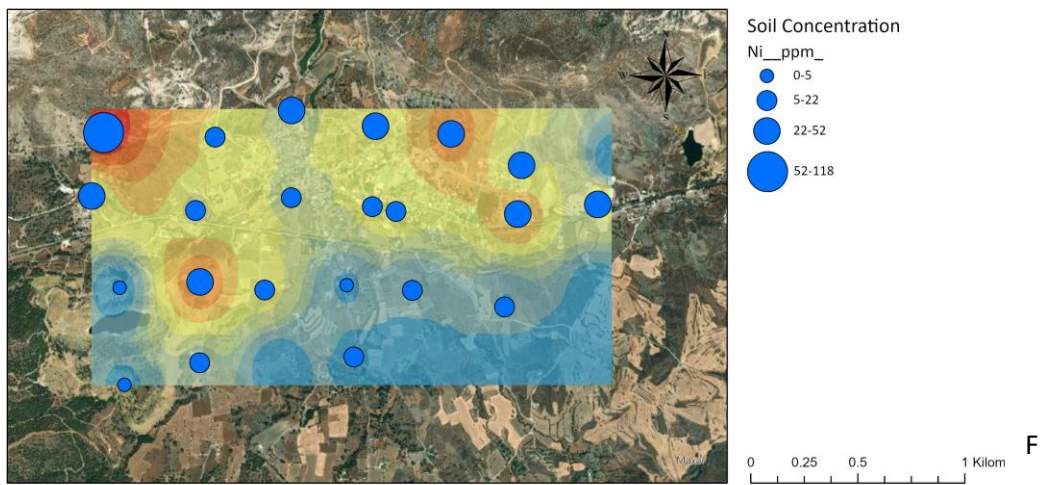
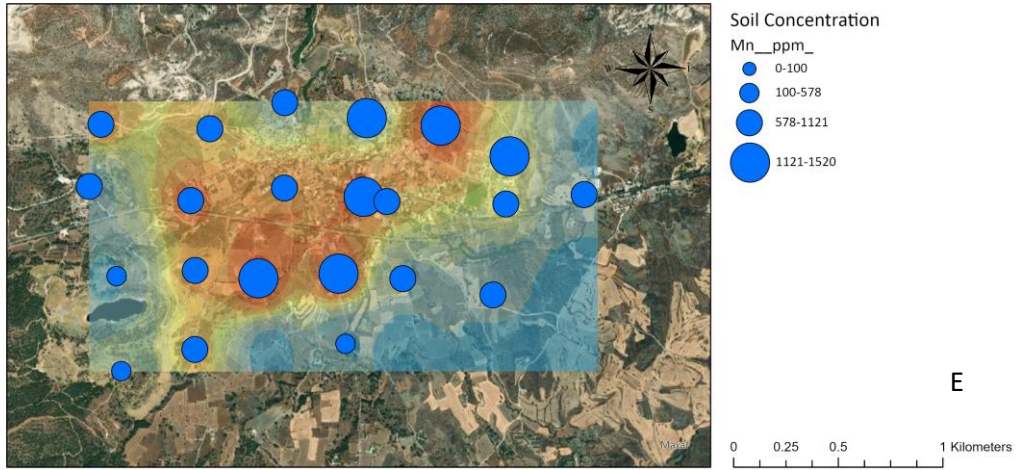
pillow lavas demonstrate higher concentration of Cr and Ni, particularly at boundary between upper and lower pillow lavas (Figure 4.3). Furthermore, Mn shows positive correlation with Ni supporting its geogenic origin and association with ultramafic rocks.

Table 4.3. Pearson correlation coefficient matrix between As, Cr, Fe, Mn, Ni, Pb, and Zn.

	Correlations	As	Cr	Cu	Fe	Mn	Ni	Pb	Zn
As	Pearson Correlation	1	-0.414	.557*	.783**	-.731**	-.566*	-0.133	-0.006
	Sig. (1-tailed)		0.08	0.024	<.001	0.002	0.022	0.377	0.493
	N	13	13	13	13	13	13	8	13
Cr	Pearson Correlation	-0.414	1	-0.099	-.417*	0.265	.918**	0.478	-0.185
	Sig. (1-tailed)	0.08		0.33	0.027	0.117	<.001	0.081	0.205
	N	13	22	22	22	22	22	10	22
Cu	Pearson Correlation	.557*	-0.099	1	.701**	-0.316	-0.314	0.248	.698**
	Sig. (1-tailed)	0.024	0.33		<.001	0.076	0.077	0.245	<.001
	N	13	22	22	22	22	22	10	22
Fe	Pearson Correlation	.783**	-.417*	.701**	1	-0.233	-.516**	0.179	.521**
	Sig. (1-tailed)	<.001	0.027	<.001		0.149	0.007	0.311	0.006
	N	13	22	22	22	22	22	10	22
Mn	Pearson Correlation	-.731**	0.265	-0.316	-0.233	1	.380*	-0.122	0.05
	Sig. (1-tailed)	0.002	0.117	0.076	0.149		0.041	0.369	0.413
	N	13	22	22	22	22	22	10	22
Ni	Pearson Correlation	-.566*	.918**	-0.314	-.516**	.380*	1	0.059	-0.255
	Sig. (1-tailed)	0.022	<.001	0.077	0.007	0.041		0.436	0.127
	N	13	22	22	22	22	22	10	22
Pb	Pearson Correlation	-0.133	0.478	0.248	0.179	-0.122	0.059	1	0.526
	Sig. (1-tailed)	0.377	0.081	0.245	0.311	0.369	0.436		0.059
	N	8	10	10	10	10	10	10	10
Zn	Pearson Correlation	-0.006	-0.185	.698**	.521**	0.05	-0.255	0.526	1
	Sig. (1-tailed)	0.493	0.205	<.001	0.006	0.413	0.127	0.059	
	N	13	22	22	22	22	22	10	22
* Correlation is significant at the 0.05 level (1-tailed).									
** Correlation is significant at the 0.01 level (1-tailed).									







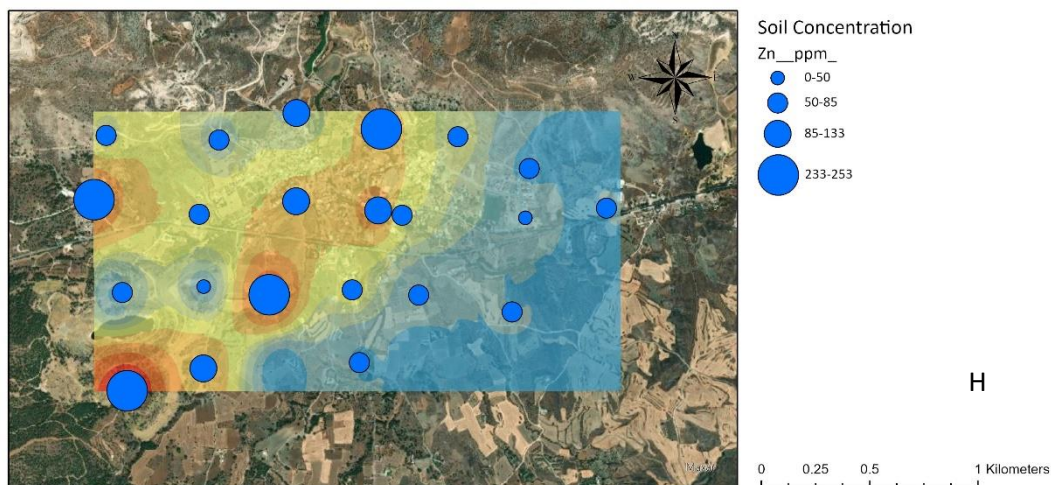


Figure 4.2. Proportional dot plots of the distribution of selected elements extracted by aqua regia in soil samples. A=As, B=Cr, C=Cu, D=Fe, E=Mn, F=Ni, G=Pb, H=Zn.

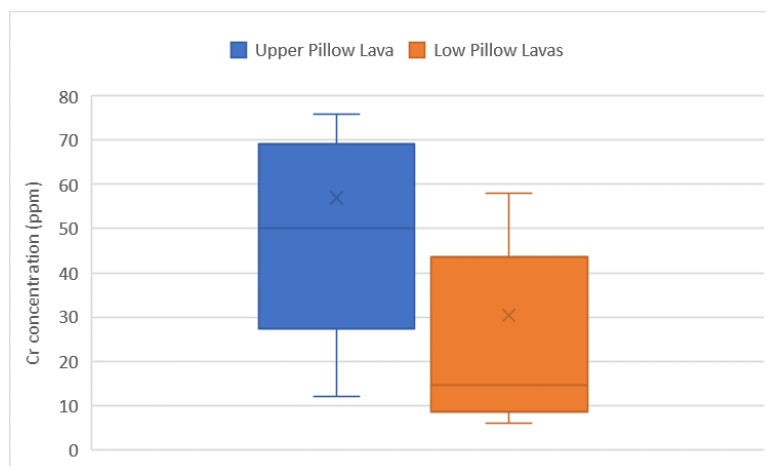


Figure 4.3 Cr concentration in soils base on sampling area of Mitsero.

4.1.4 Enrichment factor & Principal Component Analysis of soil

The geochemical variation in an element in the surficial environment is considered when calculating the element EFs relative to a local baseline (Kelepertzis et al., 2020). Additionally, it addresses the issue of under- or over-estimation of the natural geogenic contributions by incorporating elements like the influence of mineralization and diffused anthropogenic impact (Barbieri, 2016; Klinčić et al., 2021). Natural conditions are indicated by an enrichment factor (EF) of less than 2, while anthropogenic influence is suggested by an EF of more than 2. (Kelepertzis et al., 2019). In the soils from the studied areas, Enrichment Factor (EF) was determined three times for three different reference elements, including Al,

Fe, and Mn, for 8 metal(oid)s. The results of EF which had Mn as reference element shown the highest values in all cases, but without significant difference from the others. The values were less than 2 for all examined elements for each EF, showing that natural sources control their concentration levels (Table 4.8; Appendix III). The EFs which had Mn as the reference element had the highest average values than the other 2 and were followed by Fe and Al. Mitsero had solely natural factors as a major source of these elements.

Principal Component Analysis (PCA) was used to group the metal(loid)s in the soil data set (Appendix IV). According to the rotated component matrix (reference to figure of X Appendix), the cumulative explained variance of the cumulative explained variance of PC1, PC2, PC3 accounted for 28.3%, 18.4%, and 17.4% respectively, of the total variance. The outcome of PCA added confidence to the EFs' interpretations. Particularly, the presence of elements such as As, Fe, S, and Cu in the PC1, reflects the ore's constituents. These elements showed negative loadings, whereas Mg and Mn had positive loading in the first factor. Probably, PC1 shows a close relation of the mineralization (Appendix IV). Al, Cr, and Ni were found in PC2 and show that ophiolitic parent rocks affect the soil composition and the geogenic source has enriched soils with these elements. Moreover Pb, S, Zn and Cu constitute the third factor and might probably relate to minor minerals of the mineralisation such as sphalerite and galena.

4.1.5 Oral Bioaccessibility and Human Health Risk Assessment

The Relative Percent Difference of the bioaccessible concentrations appears in Table 4.4, where all difference values are lower than the acceptable value of 20% and all blank samples were lower than the instrument detection limit. In this method, CRMs 2709a and 2710 were inducted. The bioaccessible concentrations of PTEs in CRMs were recorded: Zn=61 mg/Kg; Ni=14.7 mg/Kg; Cu=6. mg/Kg; Mn=179.2 mg/Kg; Cr=15.9 mg/Kg; Fe=876.7 mg/Kg for CRM2709a and Zn=971 mg/Kg; Ni=2.2 mg/Kg; Cu=973 mg/Kg; Mn=1112 mg/Kg; Cr=16.1 mg/Kg; Fe=807 mg/Kg) for CRM2710.

Table 4.4 Relative Percent Difference (RPD) of soil sample for bioaccessible concentration.

RPD/Elements	Zn SBET	Ni SBET	Cu SBET	Mn SBET	Cr SBET	Fe SBET
--------------	---------	---------	---------	---------	---------	---------

MSS03	3.579098	4.081633	11.42492	2.813599	14.86129	15.92697
MSS09	11.956	2.666667	5.159959	8.668489	17.67016	4.06793
MSS13	2.511301	0	1.813565	4.495747	0.681818	4.135253
MSS17	9.23361	3.773585	10.06036	9.584188	7.048872	12.97663
MSS21	1.877112	0	8.773315	17.30104	3.290917	3.93141
MSS25	2.511301	10.16949	3.291639	0.21645	9.969143	8.164132
MSS29	2.048341	2.197802	4.677268	6.879607	8.214356	5.339199
MSS33	0	0	0	2.375514	7.917466	2.588311
MSS37	4.332756	2.247191	0.378587	0.862689	8.152174	2.5228
CRM 2709a	3.27869	3.41297	1.65289	1.11607	1.88088	1.28900

Across the 23 soil samples from Mitsero, oral bioaccessibility percentages based on the SBET extraction were calculated for six elements (Zn, Cr, Ni, Mn, Cu, and Fe). Median of elements bioaccessible percentages which break down from gastric fluids for soils was found to be 59.1%, 35.8%, 31.14%, 23.4%, 10.9%, and 0.64%, respectively (Figure 4.5). The highest median percentage of bioaccessibility was observed for Zn (59.1 %), and the lowest for Fe (0.64%) where their property as nutrients show that risk does not exist (Figure 4.5). Chromium and Ni had almost the same median percentage around 35% (mean 50%), indicating that these elements are hosted by equally reactive phases in the stomach solution and may in high concentrations cause a health issue at the children under of 2 years of age. These properly originated from secondary minerals such as clays and zeolites (cowlesite and notronite; XRD patterns) which absorb trace elements in their structure. Compared to the pseudototal (aqua regia extracted), bioaccessible concentrations as estimated by SBET, are high only for Zn. Iron had the highest pseudototal concentrations followed by Mn, however, the bioaccessible concentrations were low (Figure 4.4). Ni and Cr had the lowest aqua-regia extracted concentrations and bioaccessible concentrations.

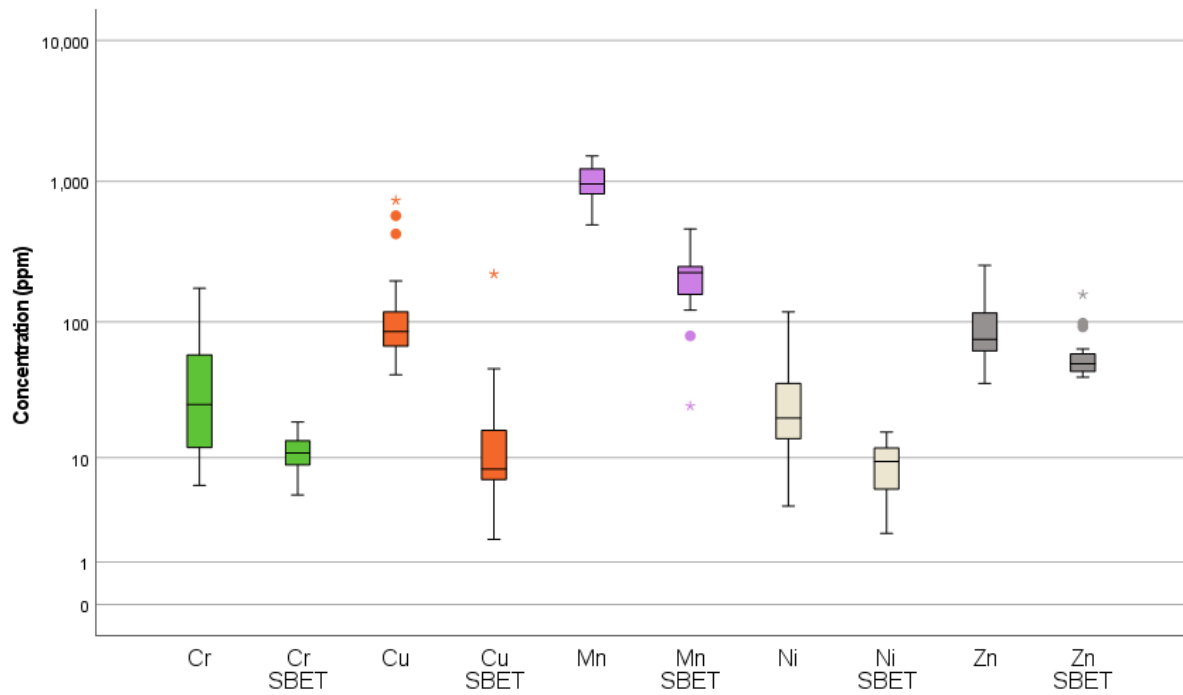


Figure 4.4. Comparison of aqua regia concentration and SBET extracted concentration in soil for 5 elements.

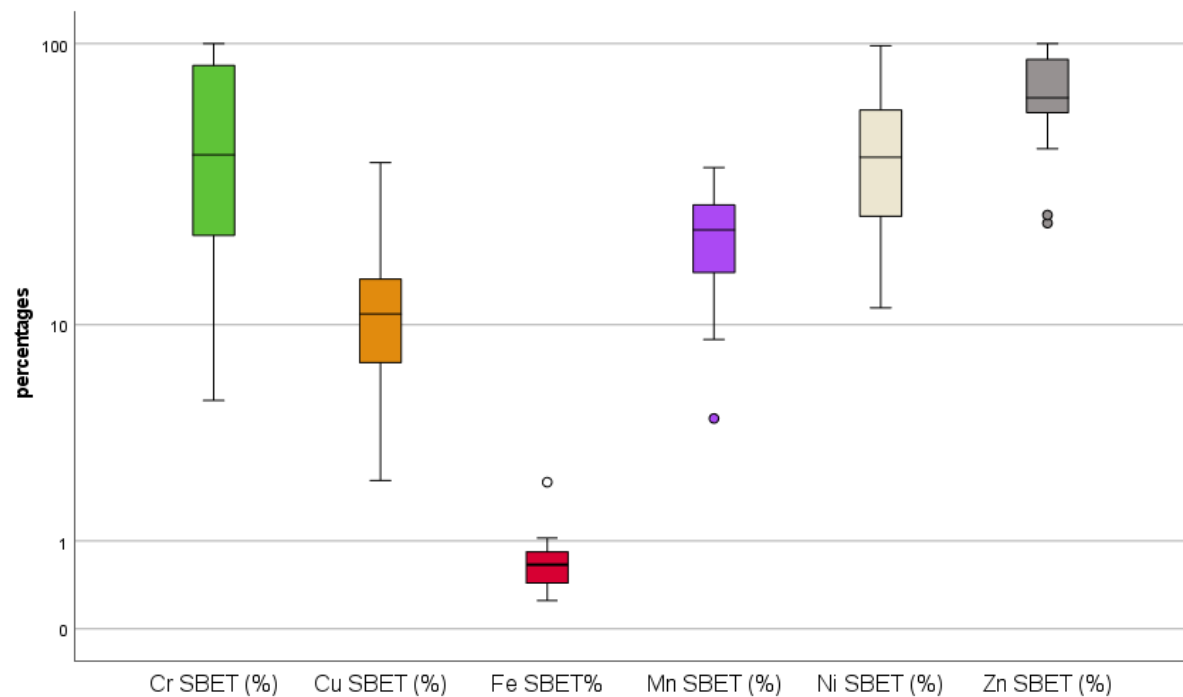


Figure 4.5. Percentages of oral bioaccessibility in soil for 6 elements.

Hazard quotient (HQ) values of the PTEs were calculated for dermal contact, inhalation, and ingestion exposure for the children 2 years of age, based on the pseudototal contents. The highest non-carcinogenic risk was calculated for Mn, followed by Cu > Zn > Cr >

Ni > Pb > As (Table 4.3) and HQ results were below the recommended level (1) (Cao et al., 2020; Isley et al., 2022). On the other hand, the upper limit of negligible risk (1×10^{-6} ; 1 case per every 1 000 000 people), and the level of unacceptable risk (1×10^{-4} ; 1 case per every 10 000 people) can be used to define the carcinogenic target risk (TR) (Isley et al 2022). Carcinogenic risk has the highest value for ingestion pathway and then for dermal. In addition, As showed negligible risk for ingestion pathway, while Cr and Ni appeared to have unacceptable target risk in ingestion pathway and negligible risk in dermal (Table 4.3). Moreover, according to Isley et al., 2022 Cr may shift between its trivalent (CrIII) and hexavalent form (CrVI). In order to prevent overrepresentation of the total Cr health risk, a conservative ratio of 0.25:1 CrVI: total Cr was adopted (Isley et al., 2022) and imputed for RfC, DRfD, OSF, and DSF values.

Table 4.5 Results of HQ and TR health risk expose calculations for under 2 years old children for 7 elements in Soil via ingestion, inhalation and dermal exposure.

Mitsero Soils						
Elements	Non carcinogenic hazard quotient (HQ)			Carcinogenic target risk (TR)		
	Ingestion	Inhalation	Dermal	Ingestion	Inhalation	Dermal
Cr	6.214E-05	8.08723E-07	5.979E-06	1.71E-04	2.14E-07	1.64E-06
Mn	0.0014108	1.83598E-05	0.0001357			
Ni	3.903E-05	5.07885E-07	3.755E-06	0.00013	2.91E-09	7.52E-06
Cu	0.0002208	2.87307E-06	2.124E-05			
Zn	0.0001405	1.83E-06	1.352E-05			
As	9.97E-06	1.29752E-07	9.592E-07	8.8E-06	3.3E-10	8.57E-07
Pb	1.111E-05	1.45E-07	1.069E-06	4.29E-08	7.89E-13	1.02E-07

4.2 House Dust

4.2.1 Mineralogy and natural properties of house dust samples

The XRD patterns were evaluated and the minerals which have been identified for the examined regions are Quartz, Calcite and Dolomite, except for Mitsero where the Nontronite clay mineral was identified (Appendix IIV). These minerals are probably originating from the outdoor environment. The lithology and the soil of each region play important role to the

presence of these minerals in house dust. Limassol lithologies include marine carbonates of the Pakhna and Lefkara formations, as well as younger carbonate-rich alluvium-colluvium. In addition, in Nicosia area, there are carbonate-rich lithologies that were deposited in shallow marine environments, alluvium and calcarenite and siliciclastic rocks of Apalos and Nicosia formations. Lastly, the geology at Mitsero is characterised by carbonate rock of the Pakhna formation in the north part of the village which are overlying the upper pillow lavas.

The pH was measured for 7 samples which had enough amount of dust for the application of the method, however, all samples were from Limassol area. The levels range from 6.7 to 13.05 and the household dusts were alkaline with average value 9.63.

4.2.2 Magnetic Susceptibility of house dust samples

Mean and median magnetic susceptibility values in house dust for each study area are presented in Table 4.4. The descriptive statistics of magnetic susceptibility (MS) data of the dust samples are shown in Table 4.5. The χ_{lf} values range from $0.91 \cdot 10^{-6} \text{ m}^3/\text{kg}$ to $7.6 \cdot 10^{-6} \text{ m}^3/\text{kg}$ with a median of $2.6 \cdot 10^{-6} \text{ m}^3/\text{kg}$ which show that ferrimagnetic grains are low in the household dust of Cyprus compared to values measured in soils. Moreover, all $\chi_{fd}\%$ values are lower than 2% and the median $\chi_{fd}\%$ value is 0.7 indicating the absence of viscous superparamagnetic grains. The data show significant correlations with the contents of Fe, Mn, Ni and Zn in Cyprus house dust (Appendix V). According to the literature, Fe is associated with magnetic particles that are identified in samples (Jordanova et al., 2012; Petrovsky et al., 2000; Yang et al 2017). Mn and Ni are related to natural sources (Isley et al., 2022; Klinčić et al., 2021), while Zn is attributed to vehicle activities (Gonzalez et al., 2016). Based on this observation, enhanced χ in the samples can be linked to either natural or anthropogenic causes. Furthermore, based on collected data values of χ_{lf} have a wider range and maximum values in older houses (Figure 4.6).

Table 4.4 Mean and median magnetic susceptibility values ($10^{-6} \text{ m}^3/\text{kg}$) in house dust for each region.

Magnetic Susceptibility (χ_{lf})	Limassol	Mitsero	Nicosia
Median	2.41	2.66	2.79
Mean	2.58	3.06	2.74

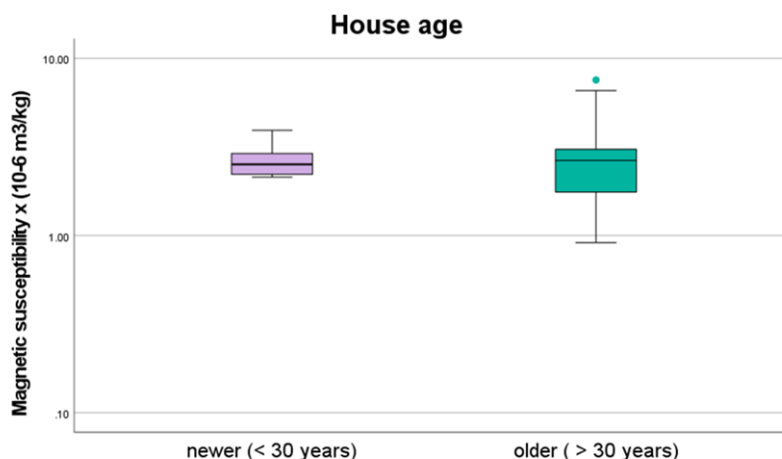


Figure 4.6. Boxplot comparison of χ between old and new houses.

The values of MS (xlf) for the 3 regions, Mitsero, Nicosia, and Limassol are presented as boxplots in Figure 4.7. The Nicosia had the highest xlf median value, followed by Mitsero and Limassol. Limassol was expected to have a higher xlf median value from Mitsero, but Mitsero as an abandoned copper-mine area showed higher values, probably due to the presence of pillow lava (likewise soil xlf in Mitsero). The correlation of the mean xlf value with population size, which had been observed by Jordanova et al (2014), might also hold in this study only between Limassol and Nicosia. Nicosia which has the highest population size exceeds Limassol, but the Mitsero village showed the highest mean xlf value recorded at $3.06 \cdot 10^{-6} \text{ m}^3/\text{kg}$ (Table 4.4).

Table 4.5 Descriptive statistics of magnetic susceptibility measurements in Cyprus house dust samples.

Magnetic Susceptibility	No samples	Mean	StDev	Median	Minimum	Maximum
xlf ($10^{-6} \text{ m}^3/\text{kg}$)	29	2.75	1.4	2.6	0.91	7.6
xhf ($10^{-6} \text{ m}^3/\text{kg}$)	29	2.73	1.4	2.6	0.91	7.5
xfd ($10^{-8} \text{ m}^3/\text{kg}$)	29	2.33	1.37	1.98	0.07	5.22
xfd%	29	0.9	0.48	0.7	0.09	1.81

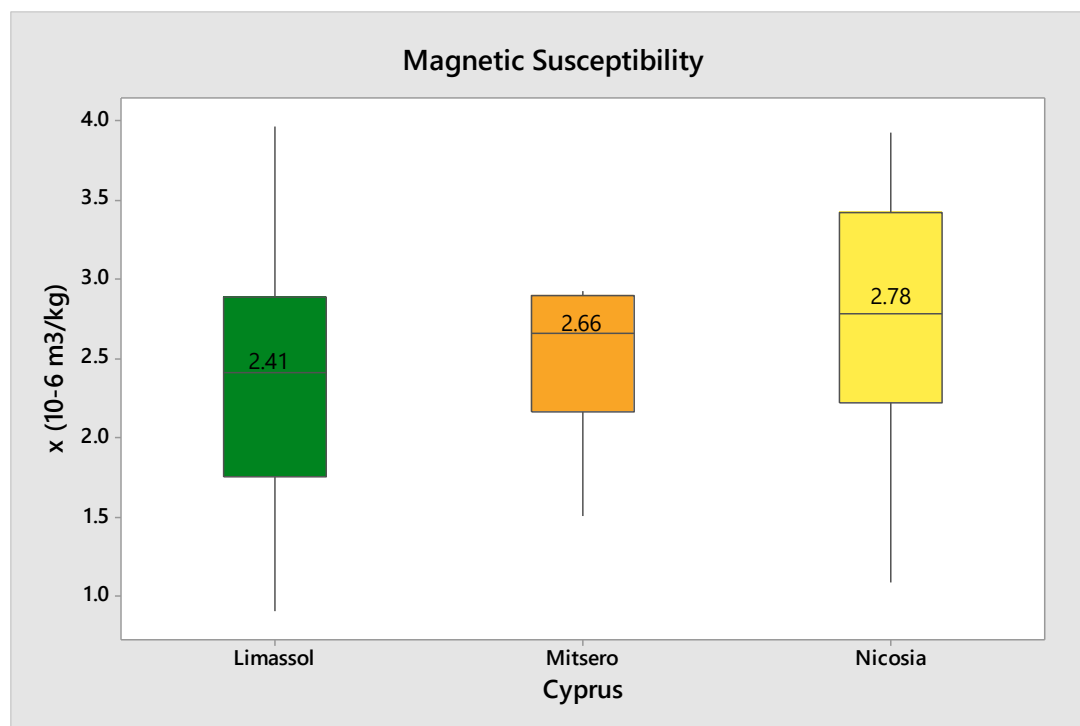


Figure 4.7. Box plots of χ values of household dust of Mitsero, Nicosia and Limassol.

4.2.3 Total elemental content in house dust samples

The statistical summary of the measured content of elements by XRF in dust samples is presented in Table 4.6.2 and the quality control was carried out with the recovery values of SRMs, which are appeared in Table 4.6.1. The order of decreasing medians of all studied elements in Cyprus house dust is Zn > Mn > Cr > Cu > Ni > Pb > As. The data are presented as box plots in Figure 4.8. Nicosia samples presented higher median values than Limassol and Mitsero for all studied elements, except Cr and Pb which had higher median values in Limassol (Table 4.6). Pearson correlation coefficient was calculated based on the log-transformed data for household dust for each different region (Appendix V).

Table 4.6.1 % recovery for standard reference materials

SRM/Elements	As	Cr	Cu	Mn	Ni	Pb	Zn
(Recovery%) BGS102	107	101.6	100.3	95.4	107.1	93.2	98.4
(Recovery%) BCR143R	-	-	94.2	115.9	83.5	104.5	100.1

Fe and Mn had a significant correlation with trace elements (Appendix V), indicating that Mn and Fe-oxides are major PTEs hosts. Furthermore, the separation of elements which have a correlation with Ni into 3 groups (Cr; As-Cu; Cu-Zn), provides 3 different origin sources. However, Pb is not associated with Ni and As with Zn. This fact divides the elements into clusters, including Pb-As-Cu, Pb-Zn-Cu, and As-Cu-Ni. The correlation test for Limassol area showed 2 groups, As-Pb and Cr-Cu-Fe-Mn-Ni-Zn. In Nicosia house dust the association of Zn-Cu, As-Cr and Mn-Fe, is observed while Pb and Ni had no correlation with the other elements. In addition, Mitsero samples displayed 4 groups of elements, and they include Cu-As, Pb-As, Pb-Mn, and Zn-Fe-Mn. Subsequently, statistically significant differences (ANOVA on log-transformed data, $p < 0.05$; Table 4.7) were observed only for Cr and Ni between Nicosia and Mitsero, and Mn and Fe between Nicosia and Limassol. However, the mining legacy of Mitsero was not evident based on the dust data of present research.

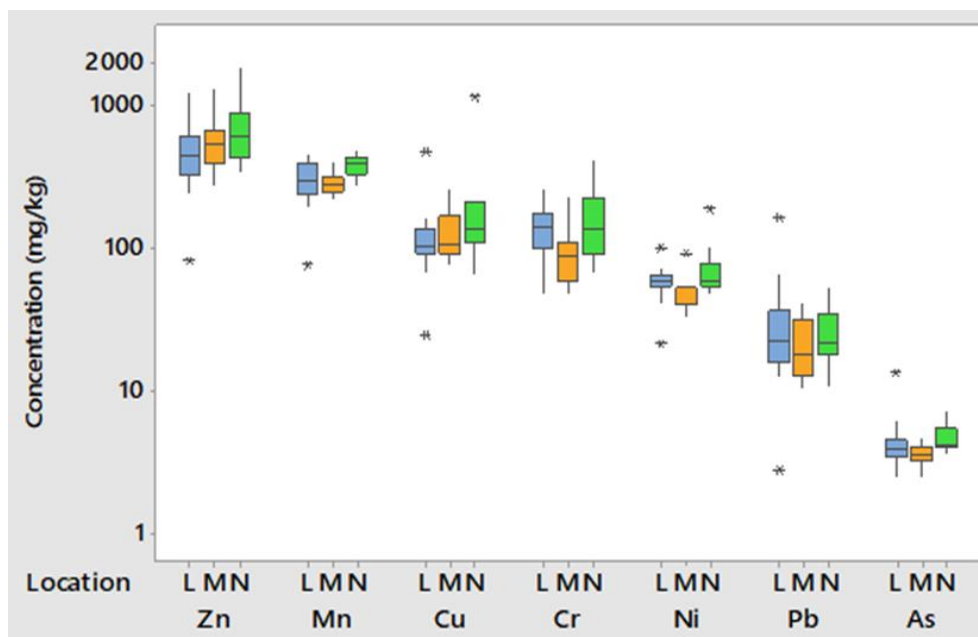


Figure 4.9. Box plots of total content of elements in house dust samples from Limassol (L), Mitsero (M) and Nicosia (N).

Table 4.6.2 Basic statistical summary for Cyprus dust data.

Descriptive statistics							
Cyprus dust							
Data	N	Units	Median	Min	Max	Mean	St. Dev
As	38	mg/Kg	4	2.5	13.3	4.3	1.8
Cr	38	mg/Kg	119.5	47.3	415	138.5	75
Cu	38	mg/Kg	113.6	24.5	1151	157	180.6
Fe	38	mg/Kg	14750.4	3000.5	37160	15642	5604
Mn	38	mg/Kg	302.4	75.4	488	315.6	86.1
Ni	38	mg/Kg	56.9	21.3	187	60	26.7
Pb	38	mg/Kg	21	2.7	162.3	28.8	26.4
Zn	38	mg/Kg	515.7	81.2	1821	579	324.3
pH	7	-	8.6	6.7	13.1	9.6	2.3
Mitsero							
Data	N	Units	Median	Min	Max	Mean	St. Dev
As	9	mg/Kg	3.5	2.45	4.7	3.5	0.65
Cr	9	mg/Kg	88	48.2	227	96.7	54.2
Cu	9	mg/Kg	105.3	76.8	255	131.4	56.6
Fe	9	mg/Kg	12900	10174.2	18817	13512	2832
Mn	9	mg/Kg	279.3	223	398	286.1	51.9
Ni	9	mg/Kg	41	32.5	90.6	47.6	17.4
Pb	9	mg/Kg	18	10.42	40.76	22	11.4
Zn	9	mg/Kg	540.5	270	1287	589	298
pH							
Limassol							
Data	N	Units	Median	Min	Max	Mean	St. Dev
As	19	mg/Kg	3.9	2.5	13.3	4.4	2.3
Cr	19	mg/Kg	140.5	47.3	264	139	52
Cu	19	mg/Kg	103	24.5	474	1265	90
Fe	19	mg/Kg	14530	3000	22825	14380	4397
Mn	19	mg/Kg	299	75.4	460	295	92
Ni	19	mg/Kg	58	21.3	100.1	58	15.6
Pb	19	mg/Kg	22	2.8	162	33.3	35.3
Zn	19	mg/Kg	449	81.2	1224	490	234
pH	7		8.6	6.7	13.1	9.6	2.3
Nicosia							
Data	N	Units	Median	Min	Max	Mean	St. Dev
As	10	mg/Kg	4	3.6	7.1	4.6	1.15
Cr	10	mg/Kg	134.7	65.6	415	172	115
Cu	10	mg/Kg	123.1	64.3	215	138	49.4
Fe	10	mg/Kg	18653	12031	25369	18045	4521
Mn	10	mg/Kg	378	273	458	369	61.3
Ni	10	mg/Kg	58.3	47.8	187	72.3	43.3
Pb	10	mg/Kg	20.8	10.6	52.3	25.8	13.7
Zn	10	mg/Kg	522	347	1090	618	248
pH							

4.2.4 Enrichment Factor

The EFs were calculated against the regional baseline (mean Cyprus soils' values; Cohen et al 2012) in order to evaluate the overall impact of anthropogenic activities on the urban indoor environment. As reference element for the determination of EF, Mn had been used. Cr, Ni, Cu, Pb and Zn returned EF > 2 in all study areas, while As, displayed EF>2 only for Mitsero dust data (Table 4.8). Overall, enrichment of Zn was the greatest, followed by Pb > Cu > Cr > Ni > As > Fe. Regional variations were present, with the greatest enrichment of Zn (EF= 18.7, 25.6, and 19.5) in Limassol, Mitsero and Nicosia, respectively and the lowest enrichment of Fe, as physical source enrichment element.

Table 4.7. Enrichment factor averages for eight trace elements of Mitsero Soils and Cyprus dust. RE is the reference element that was used for calculating the enrichment factor.

Enrichment Factor Average (CPI)					
Elements	Mitsero Soil	Cyprus Dust	Nicosia Dust	Limassol Dust	Mitsero Dust
As	0.69	2.03	1.39	1.9	3
Cr	0.45	7.4	7.8	4.6	13
Cu	1.02	5.97	7.9	5.2	5.2
Ni	0.19	3.98	3.6	2.1	8.33
Mn	0.73	RE	RE	RE	RE
Zn	0.96	20.59	19.5	18.7	25.6
Pb	0.42	7.89	5.9	7.05	11.8
Fe	RE	1.08	1.17	1.1	0.9

4.2.4 Metadata Analysis

Participants from Cyprus submitted metadata that offered insights into the significance of housing attributes and their correlation with higher dust trace-metal concentrations. Home age is a strong predictor of indoor dust concentrations of As, Cu, Mn, Ni, Pb, and Zn globally (Taylor et al., 2020). According to statistics, equations were found between house age and the concentration of significantly correlated studied elements. These equations allow the calculation of the concentration of each element based on house age, where x is the age of the house and y is the concentration of elements (Appendix VI). The annual increase was determined by subtracting the concentration of the PTEs for one year of house age from the concentration for two years of house age. The results showed that houses

in Cyprus have had a yearly increase in 0.43 mg/kg As, 0.43 mg/kg Pb, 1.1 mg/kg Cu, and 2.28 mg/kg Zn in dust), but a decrease in Mn, Ni, Cr, and Fe. There were higher levels of As and Pb in homes with access to a garden, and when the paint on the interior and/or exterior was peeling (Appendix VI), but there was not significant difference between them (Table 4.8). Recently renovated homes had somewhat lower Ni levels (Appendix VI, Figure 12), but they had significantly different Mn, Fe, and Pb (Table 4.8). The dwellings near main roads had the highest Ni levels, due to vehicle emissions that are one possible source of Ni that could undermine this finding (Doyi et al., 2019).

Table 4.8. Metadata statistics between home characteristics.

Characteristic	p value for presence versus absence of characteristic or for increase							
Elements	As	Cr	Cu	Fe	Mn	Ni	Pb	Zn
Pet	0.876	0.052	0.691	0.694	0.727	0.382	0.75	0.257
Garden	0.376	0.973	0.414	0.431	0.193	0.609	0.981	0.582
Smoking	0.615	0.511	0.43	0.694	0.851	0.69	0.367	0.7
Exterior peeling paint	0.617	0.88	0.878	0.379	0.438	0.727	0.124	0.713
Interior peeling paint	0.717	0.8	0.909	0.6	0.71	0.518	0.094	0.814
Renovation	0.309	0.95	0.353	0.031	0.01	0.208	0.037	0.169
Shoes	0.8	0.71	0.633	0.744	0.8	0.903	0.94	0.789
Industry	0.25	0.2	0.8	0.68	0.87	0.1	0.347	0.63
Main road	0.984	0.36	0.22	0.39	0.33	0.33	0.948	0.206
Humidity	0.13	0.27	0.27	0.99	0.99	0.44	0.612	0.33
Heating fuel	0.722	0.49	0.65	0.91	0.82	0.33	0.62	0.84
Construction	0.068	0.004	0.033	<0.001	<0.001	0.025	0.007	0.098
House type	0.82	0.9	0.49	0.57	0.46	0.46	0.65	0.31
floor type	0.13	0.68	0.79	0.81	0.69	0.95	0.53	0.63
Hobbies	0.275	0.063	0.078	0.005	0.005	0.022	0.196	0.129
Increasing age of house	0.0003	0.94	<0.001	0.08	0.149	0.85	<0.001	0.015
Region	0.164	0.047	0.085	0.042	0.038	0.029	0.767	0.137

Residences close to industrial areas exhibited greater Zn concentrations than other homes, but interestingly, these differences were not statistically significant ($p > 0.05$; Appendix VI, Figure 10). Homes with interior paint that was flaking also had greater quantities of arsenic and lead. As levels were higher in detached homes and the houses with access to gardens (Appendix VI, Figure 15), most likely as a result of outdoor legacy trace-metal

infiltration, which frequently includes inputs from treated woods (Taylor et al., 2021). As with all residences (Table 4.7), the age of the home has a substantial ($p < 0.001$) impact on the lead concentration, with detached homes' Pb concentration rising by 0.43 mg/ kg every year of age (Appendix VI, Figure 16), and also according to literature and boxplots (Appendix VI) lead origin probably came from the past use of exterior Pb paints and leaded gasoline (Taylor et al., 2021). High Mn, Fe, Cr, and Ni concentrations were found in semi-detached residences and apartments, likely as a result of soil track-in (Hunt et al., 2012). House which owner use shoes inside showed higher concentrations for elements, expect for Cr and Ni. Surprisingly, however, the concentration differences between dwellings with and without garden access were not statistically significant ($p > 0.05$), however, Mn, Fe, Cu, Zn and As showed higher ranges when a garden was present.

The amounts of Mn, Fe, Cr, Cu, Ni, and Zn in detached homes were not significantly higher, indicating that indoor sources may be more important for these trace-elements than the type of dwelling. There are no notable differences in the heating method. The usage of gas, oil and wood for heating appeared to have high Ni, As and Pb concentrations in indoor dust, respectively (Appendix VI). Regarding the construction materials, houses built with metal contain significantly higher contents of Cr and Fe (Table 4.7) and higher concentrations of As and Zn. Mn, Ni, Cu, and Pb were related to brick-built homes. Higher concentrations of Mn, Fe, and Ni were found in metalworkers (Appendix VI, Figure 1), possibly because Mn and Fe are steel additives (Kaar et al., 2018) and Ni is a common component of paint, stainless steels (Isley et al., 2022; Klinčić et al., 2021) and products from wood treatments (Cao et al., 2020; Isley et al., 2022). Cr, Mn, Fe and Ni associated with region (table 4.7). Chromium and Nickel had statistically difference (0.042 and 0.024 respectively) between Nicosia and Mitsero, and Iron and Mn (0.045 and 0.035 respectively) between Limassol and Nicosia. Mn and Fe are associated with construction, renovation, and metalworkers in occasion of Limassol than Nicosia, which associated with smoking for Fe and home age about Mn. In Mitsero, Cr concentrations were consorted with metal homes and carpet floor (statistically difference 0.017 only for Cr), but in Nicosia, expect for metal homes ($p=0.045$), indoor anthropogenic activities sources are main provision of these elements, such smoking ($p=0.44$). Ni are not observed statistically difference with any examined house information.

4.2.5 Principal Component Analysis of household dust.

According to PCA results, there are three major components. Three factors, "Pb-As," "Zn-Cu," and "Mn-Fe-Cr-Ni" (Appendix VII), were discovered to run consistently throughout the combined Cyprus data set (Appendix VII, Figure 1). The precise ratio of these elements' elemental combinations varied by region (Appendix VII). This method captures a variety of distinct emission sources in household dust so it cannot determine the fixed and defined emission sources in Cyprus dust (Isley et al., 2022).

The first factor includes Pb which is a known historical pollutant that frequently shows a tendency of concentration increasing with housing age (Kelepertzis et al., 2020; Rasmussen et al., 2013) and As. Lead and As contents are greatly enriched relative to soil values and this is appears to table 4.7. Residential soils tracked indoors, plastic, metals, industries influence, and tobacco have been linked to indoor dust Pb and As (Cao et al., 2020; Isley et al., 2022). In this study table 4.8 shows that Pb and As concentrations rose as a function of home age, brick-type, and re-modelling (for As). Older homes continue to pose a risk for elevated levels of trace elements (table 4.8; for Pb, As, Cu, and Zn) in indoor dust because they may still contain Pb-based paints.

The probable source of elements in the second factor according to Kennedy et al. (2018) includes building materials used in urban areas, such as paints, metal coatings, wood preservatives, and galvanized surfaces that contain Cu and Zn (Cao et al., 2020; Isley et al., 2022; Kennedy et al. 2018). Copper and Zn enrichment compared with crustal values have an anthropogenic source (Appendix VII) (Taylor et al., 2021; Isley et al., 2022). However, no correlation between home construction materials and Zn was found, while Cu was significantly lower in cement-brick homes, and data showed an increased Zn concentration with increasing property age (Appendix II, Figure 16), also indicating contribution from building material degradation (table 4.7). Cu and Zn concentrations have been found to be higher in metropolitan environments in Europe where there has been braking activity, such as tire and brake wear (Gonzalez et al., 2016).

The third factor of PCA (Appendix VII) consist of Mn-Fe-Cr-Ni. These elements are often linked to a natural soil source (Isley et al., 2022). This is supported by Mn-Fe-Cr-Ni concentrations depend on region and the low Enrichment Factor for Fe (Table 4.8), where the

potential for track-in is higher. Manganese is the eighth most abundant crustal metal (Morgan, 2000) and iron as the fourth most abundant element, constituting about 4.7% of the earth's crust (Kamble et al., 2013). These elements are commonly associated with outdoor soils (Fergusson and Kim, 1991; Yoshinaga et al., 2014), particularly from dead plant biomass, and are internationally associated with wildfire activity, sea spray, volcanic activity, and animal wastes (Isley et al., 2022). Dingle et al. (2021) suggests that high contents at the house entrances indicates the transport of outdoor soil through foot traffic and deposition of these PTEs at entranceway. On the contrary, Mn-Ni-Fe has been linked to industrial sources (Cohen et al., 2016), steel mills, ore processing and welding, and potentially fuel additives (Cohen et al., 2005), which have been found in contributing Mn-Ni-Fe inputs to the environment. The origin of Cr, Mn, Fe, and Ni in Cyprus soil has been attributed to natural sources, namely, ultramafic rock (Cohen et al., 2012; Zissimos et al., 2018; Zissimos et al., 2020). Additionally, house renovation and industrial sources also contributing, including timber treatments, construction materials and carpet dyes that associate with metalworkers (Appendix VI)

4.2.6 Human Health Risk Assessment and Oral Bioaccessibility

In Cyprus, Cr presented the highest noncarcinogenic risk, followed by Mn > As > Cu > Pb > Ni > Zn (table 4.9). The HI values for each metal(loid) through dermal contact, inhalation, and ingestion exposure for the children are shown in Table 4.9. The HI readings were mostly below the recommended level (1) (Cao et al., 2020; Isley et al., 2022). Additionally, the ingestion exposure pathway carried the highest non-carcinogenic health risk, with a mean cumulative risk estimate of 0.16 from all trace-metals evaluated across all locations evaluated. Inhalation and dermal exposure pathways came in second and third, with mean cumulative risk values of 0.011 and 0.006, respectively (table 4.9). This indicates that exposure to household dust containing heavy metals have non-carcinogenic health impacts on children living in urban and abandoned copper mining areas in Cyprus. There were differences in ranking between pollution levels and health risks of different heavy metals (loids), which is explained by the fact that contamination levels, toxicity of the contaminants, and exposure behaviour patterns are all thought to contribute to the potentially harmful health risks (Cao et al., 2020).

Following dermal and inhalation pathways, ingestion posed the highest carcinogenic risk, with median cumulative risk of 1.4×10^{-4} , 3.40×10^{-5} , and 9.24×10^{-8} , respectively (table 4.11). The upper bound of negligible risk (1×10^{-6}) was overdrawn for all elements (Pb TR= 1.17×10^{-6} ; As TR= 9.89×10^{-6} ; Cr TR = 3.71×10^{-3} ; Ni TR = 2.67×10^{-5}) and the level of unacceptable risk (1×10^{-4}) indicated no possible exceedance in Cyprus house dust. In a comparison of different heavy metal(loid)s, the integrated HI from indoor dust exposure was mainly attributed to Cr, followed by Ni > As > Pb. The highest carcinogenic risk for ingestion (Nicosia TR= 5.66×10^{-5}), inhalation (Nicosia TR= 3.89×10^{-8}) and dermal (Nicosia TR= 1.37×10^{-5}) was found in urban areas, especially in Nicosia, while in abandoned copper mining area is observed the lowest risk for all exposures (see table 4.10). The assessment showed that the children who live in Cyprus would be exposed to the target metals through household dust, which could result in carcinogenic health hazards in case of Cr.

Table 4.9.1 Results of non-carcinogenic (HQ) and carcinogenic (TR) health risk calculations for children (< 2 years of age) exposed to trace metals in dust via ingestion, inhalation and dermal in region.

Region	Non carcinogenic hazard quotient (HQ)			Carcinogenic target risk (TR)		
	Ingestion	Inhalation	Dermal	Ingestion	Inhalation	Dermal
Limassol	0.50	0.08	0.11	4.72E-05	3.15E-08	1.15E-05
Mitsero	0.57	0.08	0.10	3.54E-05	2.20E-08	8.95E-06
Nicosia	0.40	0.08	0.12	5.66E-05	3.89E-08	1.37E-05
Median	0.50	0.08	0.11	0.000139	9.24E-08	3.40E-05
Median	0.03	0.08	1.10	0.000139	9.24E-08	3.40E-05

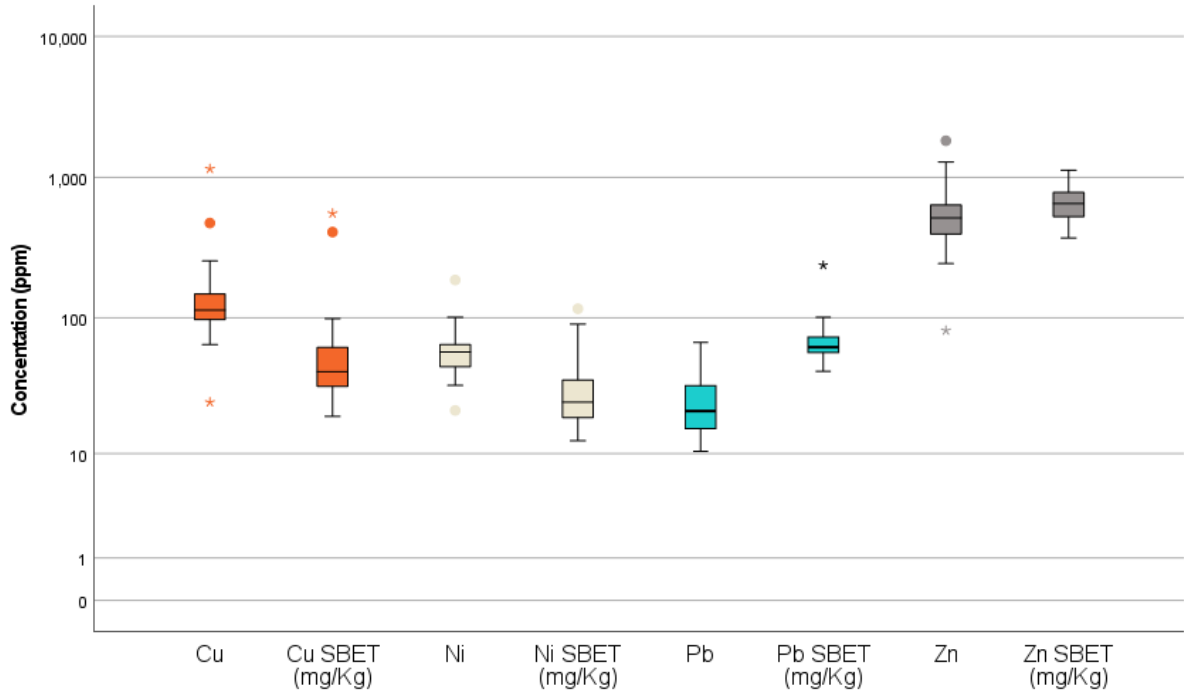
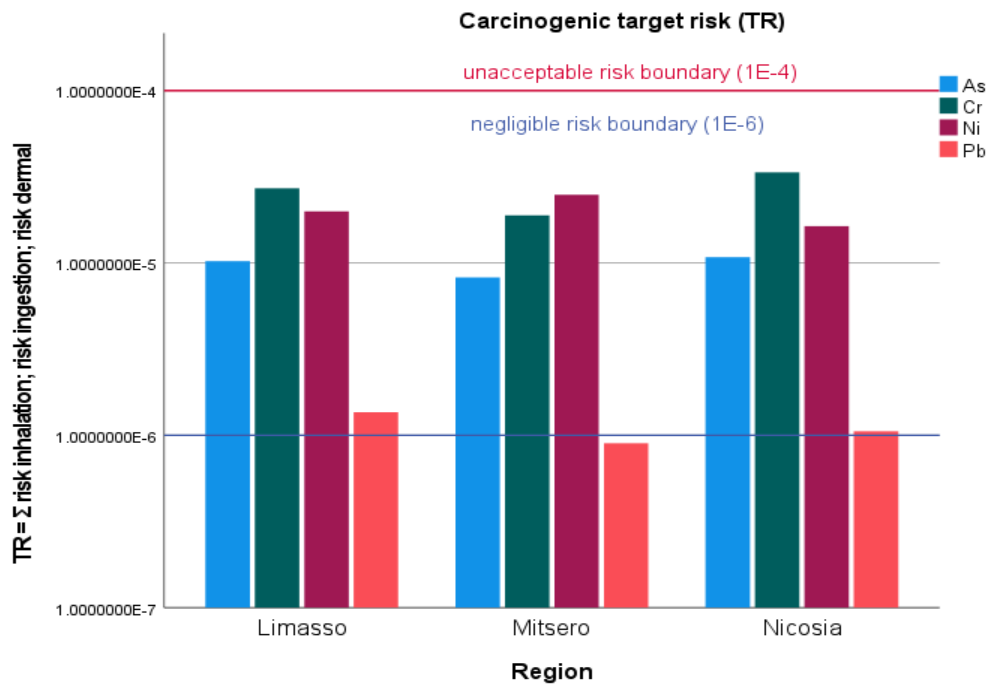


Figure 4.9 Box plot of total concentration and oral bioaccessibility (SBET) of Cyprus Dust.



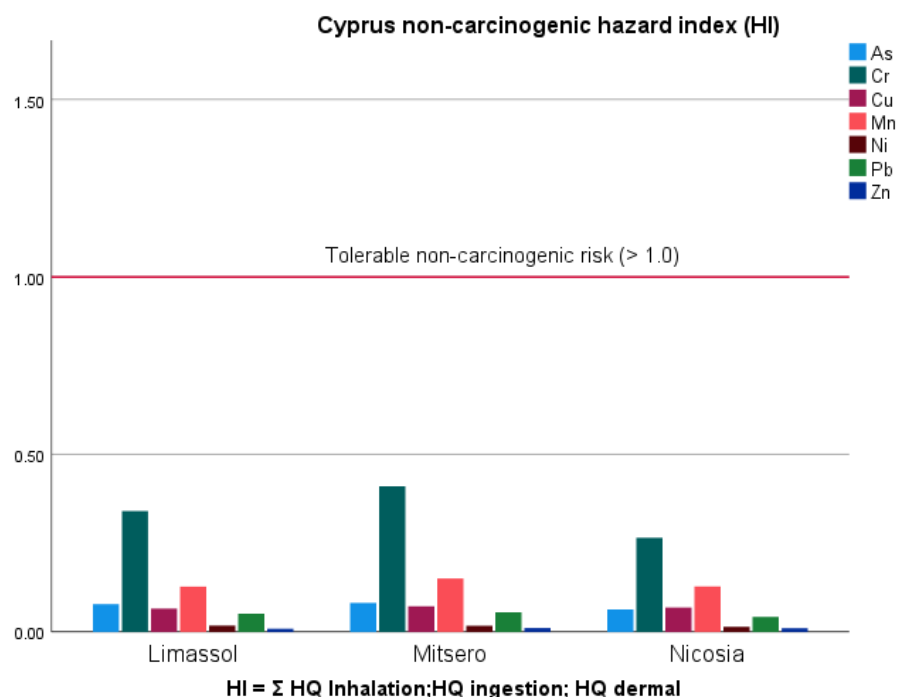


Figure 4.8 The results of Health and Risk Assessment. The figure shows the bar chart of non-carcinogenic hazard quotient and the carcinogenic target risk of Cyprus dust .

This model does not take into consideration the dangers posed by other indoor pollutants or the effects of cumulative trace metal exposure. Additionally, because we are unable to take into consideration the complexity of each person's living circumstances, such as home characteristics like the presence of gardens, pets, or renovations (Appendix II), nor specific activities that can alter exposure, the health risk assessments are estimates (Isley et al., 2022). A probable exceedance value (PEV) was generated based on the factors used in the health risk assessment for more accurately quantify risk levels and comprehend the vacuum dust concentrations at which health hazards may be posed. Tolerable risk levels for noncarcinogenic risk (>1.0) for a child (2 years) exposed to trace-metals in vacuum dust are defined as the PEV, which can subsequently be used to assess probable exceedance (Isley et al., 2022). The PEV for Zn was > 10,000 mg/kg and followed by Ni (2600 mg/kg), Cu (1800 mg/kg), Mn (1600 mg/kg), Pb (460 mg/kg) and As (50 mg/kg). They were not exceeded in any vacuum dust samples measured in this study. However, the PEVs were most exceeded only for Cr, where 5.2% of Cyprus samples and 20% of Nicosia samples were above the PEV of 290 mg/kg. No PEVs were exceeded in vacuum dust samples from Mitsero and Limassol. The PEV

calculations rely on general input parameters that might not account for possible geographical variations in trace-metals and way of life.

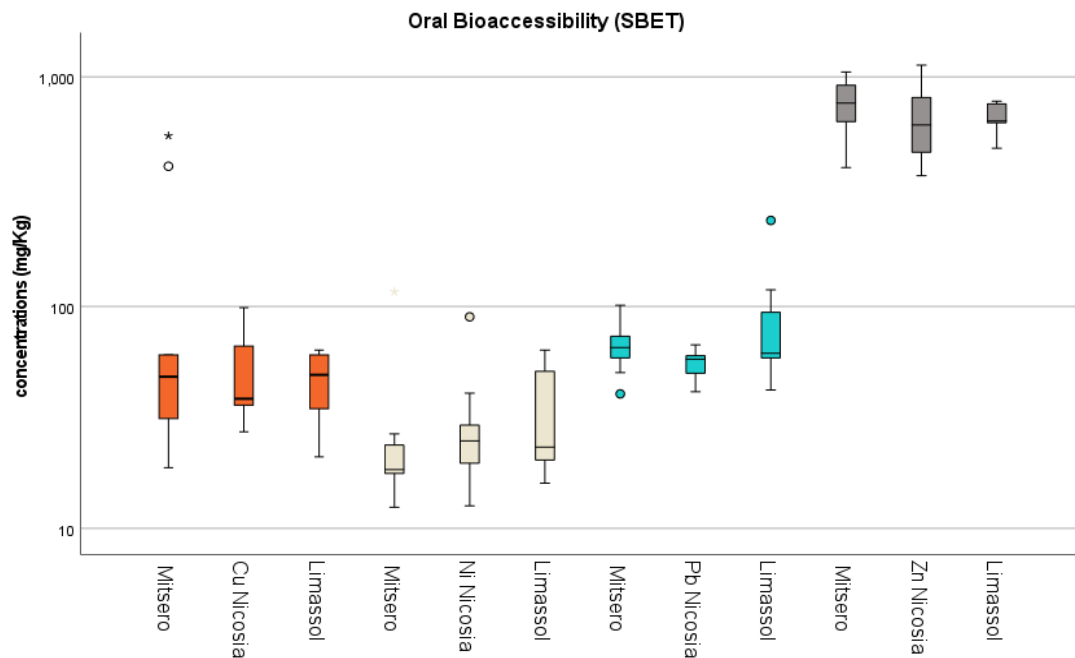


Figure 4.10 Box plot of oral bioaccessibility (SBET) of Dust in each area.

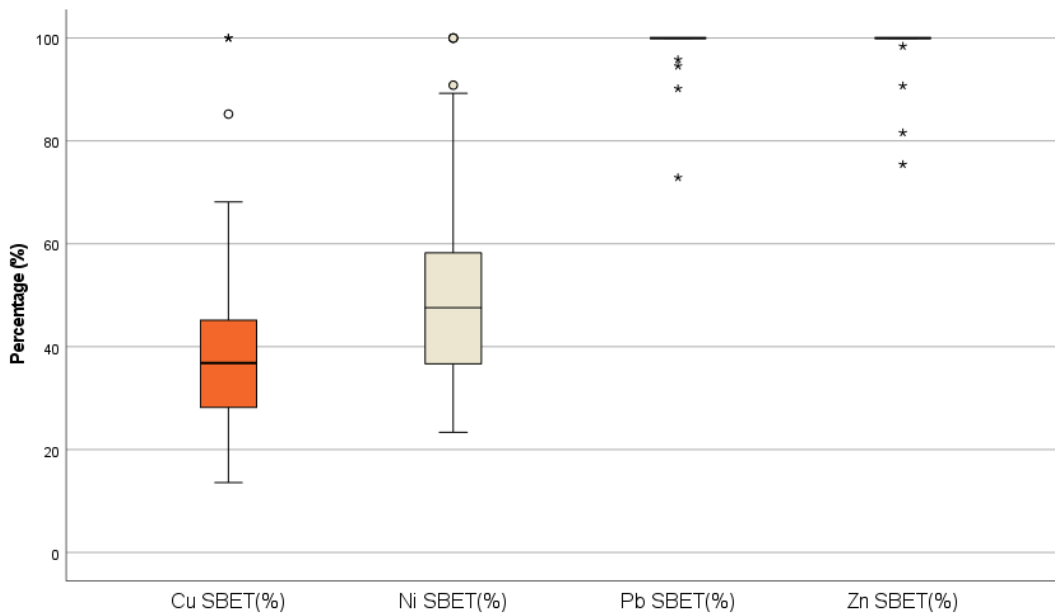


Figure 4.11. Box plots of the concentrations and the percentage of household dust oral bioaccessibility

The bioavailability and bioaccessibility of trace metal elements should also be considered in further and more thorough risk evaluations, even though all exposures to PTEs in home dust are concerning (Doyi et al., 2020). In order to establish bioaccessibility, a specific gastric digestion is carried out. It entails imitating the stomach's digestion of metals using acids, particular pH and temperature levels, and for particular lengths of time. To record precision and accuracy, duplicates were assessed, and the relative percent difference show in Table 4.9.2. All recovery values are lower than 20 %, which the acceptance boundary.

Table 4.9.2 Relative Percent Difference (RPD) for bioaccessible contents analysis in house dust

RPD%/Elements	Pb SBET	Zn SBET	Ni SBET	Cu SBET
LimDS05	0.13	4.90	6.01	7.25
LimDS11	8.73	10.48	3.62	15.61
LimDS13	3.95	11.52	7.30	6.24
LimDS14	9.47	1.27	9.16	2.65
MDS01	2.70	0.92	0.73	0.54
MDS03	1.71	3.04	11.96	0.93
MDS07	5.93	4.94	9.42	8.31
NicDS03	3.49	5.74	6.47	0.70
NicDS04	2.87	6.60	5.49	6.08

Four elements' bioaccessibility has been verified, as shown in the Figure 4.12. In Cyprus, across 33 samples from Nicosia, Limassol and Mitsero, the mean bioaccessibility percentages of Zn, Pb, Ni, and Cu in dust was found to be 98.42 %, 95.81 %, 52.38 % and 41.87 %, respectively. The largest bioaccessibility percentage in trace metal concentrations is Zn, followed by Pb > Ni > Cu. Zn and Pb had the highest percentage of dissolution in the gastric fluids (98.42 % and 95.81%, respectively) and these elements are carried into weak phases into household dust and they have immediate touch with health risks. In contrast, Ni and Cu exist in power bonds and phases, so they dissolved in a lower percentage (Ni=52.38%; Cu=41.87%) through oral bioaccessibility (Figure 4.13). Moreover, the Mitsero area are showed that the Cu and Zn concentration which break down into stomach, are highest than Limassol and Nicosia (Figure 4.8), whilst in case of Ni, Mitsero displayed the last position. Nicosia had the lowest oral bioaccessibility concentrations for all elements, except for Ni which is given the highest numbers. Lastly, Pb is provided the highest values in Limassol which this city had the highest total concentration of Pb in household dust, as well.

4.2.7 Comparison with other studies

Comparisons based on the median values which are reported to literature are showed in Figure 4.12. Compared to the global DustSafe study, Cyprus dust showed a slight enrichment in Mn, Cr, and Ni, probably attributed to geogenic origin of these elements in Cyprus. In addition, the same pattern is observed in comparison with Greek dusts. In case of Volos, an industrial city in Greece (Kelepertzis et al., 2020), Mn contents are lower than in house dust of Cyprus (Table 4.11). Subsequently, house dust in Cyprus is enriched in Cr, Cu, Ni, Pb and Zn against respective contents in Cyprus soil pseudo-total (Cohen et al., 2012), while Mn and As concentrations are prevailed in Cyprus soil than house dust (Cohen et al. 2012; Zissimos et al. 2018; Zissimos et al. 2021).

Health risk calculations for children (< 2 years of age) exposed to trace metals in dust via ingestion and inhalation in each country. Risk estimates that exceed tolerable non-carcinogenic risk (> 1.0) and the upper-bound of negligible carcinogenic target risk (> 1×10^{-6} ; 1 case per every 1,000,000 people) are shaded. Bolded values exceed the level of unacceptable carcinogenic target risk (> 1×10^{-4} ; 1 case per every 1,000 people) (source; Isley et al., 2022). Comparing, the noncarcinogenic hazard index (HI) for children (<2 years old) between the DustSafe project (Isley et al., 2022) and the present study shows that the Cyprus noncarcinogenic health risk from all elements had the lowest values for all countries, except for Cr which had the second highest value after New Caledonia.

Cr presented the highest non-carcinogenic risk worldwide, it was followed by As > Pb > Mn > Cu > Ni > Zn, whilst for Cyprus followed by Mn > As > Pb > Cu > Ni > Zn (figure 4.14). The Mn had a higher risk than As and Pb in Cyprus, while in other countries are at greater risk for As and Pb than Mn. This fact may be due to the high concentrations of Mn in household dust, in comparison with other countries (figure 4.13). Generally, non-carcinogenic health risk was greatest via the ingestion exposure pathway across all locations.

Table 4.11 Summary statistics of elemental concentrations (mg/kg) of Cyprus dusts with literature data for dust and soil.

Element	As	Cr	Cu	Mn	Ni	Pb	Zn
Mean	4.30	139	157	316	60.0	28.8	579
Standard Deviation	1.79	75.0	181	86.1	26.7	26.4	324

Median	3.97	120	114	302	56.9	21.0	516
Minimum	2.45	47.3	24.5	75.4	21.3	2.73	81.2
Maximum	13.3	415	1150	488	187	162	1820
DustSafe database median (Isley et al., 2022; n=1703)	13.3	86.0	176	257	39.0	94.0	1110
Greek house dust median (Kelepertzis et al., 20; n=35)	6.90	97.9	158	230	52.3	57.0	664
Volos (Greece) house dust median (Kelepertzis et al., 2019; n=24)	31.7	163	167	274	81.0	63.2	785
Cyprus soil mean. (Cohen et al., 2012; n=5377)	4.90	73.7	87.9	981	111	11.0	67.0
Nicosia soil median (Zissimos et al., 2018; n=441)	5.50	36.0	44.5	617	33.3	7.70	60.5
Limassol soil median (Zissimos et al., 2020; n=411)	4.50	55.4	42.5	531	52.2	8.69	49.0
Mitsero soil median (n=22)	4	25.5	85.35	960	20	6	75

Table 4.12 Summary of the cumulative non-carcinogenic and carcinogenic risk posed by the three exposure pathways assessed (ingestion, inhalation and dermal contact) for each country. The cumulative risk displayed is the sum of hazard index (HIs) for each trace metal assessed (source 1; Isley et al., 2022). Grey highlight colour shows the values which exceed the tolerable level for non-carcinogenic risk and negligible risk for carcinogenic risk. The values which exceed the unacceptable risk appear bolded.

Cumulative non-carcinogenic risk				Cumulative carcinogenic risk		
Σ HI As, Cr, Cu, Mn, Ni, Pb, Zn				Σ Risk As, Cr, Ni, Pb		
Country ¹	Ingestion	Inhalation	Dermal	Ingestion	Inhalation	Dermal
Australia ¹	4.06	0.52	1.6	2.30E-04	8.00E-07	6.60E-06
China ¹	1.15	0.08	0.56	9.50E-05	1.80E-07	1.60E-06
Croatia ¹	0.84	0.07	0.45	6.10E-05	1.30E-07	9.90E-07
Ghana ¹	0.68	0.06	0.34	4.70E-05	1.70E-07	1.10E-06
Greece ¹	0.78	0.07	0.43	6.50E-05	1.00E-07	9.90E-07
Mexico ¹	0.61	0.08	0.32	4.50E-05	4.60E-08	4.50E-07
New Caledonia ¹	2.21	0.2	1.49	3.80E-04	2.30E-07	9.80E-06
New Zealand ¹	1.97	0.12	0.87	1.70E-04	2.60E-07	1.90E-06
Nigeria ¹	0.64	0.11	0.52	4.90E-05	9.90E-08	6.50E-07
UK ¹	0.72	0.07	0.41	4.70E-05	1.50E-07	9.10E-07
USA ¹	1.47	0.12	0.71	1.30E-05	1.40E-07	2.40E-06
Cyprus	0.50	0.08	0.11	1.39E-04	9.24E-08	3.40E-05

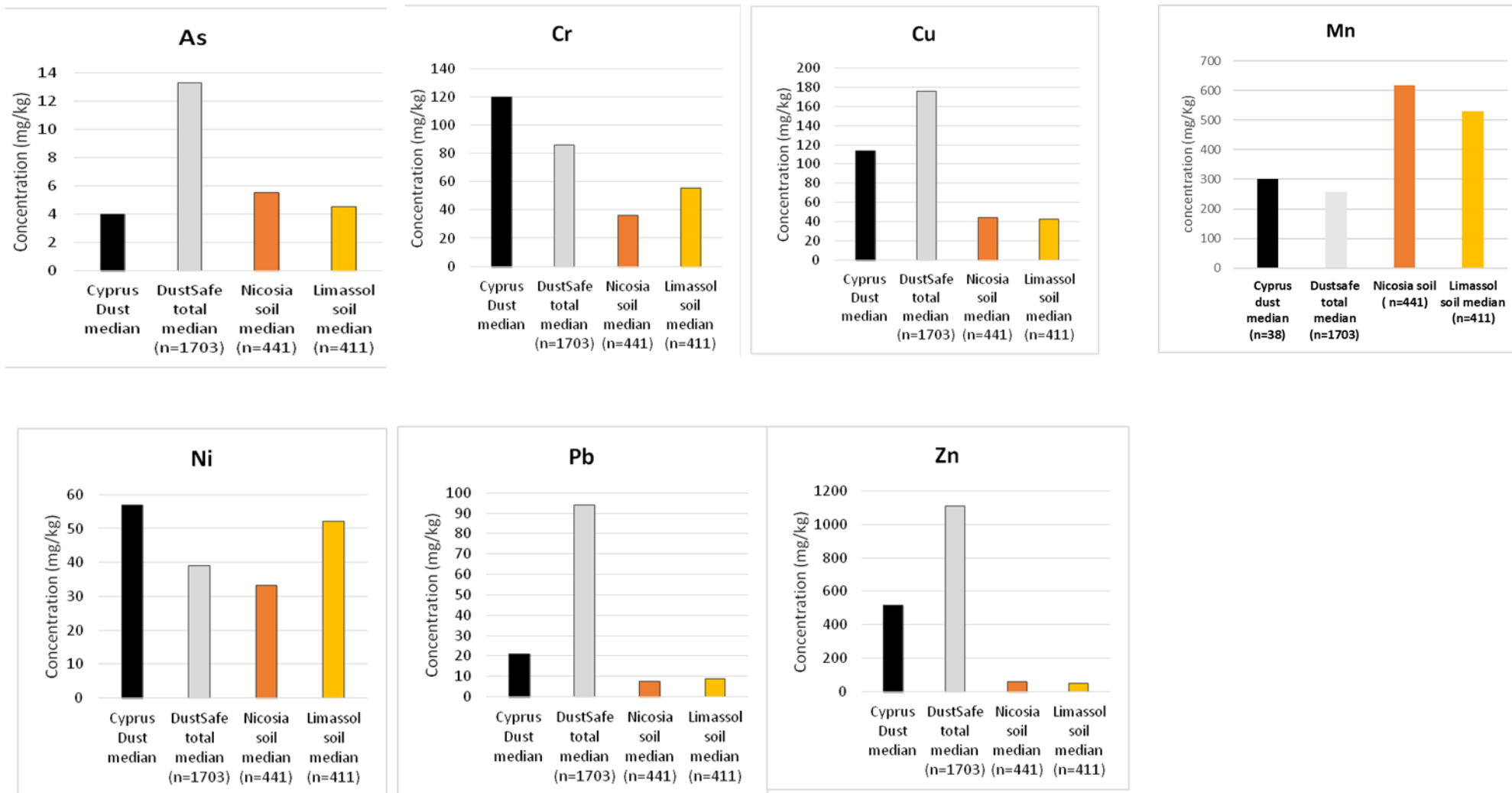


Figure 4.12. Comparison of Cyprus dust median values with data from other sources.

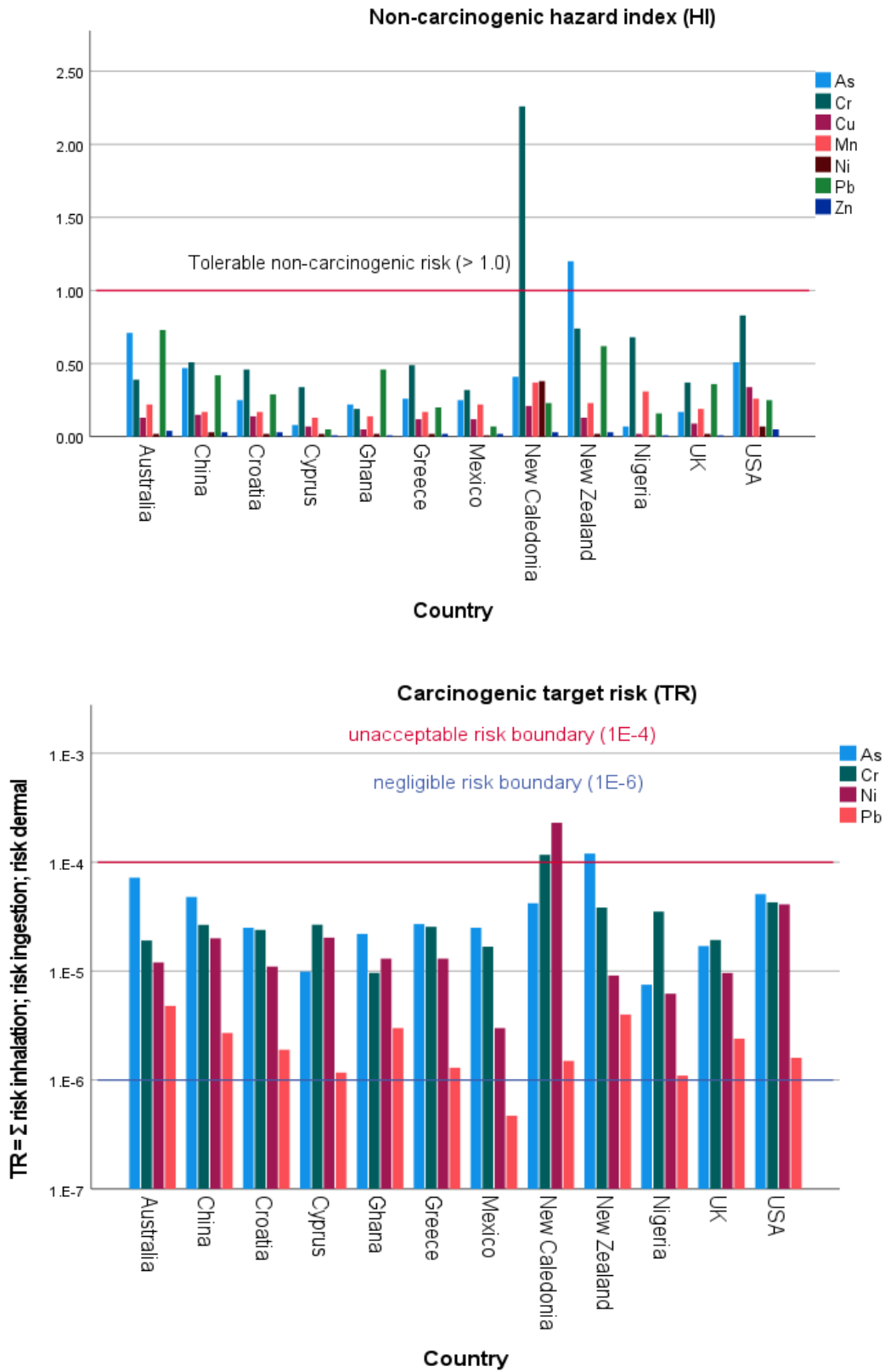


Figure 4.13. Results of non-carcinogenic (HQ) and carcinogenic (life-time cancer risk; TR)

Cyprus had the greatest carcinogenic risk for dermal exposure pathways across the assessed countries, with the highest pathway being ingestion followed by dermal and inhalation (table 4.12). The level of unacceptable risk (1×10^{-4}) indicated possible exceedance for As in New Zealand (Figure 4.13), Cr and Ni in New Caledonia (figure 4.13). The Island of Cyprus had the fourth highest carcinogenic risk in all regions in case of ingestion and the highest for dermal absorption exposure. However, Cyprus is the smallest country in terms of population and area in contrast with all other locations and it appears significant TR values the same with big countries such as USA, Australia, Greece and Mexico.

5.0 Conclusion

In this study the geochemical characteristics of Cyprus household dust from three regions (Mitsero, Limassol, and Nicosia), as well as soil from Mitsero were determined for the first time. For household dust, indoor sources such as building materials or human activities were associated with PTEs, and the results show differences between the origin of Mn, Ni, Cr and Fe for each region while Pb, As, Cu, and Zn showed a correlation with the year the houses were built. In the dust samples, three factors were found, the historical pollutant factor “Pb-As”, the construction material and vehicle activities factor “Zn-Cu” and the natural factor “Mn-Fe-Cr-Ni”. It has been observed that in the case of house dust, for some elements, the geological origin plays a key role in the supply of house dust contents. Health risk assessment was estimated for children under two years of age. Cr is the only of the examined elements that showed non-carcinogenic risk ($HI > 1$). However, Ni, Cr and As and Pb exceed the negligible carcinogenic risk ($TR > 1 \times 10^{-6}$), which there is a concern of the order 1 case per every 1,000,000 people, but none have exceeded the unacceptable carcinogenic risk ($TR > 1 \times 10^{-4}$; 1 case per every 1,000 people). The abandoned mining field of Mitsero, which initially was suspected as being contaminated, showed that its soils and dust were not enriched with PTEs, in comparison with the studied urban areas (Nicosia; Limassol). The major source of PTEs Mitsero soil was the local geological background. Health risk assessment of human exposure for children via soil indicated that there is no significant non-carcinogenic risk ($HI < 1$), while cancer risks may arise from ingestion and inhalation (due to Cr, Ni, and As). Through the ingestion pathway children under 2-year age, are under higher carcinogenic risk though exposure to household dust than from soils.

References

- Adamides N, 1984. The Cyprus volcanogenic sulphide deposits, unpubl. Ph.D. thesis, University of Leicester.
- Adamides, N.G., 2013. South Mathiatis: an unusual volcanogenic sulphide deposit in the Troodos Ophiolite of Cyprus. *Appl. Earth Sci.* 122, 194–206.
- Andonovska K, Stafilov T, Karadjova I, (2015). assessment of trace elements bioavailability – ingestion of toxic elements from the attic dust collected from the vicinity of the ferro-nickel smelter plant. *Section of Natural, Mathematical and Biotechnical Sciences, MASA, Vol. 36, No. 2, pp. 93–104.*
- Azarov G.M, Maiorova E, Oborina M. A, Belyakov A. V, 1995. wollastonite raw materials and their applications (a review). *Science for Ceramics Production. Vol. 52, Nos. 9- 10.*
- Böttcher M., 1999. Stable Isotope Fractionation during Experimental Formation of Norsethite (BaMg[CO₃]₂): A Mineral Analogue of Dolomite. *Aquatic Geochemistry* 6: 201–212, 2000.
- A. Blundell, J.A. Hannam, J.A. Dearing, J.F. Boyle, (2009). Detecting atmospheric pollution in surface soils using magnetic measurements: A reappraisal using an England and Wales database. *Environmental Pollution, Volume 157, Issue 10, October 2009, Pages 2878-2890.*
- Cao S, Chen X, Zhang L, Xing X, Wen D, Wang B, Qin N, Wei F, Duan X, (2020). Quantificational exposure, sources, and health risks posed by heavy metals in indoor and outdoor household dust in a typical smelting area in China. *Indoor Air.* 30:872–884.
- Charlesworth S., De Miguel E, Ordóñez A (2011). A review of the distribution of particulate trace elements in urban terrestrial environments and its application to considerations of risk. *Environmental Geochemistry and Health* volume 33, pages103–123.
- Cohen, D.; Gulson, B.; Davis, J. M.; Stelcer, E.; Garton, D.; Hawas, O.; Taylor, A, 2005. Fine-particle Mn and other metals linked to the introduction of MMT into gasoline in Sydney, Australia: Results of a natural experiment. *Atmos. Environ.*, 39, 6885–6896.
- Cohen DR, Rutherford NF, Morisseau E, Zissimos AM, 2012. Geochemical patterns in the soils of Cyprus. *Sci Total Environ* 420:250–262.
- Cohen, D. D.; Atanacio, A. J.; Stelcer, E.; Garton, D. Sydney Particle Characterisation Study; 2016. <https://www.epa.nsw.gov.au/your-environment/air/regional-air-quality/sydney-particle-characterisation-study>.
- Cohen, D.R., Rutherford, N.F., Morisseau, E. and Zissimos, A.M., 2011. *Geochemical Atlas of Cyprus.* UNSW Press, Sydney, 2011.
- Cohen D, Zissimos A, Schifano J, Rutherford N., 2021. Biogeochemical response of *Pinus brutia* and *Olea europaea* to lithological variations and Cu mineralisation in Cyprus. *Science of the Total Environment* 759, 143434.
- Constantinou G, Govett G (1973) Geology, geochemistry, and genesis of Cyprus sulfide deposits. *Econ Geol* 68:843–858.
- Davis JC. *Statistics and data analysis in geology.* 3rd edition. New York: John Wiley & Sons; 2002. 638 pp.
- Dearing J.A, R. J. L. Dann, K. Hay, J. A. Lees, P. J. Loveland, B. A. Maher and K. O'Grady (1996). Frequency-dependent susceptibility measurements of environmental materials. *Geophys. J. Znt.* (1996) 124,228-240.
- Dingle J, Kohl L, Khan N, Meng M, Shi Y.A, Pedroza-Brambila M, Chung-Wai Chow, Chan Arthur W.H, 2021. Sources and composition of metals in indoor house dust in a mid-size Canadian city. *Environmental Pollution* 289, 117867.
- Doyi, I. N.; Strezov, V.; Isley, C. F.; Yazdanparast, T.; Taylor, M. P., The relevance of particle size distribution and bioaccessibility on human health risk assessment for trace elements measured in indoor dust. *Sci. Total Environ.* 2020, 137931.
- Fergusson, J.E. & Kim, N.D., 1991. Trace elements in street and house dusts: sources and speciation. *Sci. Total Environ.*, 100, 125–150.
- Galanopoulos, E., Skarpelis, N., Argyraki, A. (2019) Supergene alteration, environmental impact and laboratory scale acid water treatment of Cyprus-type ore deposits: case study of Mathiatis and Sha abandoned mines. *Geochemistry: Exploration, Environment, Analysis, geochem2018-070* <https://doi.org/10.1144/geochem2018-070>

- Gonzalez, R., Strekopytov, S., Amato, F., Querol, X., Reche, C., Weiss, D., 2016. New insights from zinc and copper isotopic compositions into the sources of atmospheric particulate matter from two major European cities. *Environ. Sci. Technol.* 50, 9816–9824.
- Graustein, Kermit Cromack, Jr., Phillip Sollins., 1977. Calcium Oxalate: Occurrence in Soils and Effect on Nutrient and Geochemical Cycles. *Science*, Dec. 23, 1977, New Series, Vol. 198, No. 4323, pp. 1252-1254.
- Hadjipanagiotou C; Christou A; Zissimos A-M; Chatzitheodoridis E; Varnavas SP; (2020). Contamination of stream waters, sediments, and agricultural soil in the surroundings of an abandoned copper mine by potentially toxic elements and associated environmental and potential human health-derived risks: a case study from Agrokipia, Cyprus. *Environmental Science and Pollution Research* volume 27, pages 41279–41298.
- Hadjiparaskevas, C., 2008. Soil Survey and Monitoring in Cyprus. *European Soil Bureau Rpt*, 9 pp.
- Hanesch M, Rantitsch G, Hemetsberger S, Scholger R, 2007. Lithological and pedological influences on the magnetic susceptibility of soil: Their consideration in magnetic pollution mapping. *Science of the Total Environment* 382, 351–363.
- Hudson-Edwards K (2016) Tackling mine wastes. *Science* 352:288–290
- Harb M, Ebqa' ai M, Al-rashidi A, Alaziqi B, Al Rashdi M, Ibrahim B., 2015. Investigation of selected heavy metals in street and house dust from Al-Qunfudah, Kingdom of Saudi Arabia. *Environmental Earth Sciences* volume 74, pages 1755–1763.
- Hunt, A.; Johnson, D. L. Suspension and resuspension of dry soil indoors following track-in on footwear. *Environ. Geochem. Health* 2012, 34, 355–363.
- Ibanez Y, le Bot B, Glorennec P., 2011. House-dust metal content and bioaccessibility: a review. *European Journal Mineralogy* 22, pg. 629–637.
- Isley CF, Fry K.L , Liu X, Filippelli GM, Entwistle JA, Martin A, Kah M, Meza-Figueroa D, Shukle J, Jabeen K, Famuyiwa A, Wu L, Sharifi-Soltani N, Doyi I, Argyraki A, Ho KF, Dong C, Gunkel-Grillon PPAelion MC, and Taylor MP, 2022. International Analysis of Sources and Human Health Risk Associated with Trace Metal Contaminants in Residential Indoor Dust. *Environmental Science & Technology*, 56, 1053–1068.
- Jordanova, D., Jordanova, N., Lanos, P., Petrov, P., Tsacheva, T., 2012. Magnetism of outdoor and indoor settled dust and its utilization as a tool for revealing the effect of elevated particulate air pollution on cardiovascular mortality. *Geochem. Geophys. Geosy.* 13, 8.
- Jordanova D., Neli Jordanova, Petar Petrov., 2014. Magnetic susceptibility of road deposited sediments at a national scale – Relation to population size and urban pollution. *Environmental Pollution* Volume 189, Pages 239-251.
- Kaar, S.; Krizan, D.; Schwabe, J.; Hofmann, H.; Hebesberger, T.; Commenda, C.; Samek, L. Influence of the Al and Mn content on the structure-property relationship in density reduced TRIP-assisted sheet steels. *Mater. Sci. Eng., A* 2018, 735, 475–486.
- Kamble R.K, Thakare M. G, Ingle A. B, 2013. Iron in the Environment. *Indian J. Environ. Prot.*
- Kelepertzis, E., Argyraki, A., 2015. Geochemical associations for evaluating the availability of potentially harmful elements in urban soils: lessons learnt from Athens. *Appl. Geochem.* 59, 63–73.
- Kelepertzis, E., Komárek, M., Argyraki, A., Šillerová, H., 2016. Metal(loid) distribution and Pb isotopic signatures in the urban environment of Athens. Greece. *Environ. Pollut.* 213, 42–431.
- Kelepertzis, E., Argyraki, A., Botsou, F., Aidona, E., Szabó, A., Szabó, C., 2019. Tracking the occurrence of anthropogenic magnetic particles and potentially toxic elements (PTEs) in house dust using magnetic and geochemical analysis. *Environ. Pollut.* 245, 909–920.
- Kelepertzis, E., Argyraki, A., Chrastný, V., Botsou, F., Skordas, K., Komárek, M., Fouskas, A., 2020. Metal(loid) and isotopic tracing of Pb in soils, road and house dusts from the industrial area of Volos (central Greece). *Sci. Total Environ.* 725, 138300.
- Kelepertzis E, Chrastný V , Botsou F, Sigala E, Kypridou Z, Komárek M, Skordas K, Argyraki A, 2021. Tracing the sources of bioaccessible metal(loid)s in urban environments: A multidisciplinary approach. *Science of the Total Environment* 771, 144827.
- Kennedy, P.; Sutherland, S. Urban Sources of Copper, Lead and Zinc. *Auckland Regional Council Technical Report 2008/023*, 2008.
- Klinčić D, Lovaković B, Jagić K, Dvorščak M, 2021. Polybrominated diphenyl ethers and the multi-element profile of house dust in Croatia: Indoor sources, influencing factors of their accumulation

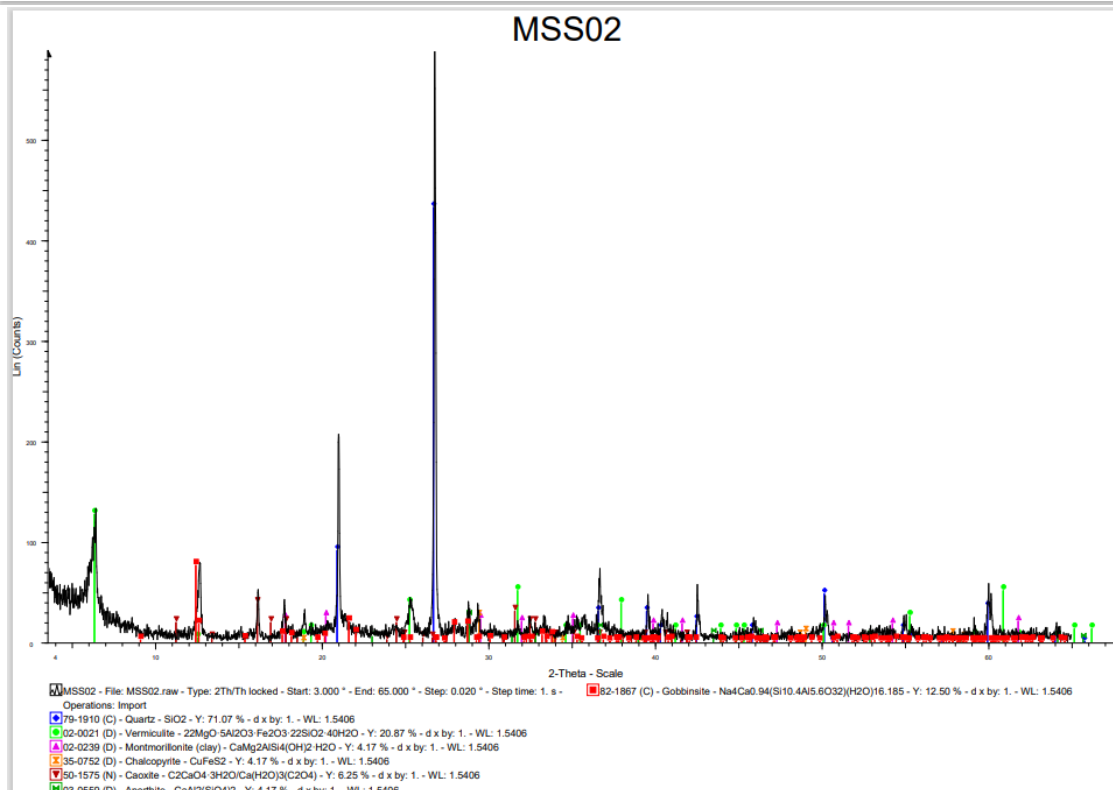
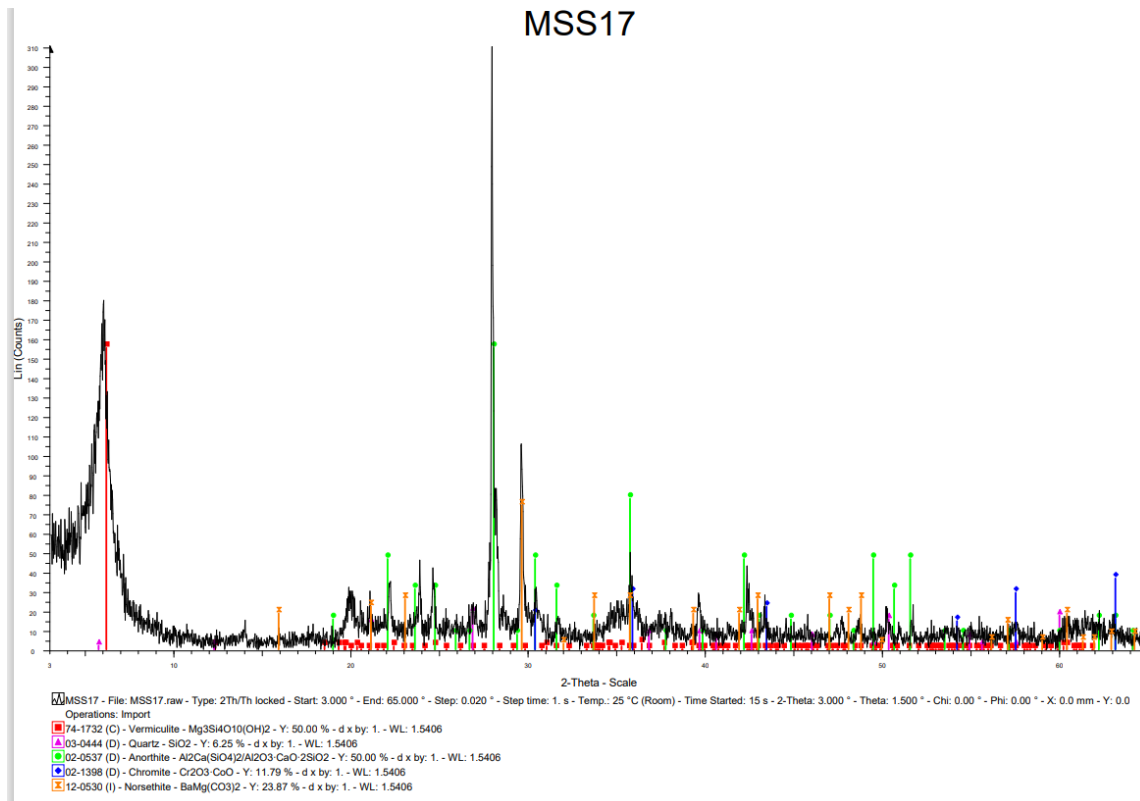
- and health risk assessment for humans. *Science of the Total Environment* 800, 149430.
- Kurt-Karakus, P. B. Determination of heavy metals in indoor dust from Istanbul, Turkey: estimation of the health risk. *Environ. Int.* 2012, 50, 47–55.
- Lisiewiczza M, Heimbürger R, Golimowski J, 2000. Granulometry and the content of toxic and potentially toxic elements in vacuum-cleaner collected, indoor dusts of the city of Warsaw. *The Science of the Total Environment* 263, 69, 78.
- Li HB, Li J, Zhu Y, Juhasz A, Ma L, (2015). Comparison of arsenic bioaccessibility in housedust and contaminated soils based on four in vitro assays. *Science of the Total Environment* 532, 803–811.
- Lu X, Liu W, Zhao C, Chen C, 2012. Environmental assessment of heavy metal and natural radioactivity in soil around a coal-fired power plant in China. *J Radioanal Nucl Chem.*, 295(3):1845–54. doi: 10.1007/s10967-012-2241-9.
- Luo, X.-s., Yu, S., Li, X.-d., 2012. The mobility, bioavailability and human bioaccessibility of trace metals in urban soils of Hong Kong. *Appl. Geochem.* 27, 995–1004.
- Martin, A. P.; Turnbull, R. E.; Rattenbury, M. S.; Cohen, D. R.; Hoogewerff, J.; Rogers, K. M.; Baisden, W. T.; Christie, A. B., 2016. The regional geochemical baseline soil survey of southern New Zealand: Design and initial interpretation. *J. Geochem. Explor.*, 167, 70– 82.
- Mercier F, Glorennec P, Thomas O, Le Bot B, 2011. Organic Contamination of Settled House Dust, A Review for Exposure Assessment Purposes. *Environmental Science & Technology* 45, 6716–6727.
- Morgan, J. J. Manganese in Natural Waters and Earth's Crust: Its Availability to Organisms. In *Metal Ions in Biological Systems*; CRC Press, 2000; Vol. 37, pp 1–34.
- Murthuza M., N. Surumbarkuzhali, C. Lakshmi Narasimhan, V. Thirukumaran, A. Chandrasekaran, Durai Ganesh, R. Ravisankar, 2022. Magnetic and soil parameters as a potential indicator of soil pollution in the district of Tiruvannamalai, Tamil Nadu, India. *Environmental Earth Sciences* 81:75.
- Pappu A., Mohini Saxena, Shyam R. Asolekar. 2005. Jarosite characteristics and its utilisation potentials. *Science of The Total Environment* Volume 359, Issues 1–3, 15 April 2006, Pages 232–243.
- Petrovský E., A. Kapičková, N. Jordanova, M. Knab, V. Hoffmann, 2000. Low-field magnetic susceptibility: a proxy method of estimating increased pollution of different environmental systems. *Environmental Geology* 39 (3–4).
- Reimann, C.; Fabian, K.; Birke, M.; Filzmoser, P.; Demetriades, A.; Négrel, P.; Oorts, K.; Matschullat, J.; de Caritat, P.; Albanese, S.; Anderson, M.; Baritz, R.; Batista, M. J.; Bel-Ian, A.; Cichella, D.; De Vivo, B.; De Vos, W.; Dinelli, E.; Ā uris, M.; Dusza-Dobek, A.; Eggen, O. A.; Eklund, M.; Ernsten, V.; Flight, D. M. A.; Forrester, S.; Fügedi, U.; Gilucis, A.; Gosar, M.; Gregorauskiene, V.; De Groot, W.; Gulán, A.; Halamic, J.; Haslinger, E.; Hayoz, P.; Hoogewerff, J.; Hrvatovic, H.; Husnjak, S.; Jähne-Klingberg, F.; Janik, L.; Jordan, G.; Kaminari, M.; Kirby, J.; Klos, V.; Kwecko, P.; Kuti, L.; Ladenberger, A.; Lima, A.; Locutura, J.; Lucivjansky, P.; Mann, A.; Mackovych, D.; McLaughlin, M.; Malyuk, B. I.; Maquil, R.; Meuli, R. G.; Mol, G.; O'Connor, P.; Ottesen, R. T.; Pasnieczna, A.; Petersell, V.; Pfliegerer, S.; Poňavic, M.; Prazeres, C.; Radusinovic, S.; Rauch, U.; Salpeteur, I.; Scanlon, R.; Schedl, A.; Scheib, A.; Schoeters, I.; Š efcik, P.; Sellersjö, E.; Slaninka, I.; Soriano-Disla, J. M.; Š orsa, A.; Svrkota, R.; Stafilov, T.; Tarvainen, T.; Tendavilov, V.; Valera, P.; Verougstraete, V.; Vidojevic, D.; Zissimos, A.; Zomeni, Z.; Sadeghi, M. GEMAS: Establishing geochemical background and threshold for 53 chemical elements in European agricultural soil. *Appl. Geochem.* 2018, 88, 302–318.
- Reich M., Palacios C., Parada, Udo Fehn, Eion M. Cameron, I. Leybourne M., Zúñiga A., 2008. Atacamite formation by deep saline waters in copper deposits from the Atacama Desert, Chile: evidence from fluid inclusions, groundwater geochemistry, TEM, and ³⁶Cl data. *Miner Deposita* 43:663–675.
- Reimann, C., Filzmoser, P., Garrett, R.G., 2002. Factor analysis applied to regional geochemical data: problems and possibilities. *Appl. Geochem.* 17, 185–206.
- Rodrigues, S.M., Pereira, M.E., Ferreira da Silva, E., Hursthouse, A.S., Duarte, A.C., 2010. A review of regulatory decisions for environmental protection: part I – challenges in the implementation of national soil policies. *Environ. Int.* 35, 202–213.
- Rutkowski R, Białowicz J.S, Rachwał M, Rogula-Kozłowska W, Rybak J, 2020. Magnetic Susceptibility of Spider Webs and Dust: Preliminary Study in Wrocław, Poland. *Minerals*, 10, 1018; doi:10.3390/min10111018.

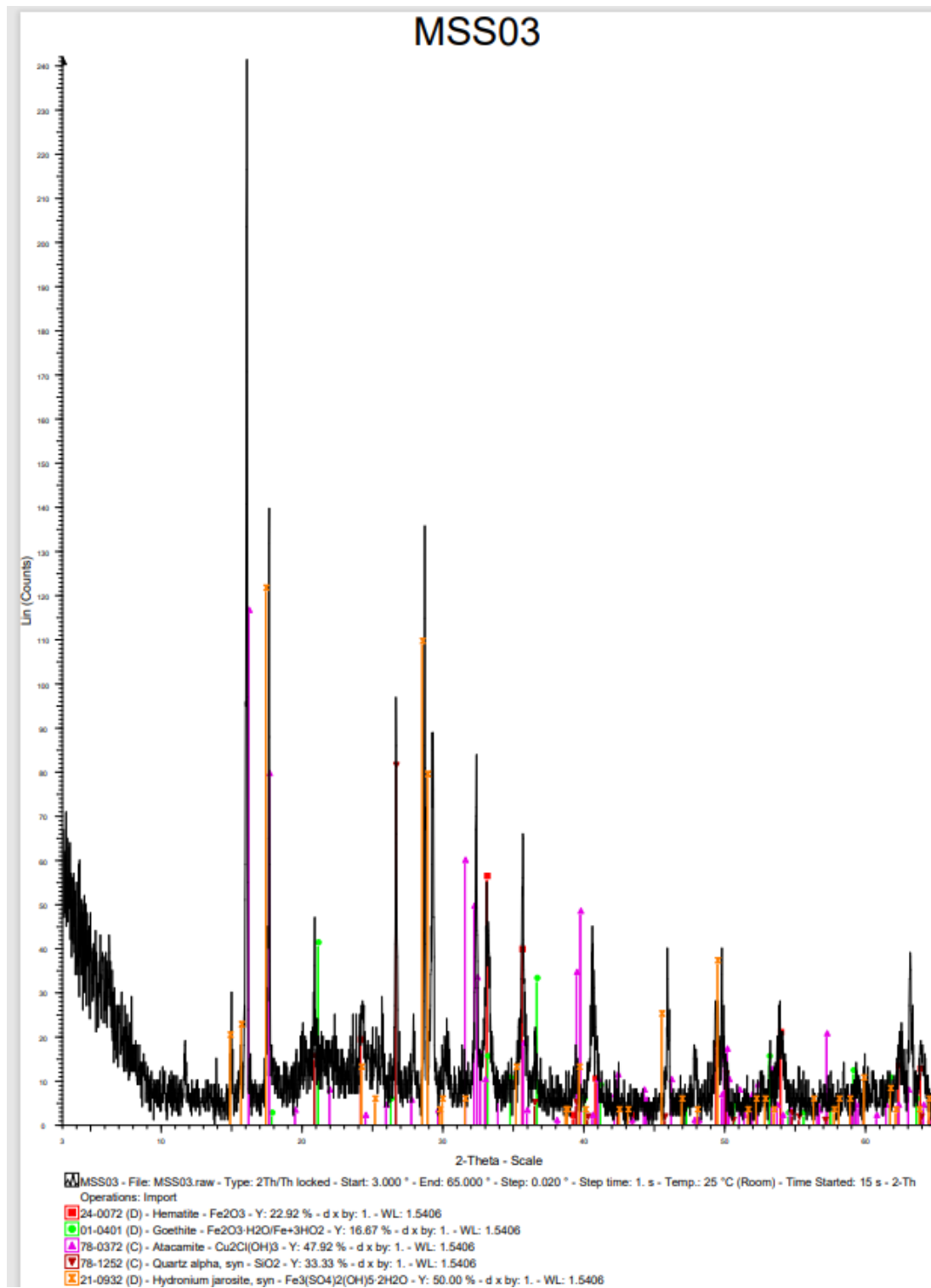
- Sabzevari E and Sobhanardakani S, 2018. Analysis of Selected Heavy Metals in Indoor Dust Collected from City of Khorramabad, Iran: A Case Study. *Jundishapur J Health Sci.* 10(3):e67382.
- Schmidt A., Richard Yarnolda, Matt Hilla, Ashmorea M. 2004. Magnetic susceptibility as proxy for heavy metal pollution: a site study. *Journal of Geochemical Exploration* 85 (2005) 109 – 117.
- Shi, G., Chen, Z., Xu, S., Zhang, J., Wang, L., Bi, C., Teng, J., 2008. Potentially toxic metal contamination of urban soils and roadside dust in Shanghai, China. *Environ. Pollut.* 156, 251–260.
- Taylor, M. P.; Isley, C. F.; Fry, K. L.; Liu, X.; Gillings, M. M.; Rouillon, M.; Soltani, N. S.; Gore, D. B.; Filippelli, G. M, 2021. A citizen science approach to identifying trace metal contamination risks in urban gardens. *Environ. Int.*, 155, No. 106582.
- Thompson, R., Oldfield, F., 1986. *Environmental Magnetism*. Springer Netherlands, Dordrecht. <https://doi.org/10.1007/978-94-011-8036-8>
- Turner, A., 2011. Oral bioaccessibility of trace metals in household dust: A review. *Environmental Geochemistry and Health*, 33, 331–341.
- Wang, W.; Wu, F.; Zheng, J.; Wong, M. H. Risk assessments of PAHs and Hg exposure via settled house dust and street dust, linking with their correlations in human hair. *J. Hazard. Mater.* 2013, 263, 627–637.
- Wragg J, Cave M, Basta N, Brandon E, Casteel S, Denys S, Gron C, Oomen A, Reimer K, Tack K, Van de Wiele T, (2011). An inter-laboratory trial of the unified BARGE bioaccessibility method for arsenic, cadmium, and lead in soil. *Science of the Total Environment* 409, 4016–4030.
- Wong, C.S.C., Li, X., Thornton, I., 2006. Urban environmental geochemistry of trace metals. *Environ. Pollut.* 142, 1–16.
- Yadav, I. C.; Devi, N. L.; Singh, V. K.; Li, J.; Zhang, G. Spatial distribution, source analysis, and health risk assessment of heavy metals contamination in house dust and surface soil from four major cities of Nepal. *Chemosphere* 2019, 218, 1100–1113.
- Yang K, Cattle S, 2015. Bioaccessibility of lead in urban soil of Broken Hill, Australia: A study based on in vitro digestion and the IEUBK model. *Science of the Total Environment* 538, 922–933.
- Yoshinaga, J.; Yamasaki, K.; Yonemura, A.; Ishibashi, Y.; Kaido, T.; Mizuno, K.; Takagi, M.; Tanaka, A. Lead and other elements in house dust of Japanese residences—Source of lead and health risks due to metal exposure. *Environ. Pollut.* 2014, 189, 223–228.
- Zissimos, A.M., Cohen, D.R., Christoforou, I.C., 2018. Land use influences on soil geochemistry in Lefkosia (Nicosia) Cyprus. *J. Geochem. Explor.* 187, 6–20.
- Zissimos, A.M., Cohen, D.R., Christoforou, I.C., Sadeghi, B., Rutherford, N.F., 2021. Controls on soil geochemistry fractal characteristics in Lemesos (Limassol), Cyprus. *J. Geochem. Explor.* 220-106682.
- <https://www.census2021.cystat.gov.cy/Announcements/18%20%CE%9C%CE%B1%CF%8A%CE%BF%CF%85%202022%20%CE%91%CE%A0%CE%9F%CE%93%CE%A1%CE%91%CE%A6%CE%97%20%CE%A0%CE%9B%CE%97%CE%98%CE%A5%CE%A3%CE%9C%CE%9F%CE%A5%202021%20%20%CE%A0%CE%A1%CE%9F%CE%9A%CE%91%CE%A4%CE%91%CE%A1%CE%9A%CE%A4%CE%99%CE%9A%CE%91%20%CE%91%CE%A0%CE%9F%CE%A4%CE%95%CE%9B%CE%95%CE%A3%CE%9C%CE%91%CE%A4%CE%91>. Published 18/05/2022.

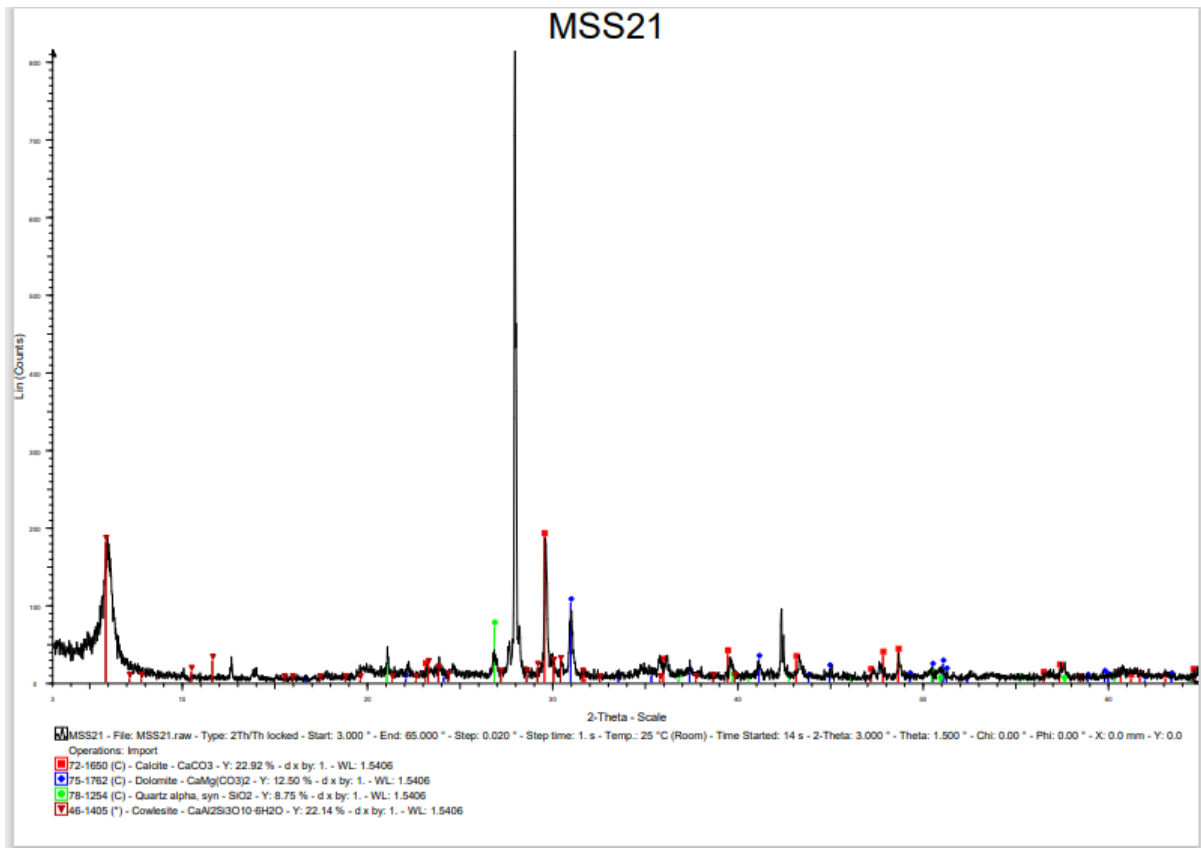
Appendix I – Basic statistical summary for Mitsero Soil Samples.

Statistics						
Elements	Units (n=22)	Mean	Median	Std. Deviation	Minimum	Maximum
Al	%	3.2914	3.175	0.86357	1.73	5.42
As	ppm	7	4	9.50438	3	38
Ba	ppm	36.3	37	19.46684	9	100
Ca	%	6.8977	7.38	4.47377	0.14	13.44
Cr	ppm	43.6364	25.5	44.23051	6	174
Cu	ppm	155.0091	85.35	180.7859	41.6	734
Fe	%	5.6614	5.04	2.6386	2.85	13.31
K	%	0.365	0.315	0.17655	0.09	0.66
La	ppm	1.9263	1.7	0.88997	0.6	4.2
Li	ppm	18.2727	15.5	13.56179	2	50
Mg	%	2.7773	2.695	1.05009	1.4	6.17
Mn	ppm	990.5455	960	283.1234	492	1517
Na	%	0.1627	0.15	0.08072	0.03	0.39
Ni	ppm	27.4091	20	24.35972	4	118
P	%	0.039	0.03	0.0359	0.01	0.17
Pb	ppm	7.8	6	5.94045	2	19
S	%	0.3105	0.06	0.79413	0.01	3.27
Sc	ppm	18.5273	18.5	4.91927	9.4	29.3
Sr	ppm	86.8364	79.6	43.26064	19.7	185
Ti	%	0.1818	0.155	0.10326	0.02	0.4
V	ppm	160.5909	148	58.45443	88	271
W	ppm	25	14.5	23.56551	11	60
Y	ppm	13.6545	12.75	7.12305	1.5	32.7
Zn	ppm	98.6364	75	60.21275	36	253
Zr	ppm	11.9182	10.05	8.0946	2	39.3
pH	-	8.23	8.42	1.25	4.37	9.91
Xfd%	-	0.90	0.95	0.47	0.02	1.71

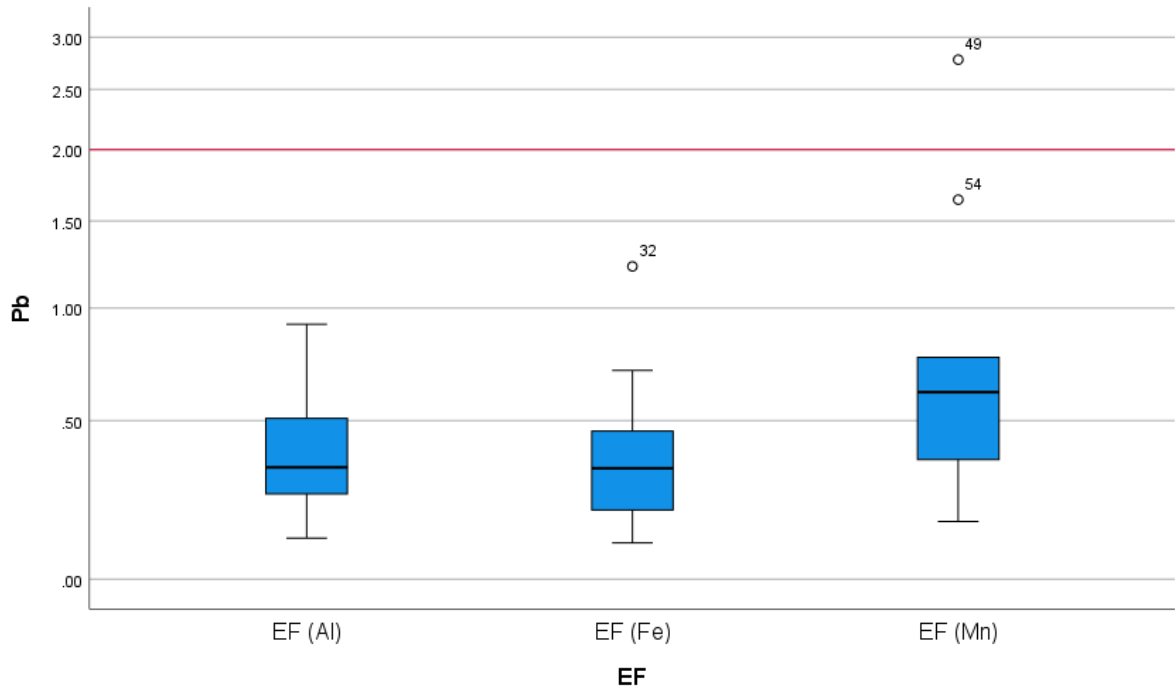
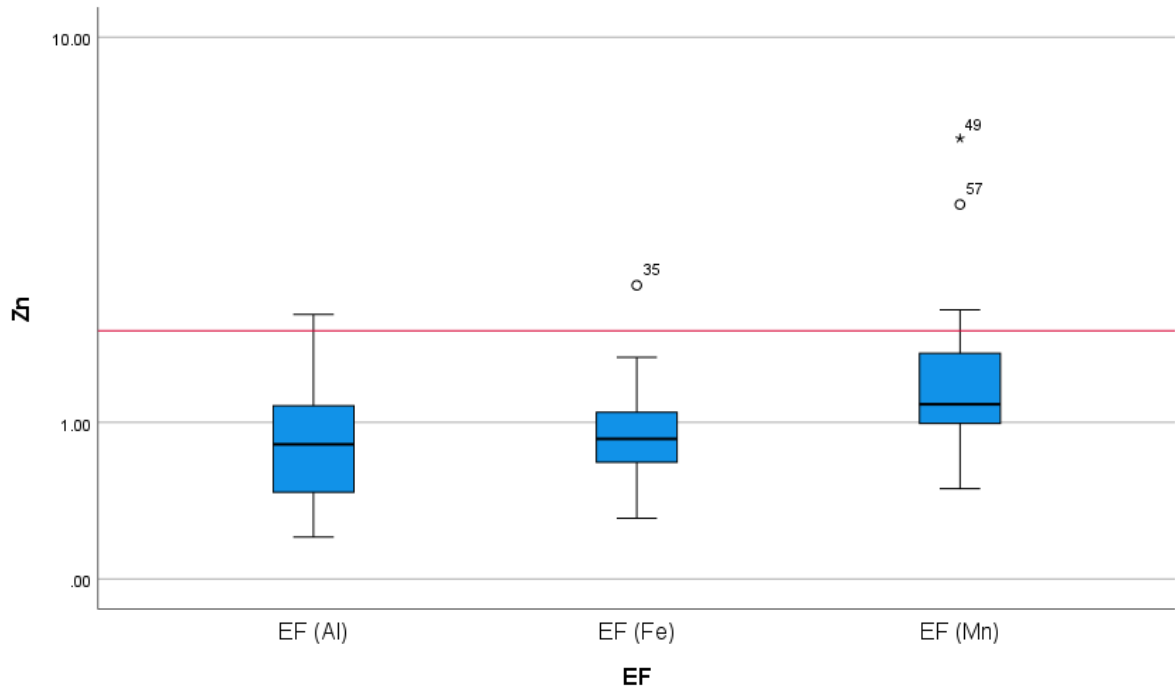
Appendix II- XRD patterns of the studied samples

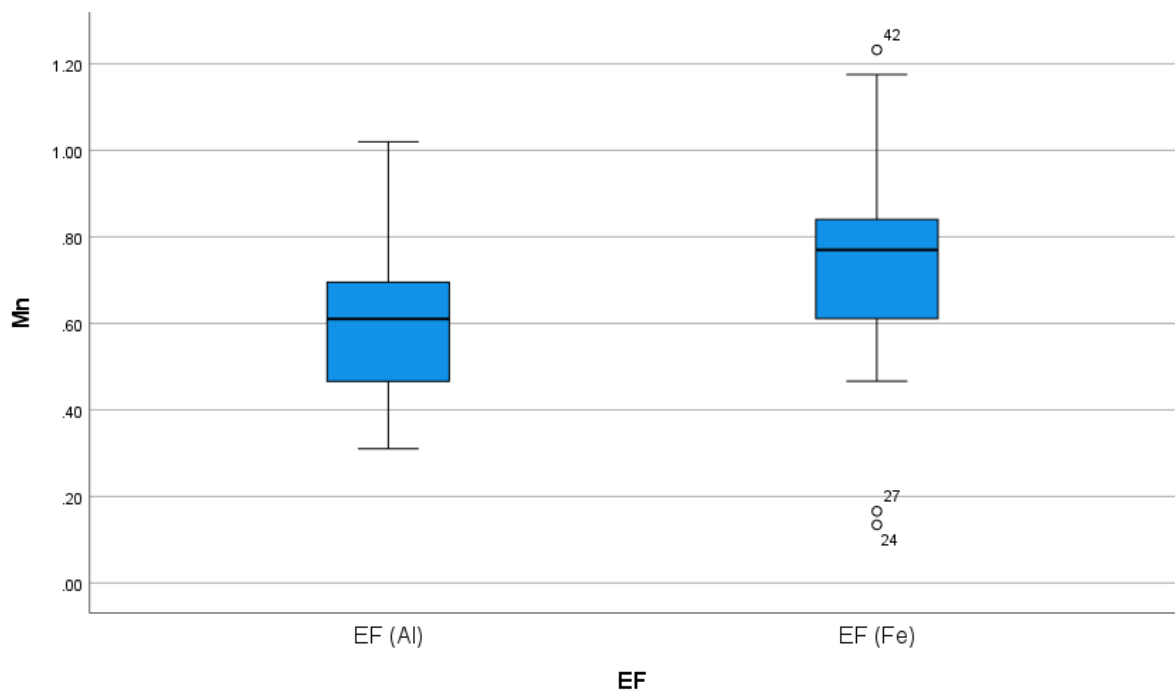
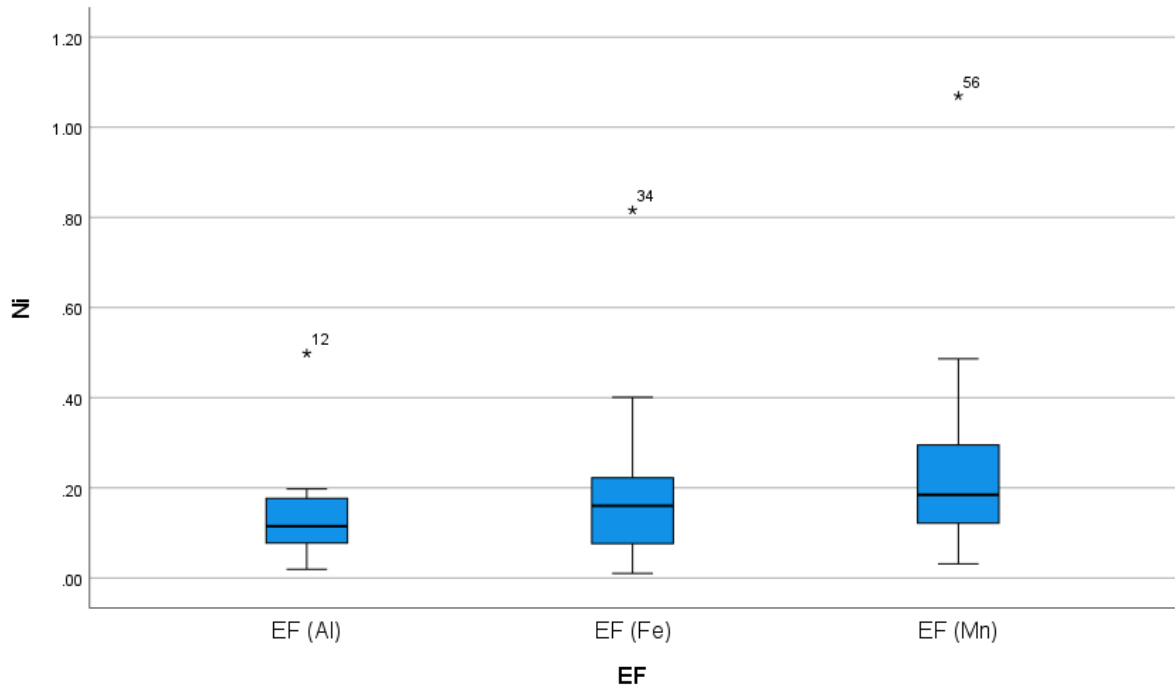


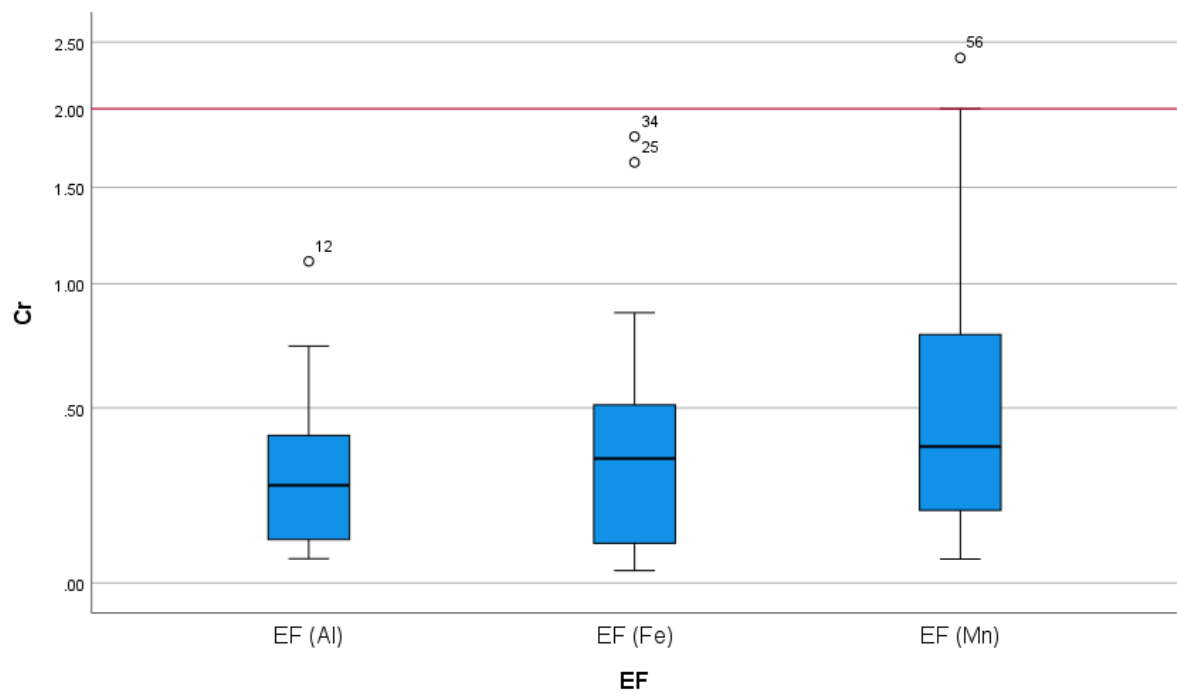
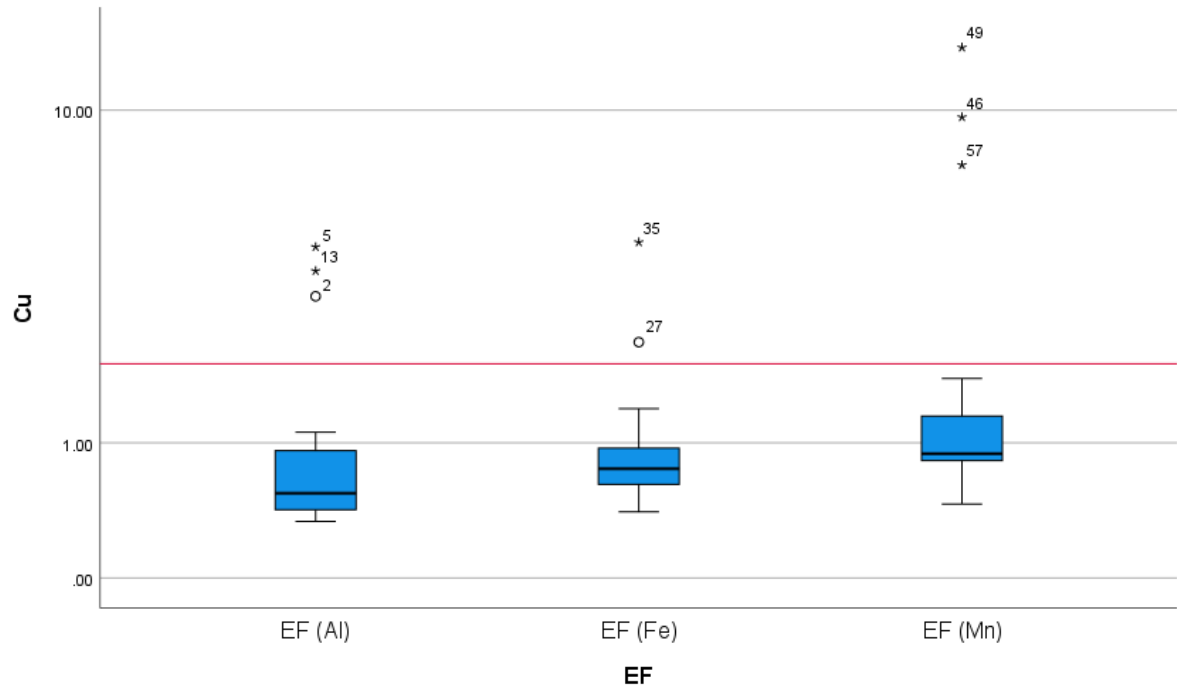


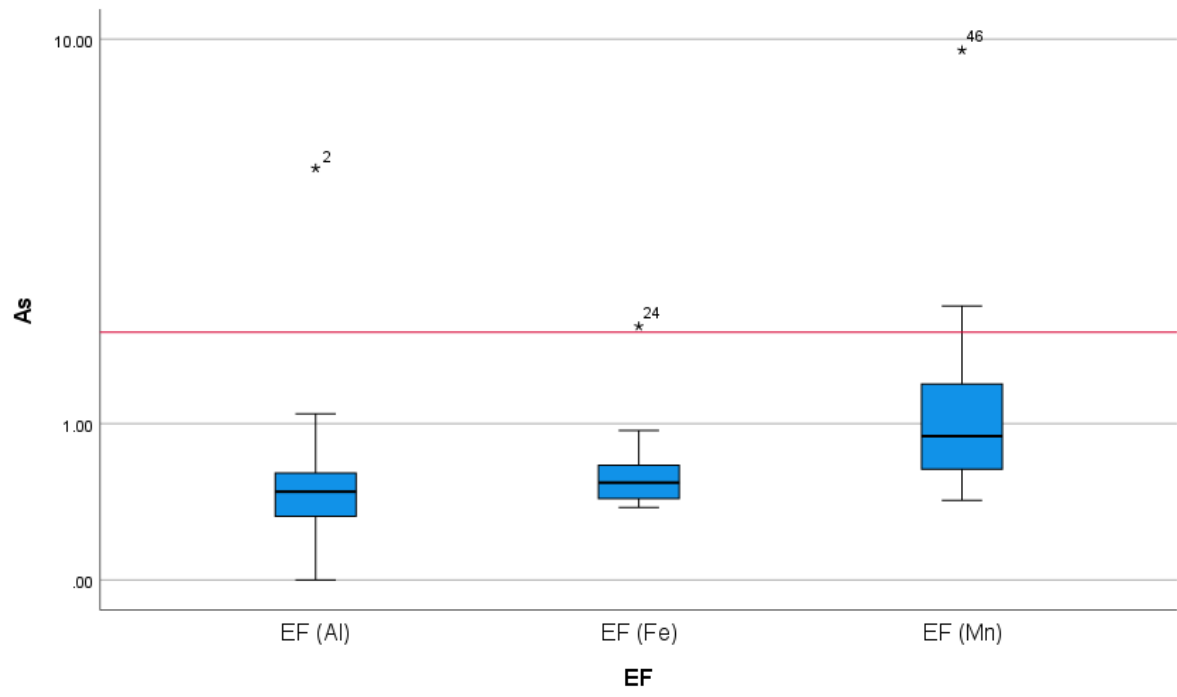


Appendix III –Enrichment factor for soil, as reference element Al, Fe, and Mn

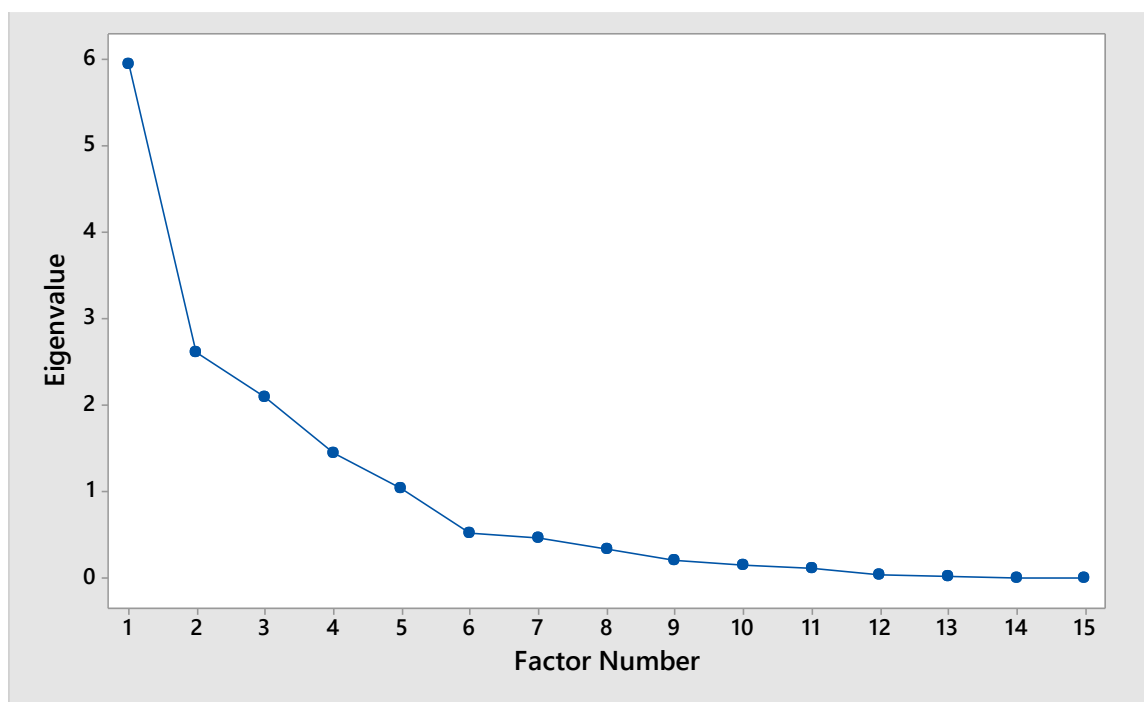








Appendix IV –Principal Component Analysis

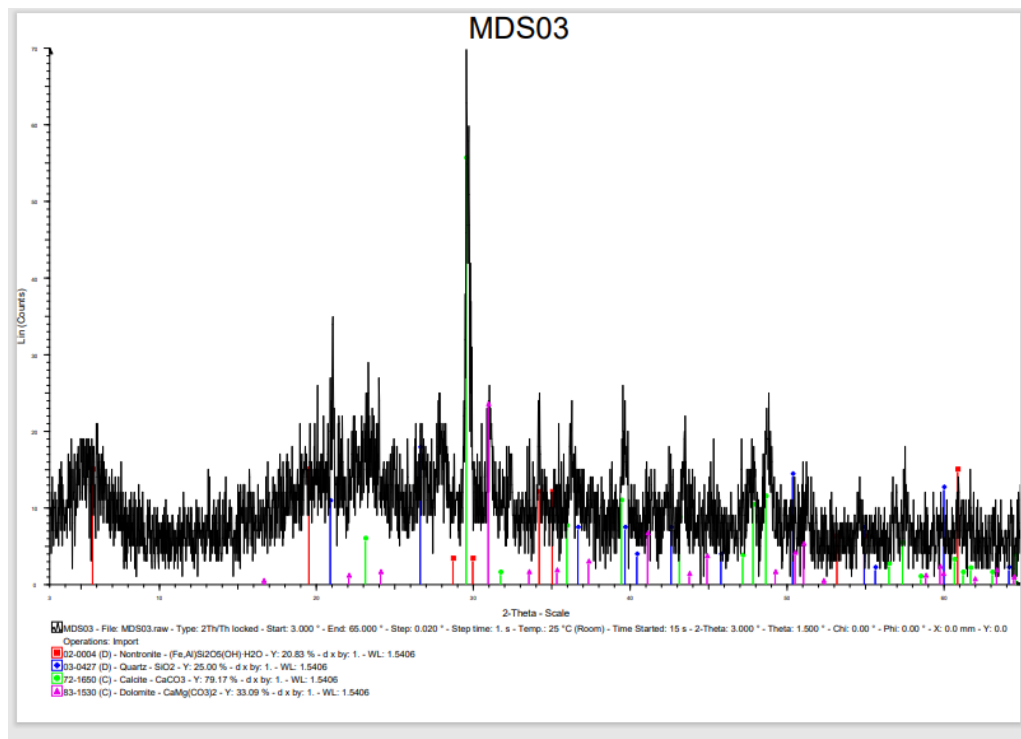
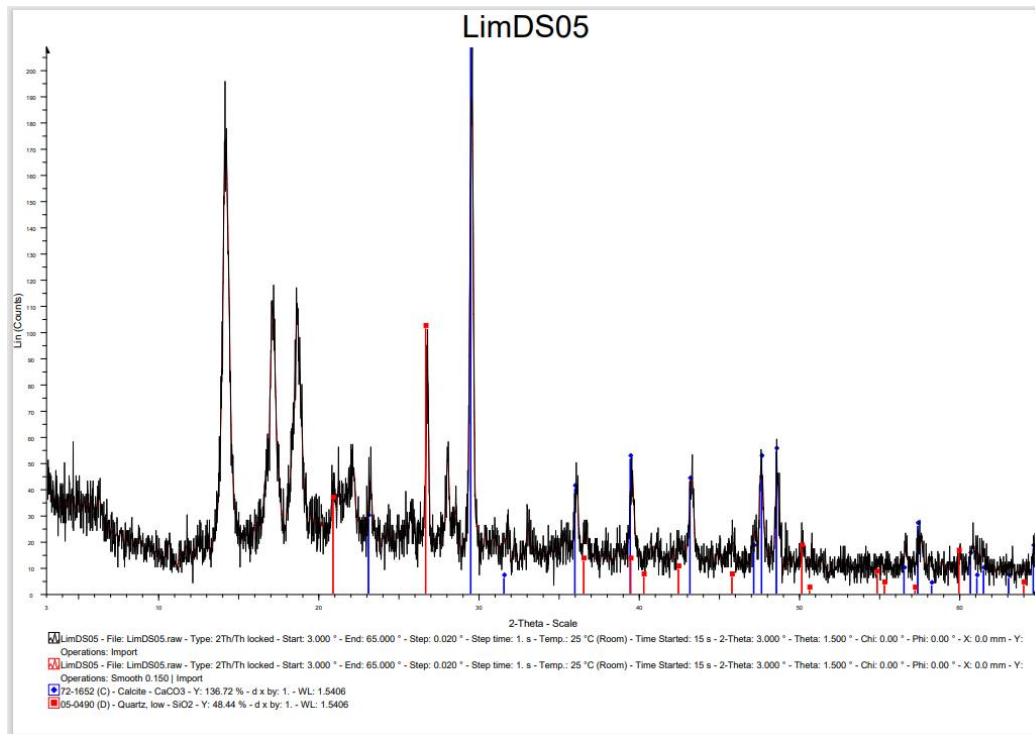


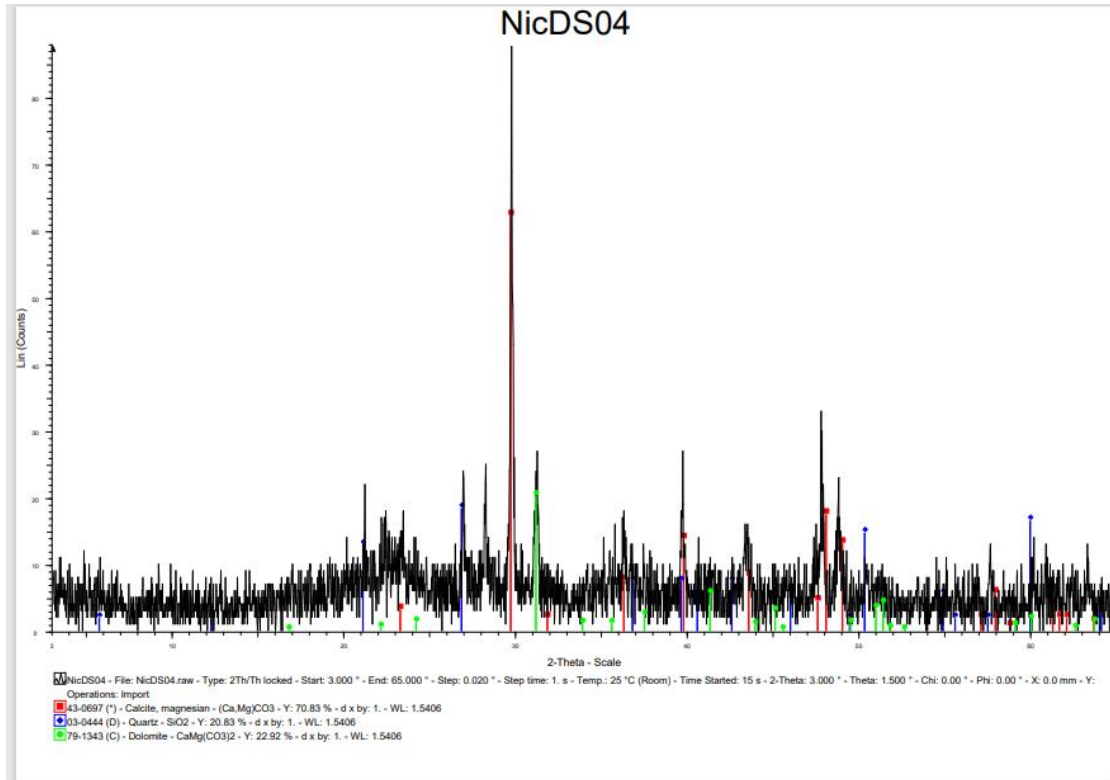
Variable	Factor1	Factor2	Factor3	Factor4
xlf	0.445	-0.376	-0.003	0.648
pH	0.856	0.106	-0.364	-0.083
Al	0.054	0.820	0.037	0.281
As	-0.919	-0.057	-0.034	0.050
Ca	0.389	0.131	-0.257	-0.770
Cr	0.090	0.948	-0.109	-0.196
Cu	-0.591	-0.003	0.728	-0.048
Fe	-0.816	-0.121	0.330	0.379
Mg	0.440	-0.032	-0.135	-0.745
Mn	0.449	0.208	-0.126	0.583
Na	-0.132	0.006	-0.027	0.006
Ni	0.116	0.885	-0.141	-0.139
Pb	-0.199	-0.140	0.787	0.057
S	-0.803	-0.101	0.482	-0.034
Zn	-0.097	-0.037	0.910	0.181

Component	% Of Variance
1	28.3
2	18.4
3	17.4

Figure 1. the results of Principal Component Analysis of Mitsero soil samples (n=22).

Appendix IIV- XRD patterns of the studied samples





Appendix V – Pearson correlation test of elements and magnetic susceptibility for household dust.

	Mitsero	As	Cr	Cu	Fe	Mn	Ni	Pb	Zn
As	Pearson Correlation	1	-0.267	.815**	0.395	0.629	0.049	.884**	0.565
	Sig. (2-tailed)		0.487	0.007	0.293	0.07	0.9	0.002	0.113
	N	9	9	9	9	9	9	9	9
Cr	Pearson Correlation	-0.267	1	-0.298	0.391	0.247	-0.02	0.069	0.216
	Sig. (2-tailed)	0.487		0.436	0.299	0.521	0.96	0.861	0.577
	N	9	9	9	9	9	9	9	9
Cu	Pearson Correlation	.815**	-0.298	1	0.263	0.32	0.05	0.602	0.479
	Sig. (2-tailed)	0.007	0.436		0.494	0.401	0.899	0.086	0.192
	N	9	9	9	9	9	9	9	9
Fe	Pearson Correlation	0.395	0.391	0.263	1	.847**	0.004	0.636	.823**
	Sig. (2-tailed)	0.293	0.299	0.494		0.004	0.993	0.066	0.006
	N	9	9	9	9	9	9	9	9
Mn	Pearson Correlation	0.629	0.247	0.32	.847**	1	-0.151	.848**	.692*
	Sig. (2-tailed)	0.07	0.521	0.401	0.004		0.699	0.004	0.039
	N	9	9	9	9	9	9	9	9
Ni	Pearson Correlation	0.049	-0.02	0.05	0.004	-0.151	1	0.008	0.409
	Sig. (2-tailed)	0.9	0.96	0.899	0.993	0.699		0.985	0.275
	N	9	9	9	9	9	9	9	9
Pb	Pearson Correlation	.884**	0.069	0.602	0.636	.848**	0.008	1	0.61
	Sig. (2-tailed)	0.002	0.861	0.086	0.066	0.004	0.985		0.081
	N	9	9	9	9	9	9	9	9
Zn	Pearson Correlation	0.565	0.216	0.479	.823**	.692*	0.409	0.61	1
	Sig. (2-tailed)	0.113	0.577	0.192	0.006	0.039	0.275	0.081	
	N	9	9	9	9	9	9	9	9
** Correlation is significant at the 0.01 level (2-tailed).									
* Correlation is significant at the 0.05 level (2-tailed).									

	Nicosia	As	Cr	Cu	Fe	Mn	Ni	Pb	Zn
As	Pearson Correlation	1	.737*	0.134	.642*	0.491	0.464	-0.222	0.175
	Sig. (2-tailed)		0.015	0.712	0.045	0.15	0.177	0.537	0.629
	N	10	10	10	10	10	10	10	10
Cr	Pearson Correlation	.737*	1	0.007	0.568	0.41	0.08	-0.396	0.196
	Sig. (2-tailed)	0.015		0.985	0.087	0.24	0.825	0.257	0.587
	N	10	10	10	10	10	10	10	10
Cu	Pearson Correlation	0.134	0.007	1	.666*	0.579	0.422	0.405	.829**
	Sig. (2-tailed)	0.712	0.985		0.035	0.079	0.225	0.245	0.003
	N	10	10	10	10	10	10	10	10
Fe	Pearson Correlation	.642*	0.568	.666*	1	.881**	0.486	-0.263	0.459
	Sig. (2-tailed)	0.045	0.087	0.035		<.001	0.154	0.463	0.182
	N	10	10	10	10	10	10	10	10
Mn	Pearson Correlation	0.491	0.41	0.579	.881**	1	0.45	-0.259	0.297
	Sig. (2-tailed)	0.15	0.24	0.079	<.001		0.192	0.47	0.404
	N	10	10	10	10	10	10	10	10
Ni	Pearson Correlation	0.464	0.08	0.422	0.486	0.45	1	0.017	0.279
	Sig. (2-tailed)	0.177	0.825	0.225	0.154	0.192		0.963	0.435
	N	10	10	10	10	10	10	10	10
Pb	Pearson Correlation	-0.222	-0.396	0.405	-0.263	-0.259	0.017	1	0.485
	Sig. (2-tailed)	0.537	0.257	0.245	0.463	0.47	0.963		0.155
	N	10	10	10	10	10	10	10	10
Zn	Pearson Correlation	0.175	0.196	.829**	0.459	0.297	0.279	0.485	1
	Sig. (2-tailed)	0.629	0.587	0.003	0.182	0.404	0.435	0.155	
	N	10	10	10	10	10	10	10	10
* Correlation is significant at the 0.05 level (2-tailed).									
** Correlation is significant at the 0.01 level (2-tailed).									

	Limassol	As	Cr	Cu	Fe	Mn	Ni	Pb	Zn
As	Pearson Correlation	1	0.104	0.357	0.425	0.403	0.209	.833**	0.081
	Sig. (2-tailed)		0.673	0.134	0.07	0.087	0.39	<.001	0.741
	N	19	19	19	19	19	19	19	19
Cr	Pearson Correlation	0.104	1	.692**	.760**	.717**	.681**	0.298	.529*
	Sig. (2-tailed)	0.673		0.001	<.001	<.001	0.001	0.215	0.02
	N	19	19	19	19	19	19	19	19
Cu	Pearson Correlation	0.357	.692**	1	.712**	.700**	.834**	0.447	.622**
	Sig. (2-tailed)	0.134	0.001		<.001	<.001	<.001	0.055	0.004
	N	19	19	19	19	19	19	19	19
Fe	Pearson Correlation	0.425	.760**	.712**	1	.975**	.776**	.649**	.583**
	Sig. (2-tailed)	0.07	<.001	<.001		<.001	<.001	0.003	0.009
	N	19	19	19	19	19	19	19	19
Mn	Pearson Correlation	0.403	.717**	.700**	.975**	1	.753**	.604**	.557*
	Sig. (2-tailed)	0.087	<.001	<.001	<.001		<.001	0.006	0.013
	N	19	19	19	19	19	19	19	19
Ni	Pearson Correlation	0.209	.681**	.834**	.776**	.753**	1	0.433	.736**
	Sig. (2-tailed)	0.39	0.001	<.001	<.001	<.001		0.064	<.001
	N	19	19	19	19	19	19	19	19
Pb	Pearson Correlation	.833**	0.298	0.447	.649**	.604**	0.433	1	0.401
	Sig. (2-tailed)	<.001	0.215	0.055	0.003	0.006	0.064		0.089
	N	19	19	19	19	19	19	19	19
Zn	Pearson Correlation	0.081	.529*	.622**	.583**	.557*	.736**	0.401	1
	Sig. (2-tailed)	0.741	0.02	0.004	0.009	0.013	<.001	0.089	
	N	19	19	19	19	19	19	19	19
* Correlation is significant at the 0.05 level (2-tailed).									
** Correlation is significant at the 0.01 level (2-tailed).									

	Correlations	pH	As	Cr	Cu	Fe	Mn	Ni	Pb	Zn
As	Pearson Correlation	-0.508	1	0.286	.341*	.499**	.468**	.331*	.691**	0.177
	Sig. (2-tailed)	0.304		0.081	0.036	0.001	0.003	0.042	<.001	0.288
	N	6	38	38	38	38	38	38	38	38
Cr	Pearson Correlation	0.373	0.286	1	0.248	.612**	.518**	.408*	0.118	0.319
	Sig. (2-tailed)	0.467	0.081		0.134	<.001	<.001	0.011	0.482	0.051
	N	6	38	38	38	38	38	38	38	38
Cu	Pearson Correlation	0.232	.341*	0.248	1	.663**	.614**	.553**	.403*	.689**
	Sig. (2-tailed)	0.658	0.036	0.134		<.001	<.001	<.001	0.012	<.001
	N	6	38	38	38	38	38	38	38	38
Fe	Pearson Correlation	0.275	.499**	.612**	.663**	1	.946**	.618**	.462**	.604**
	Sig. (2-tailed)	0.598	0.001	<.001	<.001		<.001	<.001	0.004	<.001
	N	6	38	38	38	38	38	38	38	38
Mn	Pearson Correlation	0.278	.468**	.518**	.614**	.946**	1	.568**	.494**	.553**
	Sig. (2-tailed)	0.593	0.003	<.001	<.001	<.001		<.001	0.002	<.001
	N	6	38	38	38	38	38	38	38	38
Ni	Pearson Correlation	0.281	.331*	.408*	.553**	.618**	.568**	1	0.268	.512**
	Sig. (2-tailed)	0.589	0.042	0.011	<.001	<.001	<.001		0.103	0.001
	N	6	38	38	38	38	38	38	38	38
Pb	Pearson Correlation	-0.258	.691**	0.118	.403*	.462**	.494**	0.268	1	.405*
	Sig. (2-tailed)	0.622	<.001	0.482	0.012	0.004	0.002	0.103		0.012
	N	6	38	38	38	38	38	38	38	38
Zn	Pearson Correlation	0.18	0.177	0.319	.689**	.604**	.553**	.512**	.405*	1
	Sig. (2-tailed)	0.733	0.288	0.051	<.001	<.001	<.001	0.001	0.012	
	N	6	38	38	38	38	38	38	38	38
* Correlation is significant at the 0.05 level (2-tailed).										
** Correlation is significant at the 0.01 level (2-tailed).										

	xlfr	Cr	Mn	Fe	Ni	Cu	Zn	As
Cr	0.356 0.058							
Mn	0.568 0.001	0.495 0.006						
Fe	0.630 0.000	0.574 0.001	0.960 0.000					
Ni	0.410 0.027	0.392 0.035	0.582 0.001	0.623 0.000				
Cu	0.362 0.054	0.200 0.298	0.685 0.000	0.646 0.000	0.499 0.006			
Zn	0.519 0.004	0.246 0.199	0.668 0.000	0.670 0.000	0.500 0.006	0.659 0.000		
As	0.147 0.446	0.159 0.409	0.418 0.024	0.437 0.018	0.253 0.186	0.349 0.064	0.142 0.461	
Pb	0.203 0.291	0.086 0.656	0.455 0.013	0.437 0.018	0.276 0.147	0.463 0.011	0.509 0.005	0.745 0.000

Appendix VI –Metadata

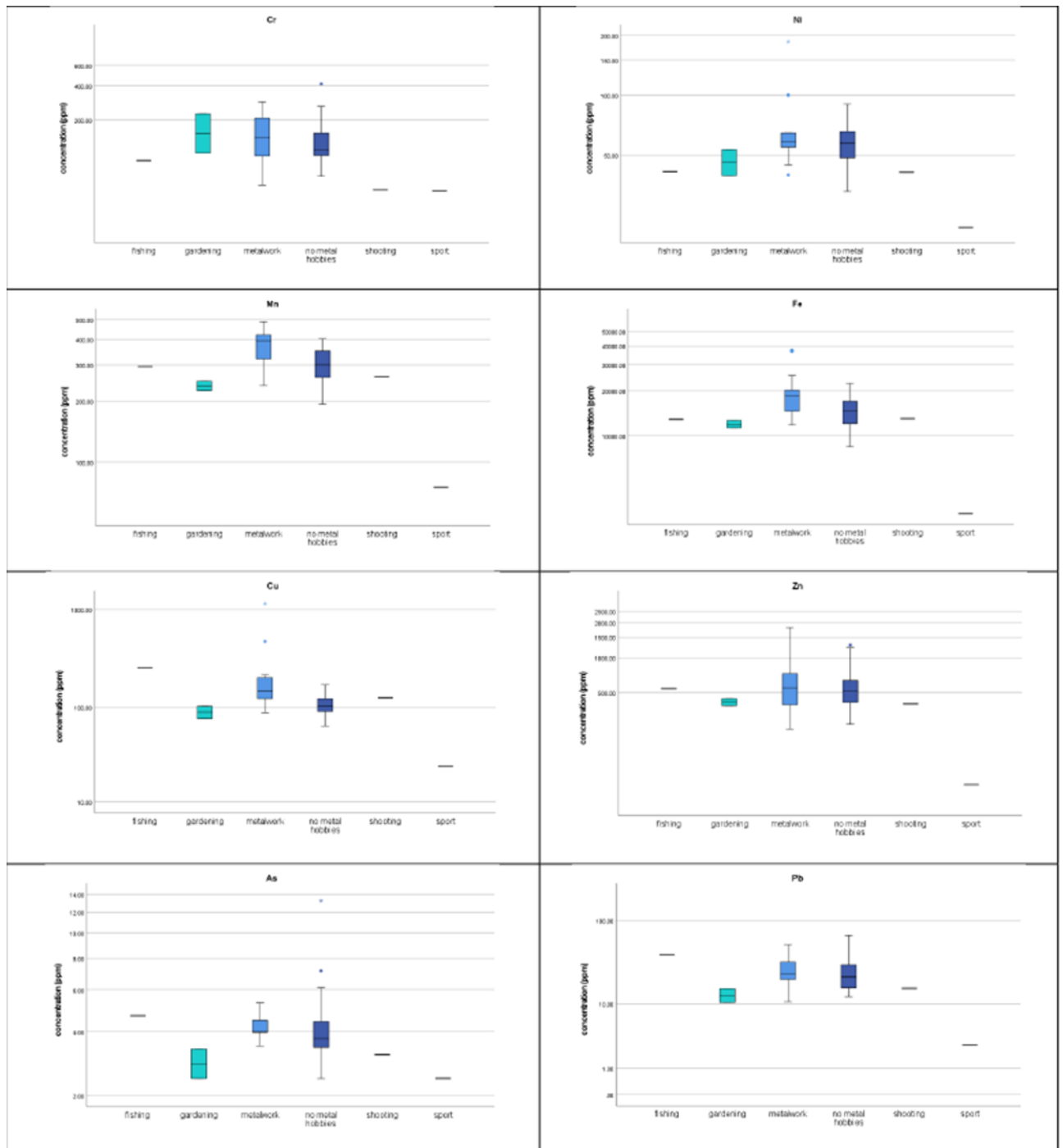


Figure 1. Box plot of trace metal concentrations for homes with and without leisure activities which related with metal exposure

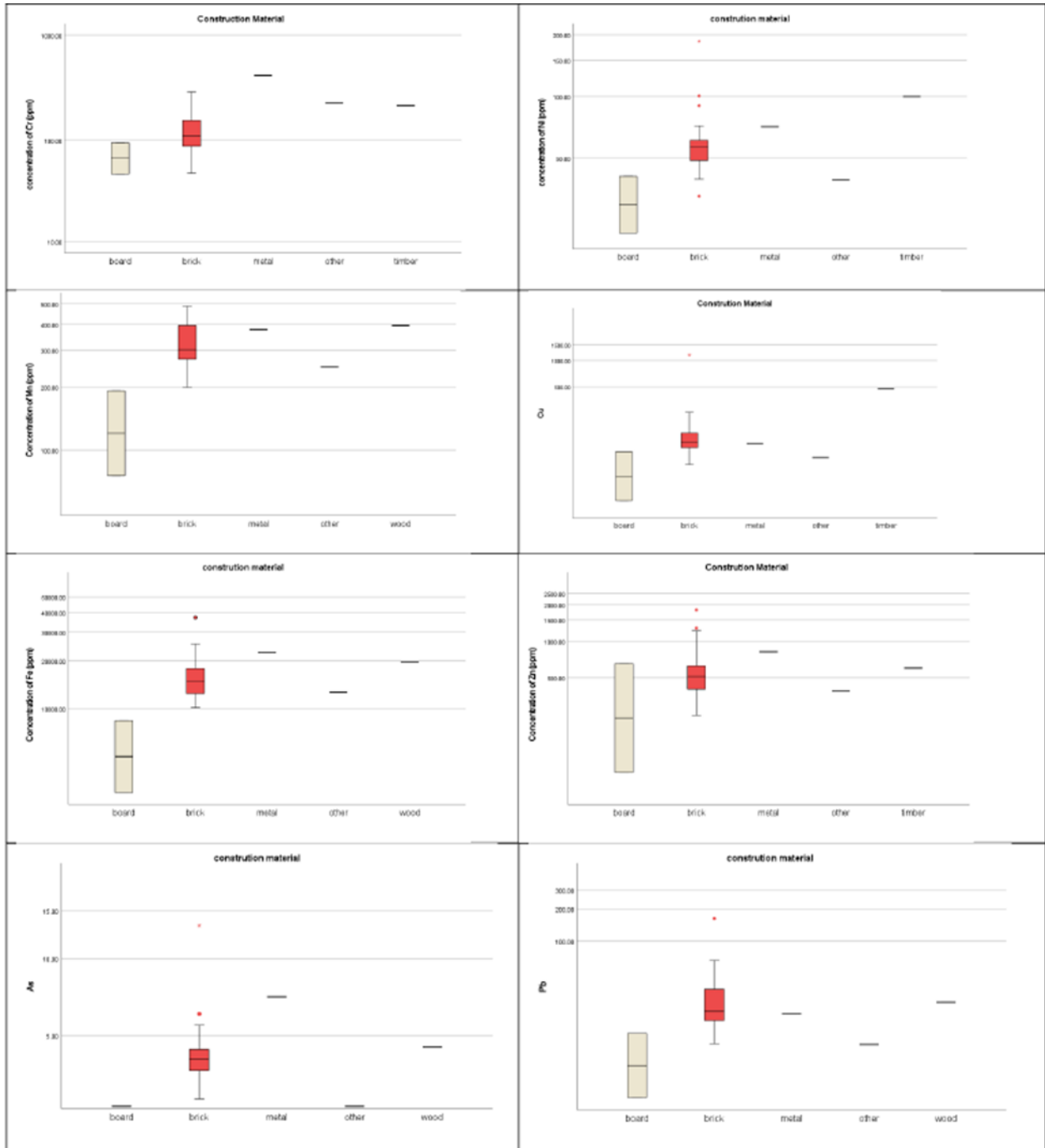


Figure 2. Box plot of elemental concentration by construction material.

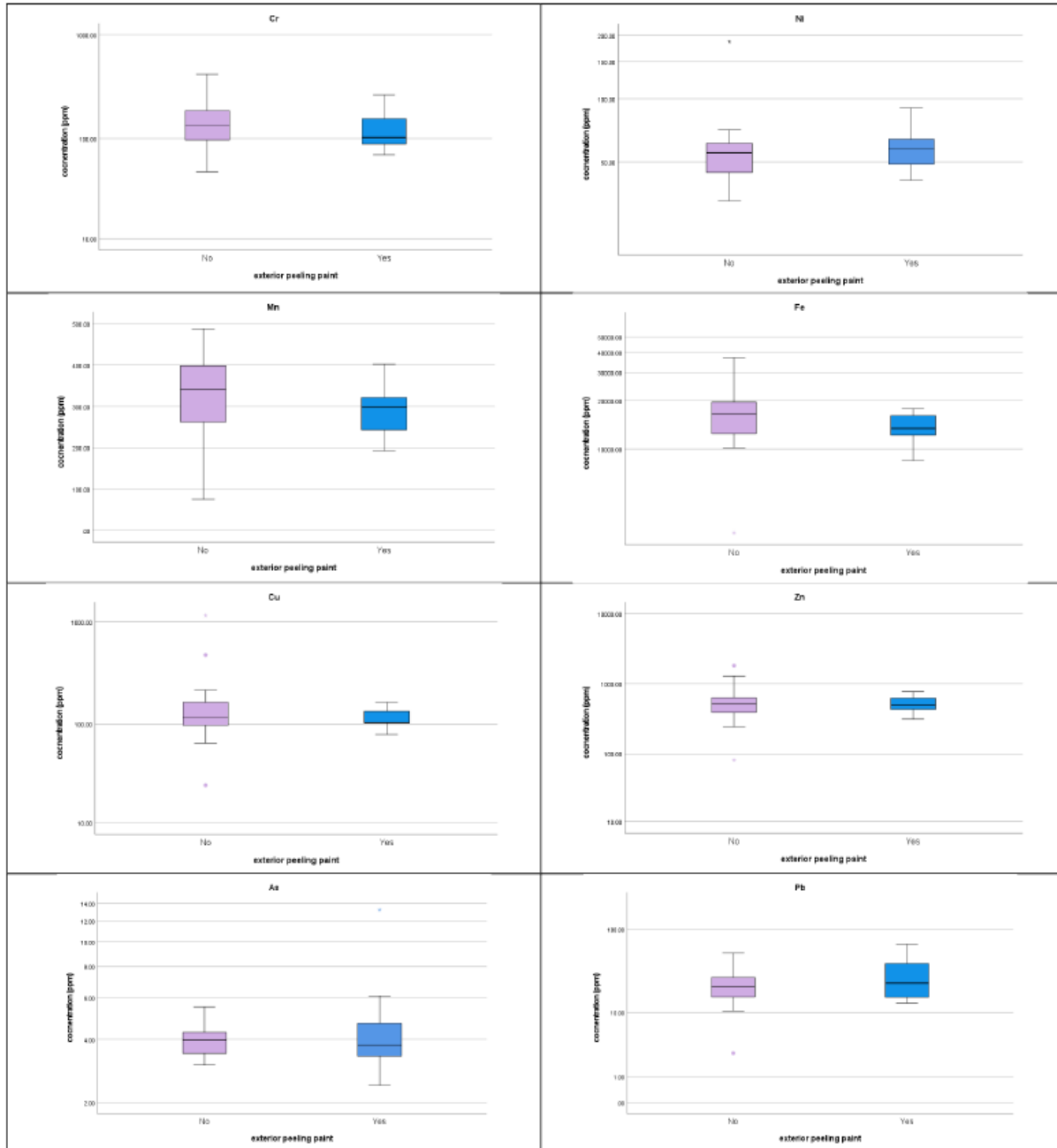


Figure 3. Box plot of trace elements of homes which had exterior peeling paint.

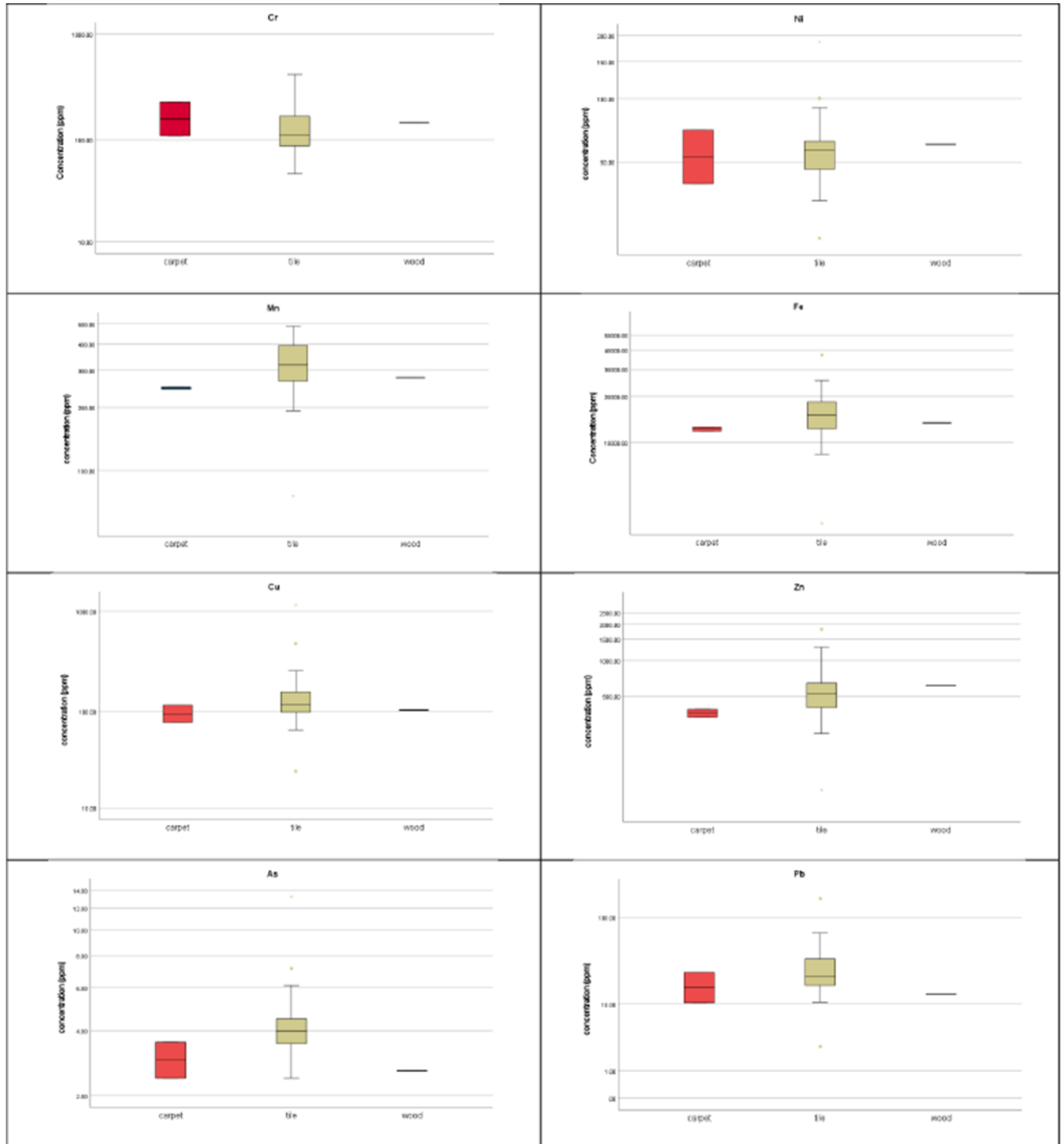


Figure 4. Box plot of elemental concentration by floor covering.

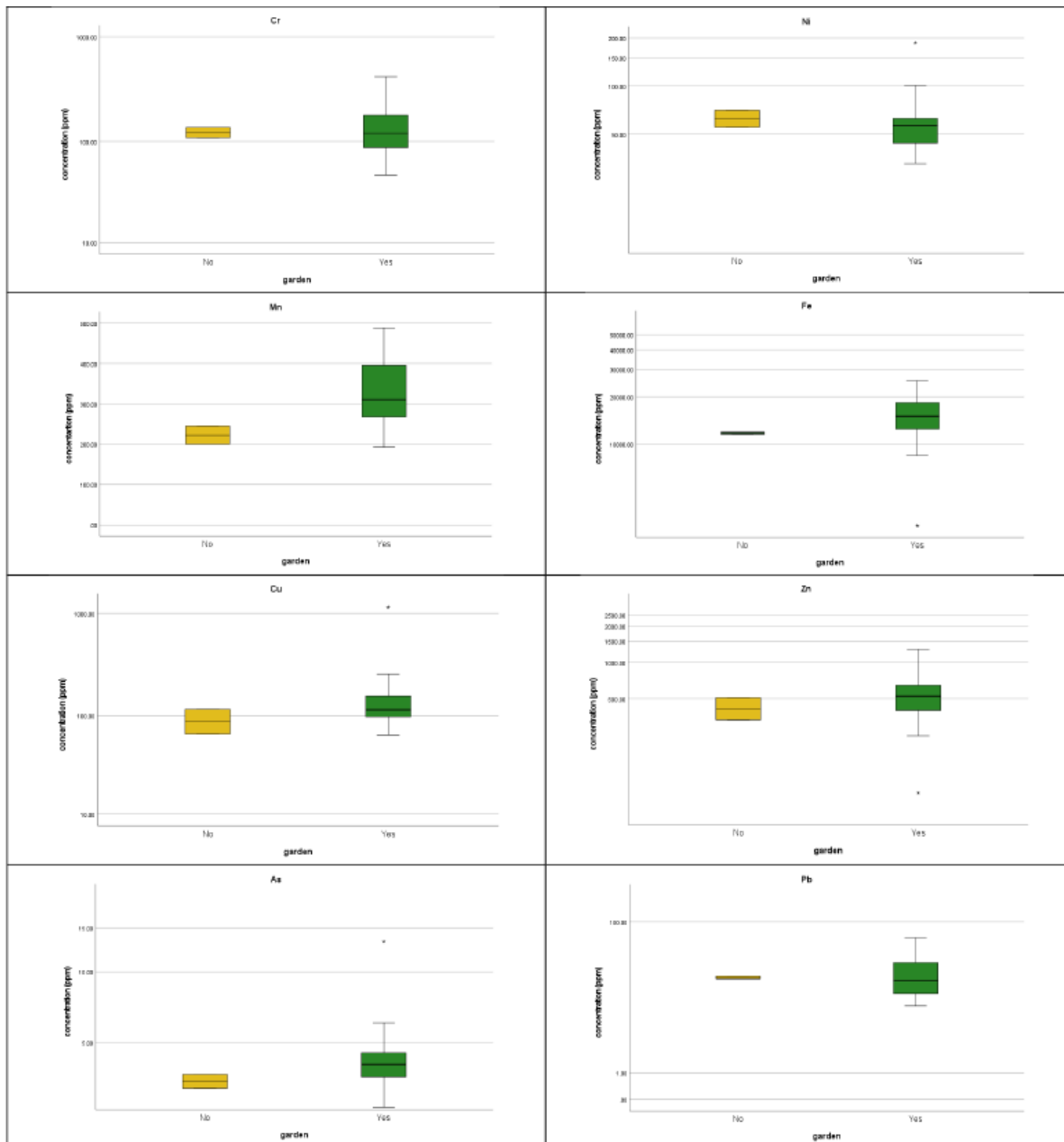


Figure 5. Box plot of elemental concentration of homes with and without access to a garden.

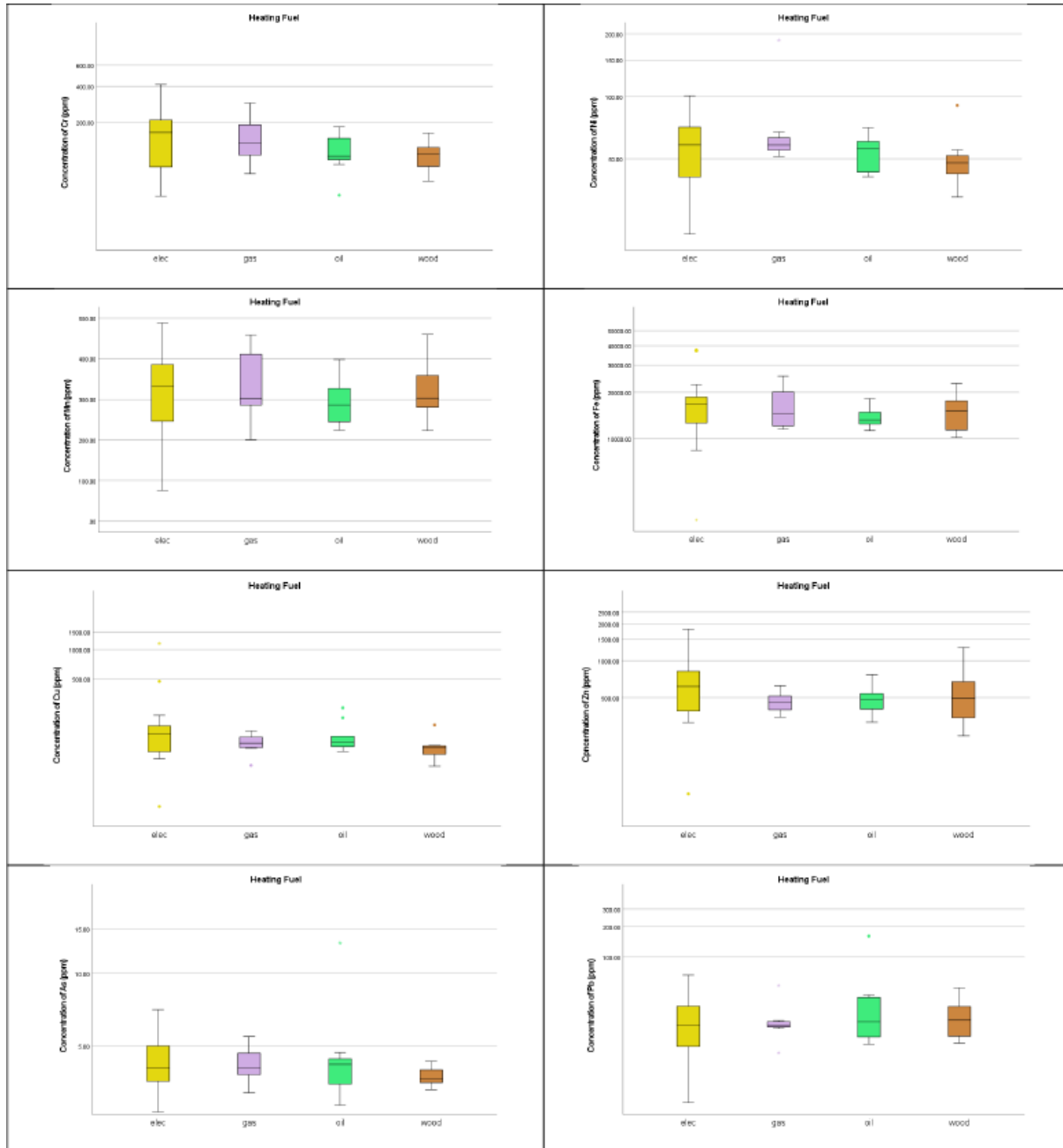


Figure 6. Box plot of elemental concentration by heating fuels.

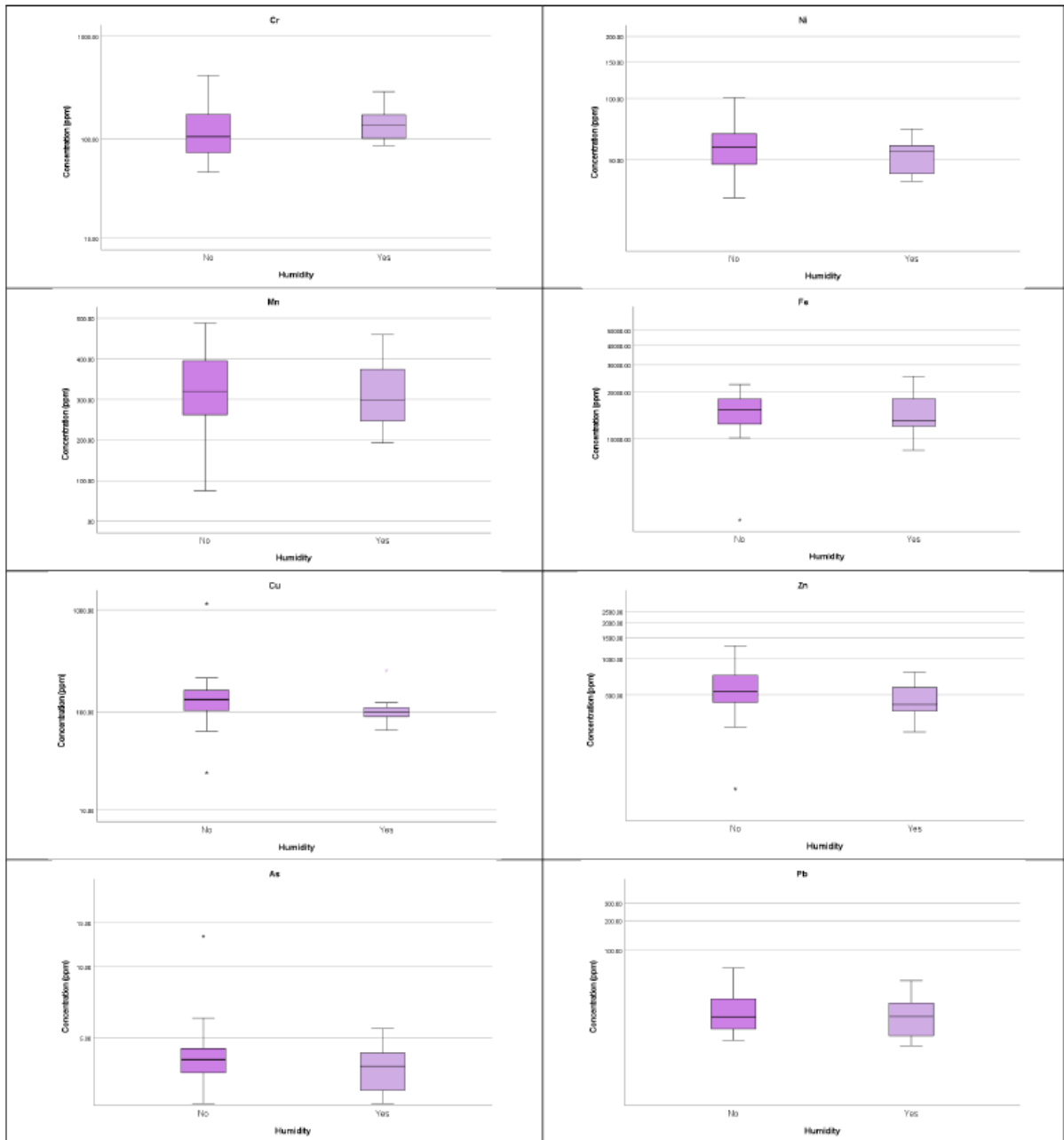


Figure 7. Box plot of elemental concentration by humidity

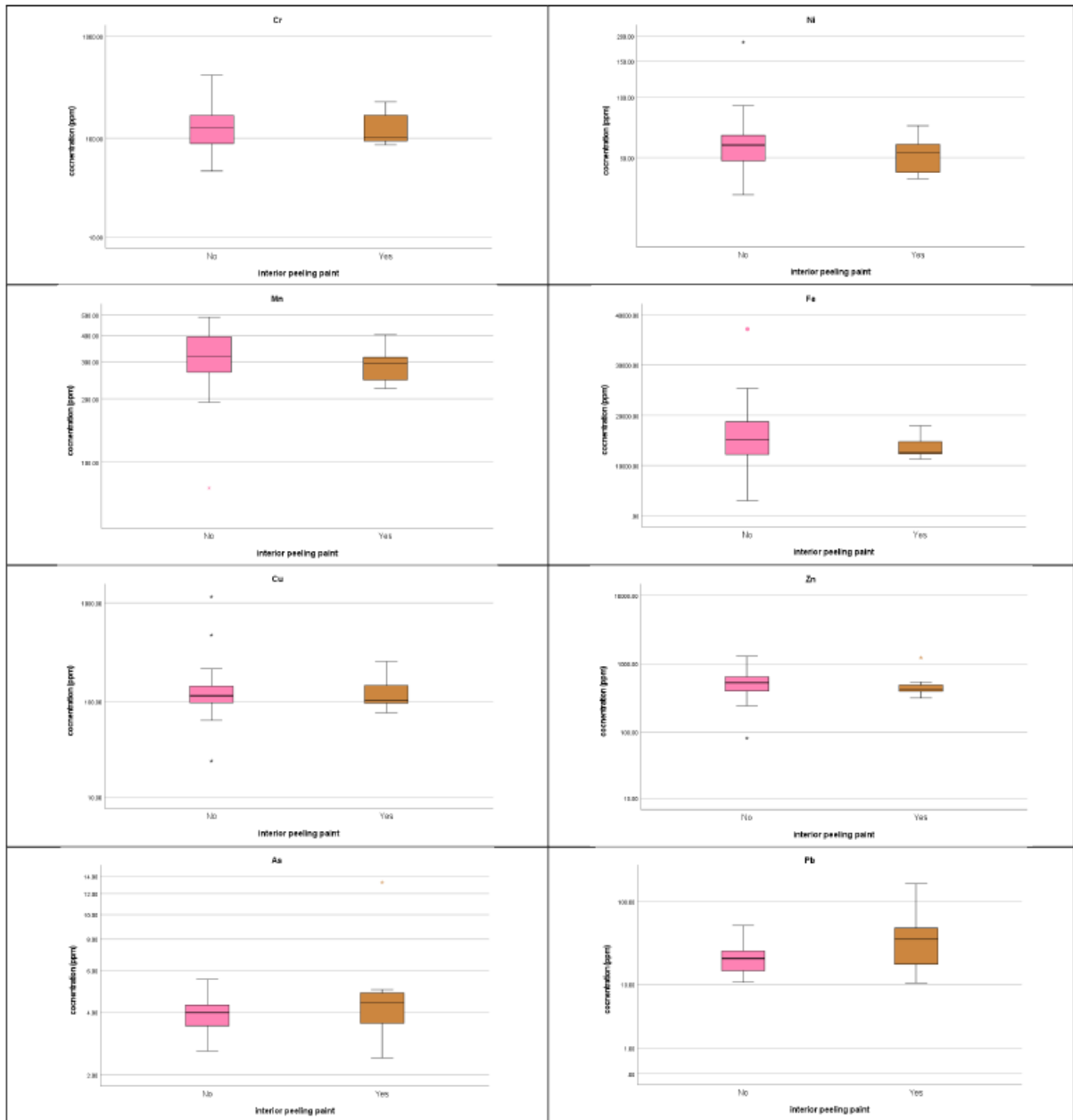


Figure 8. Box plot of elemental concentration of homes with and without interior peeling paint.

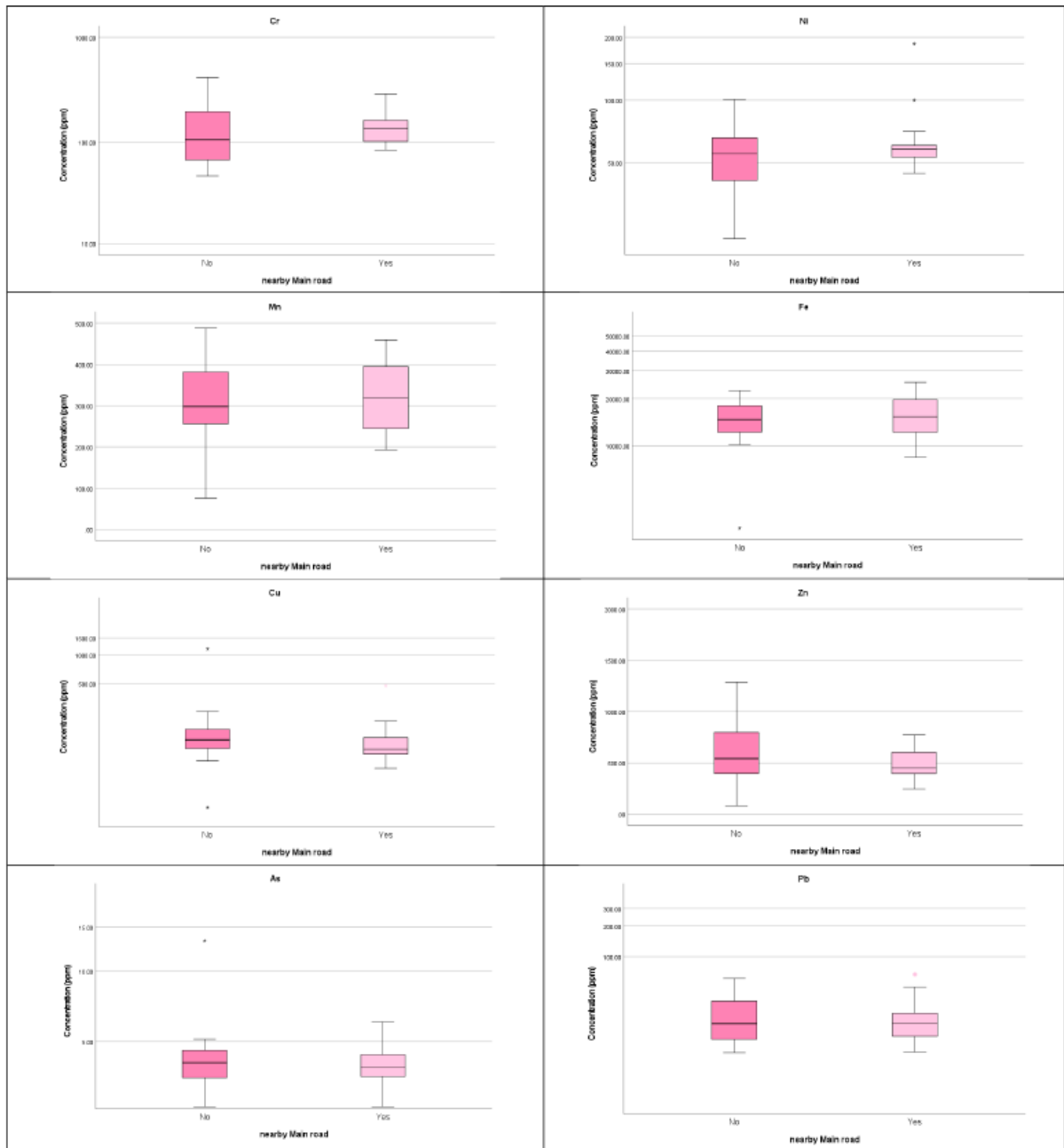


Figure 9. Box plot of elemental concentration of homes where located next to a main road.

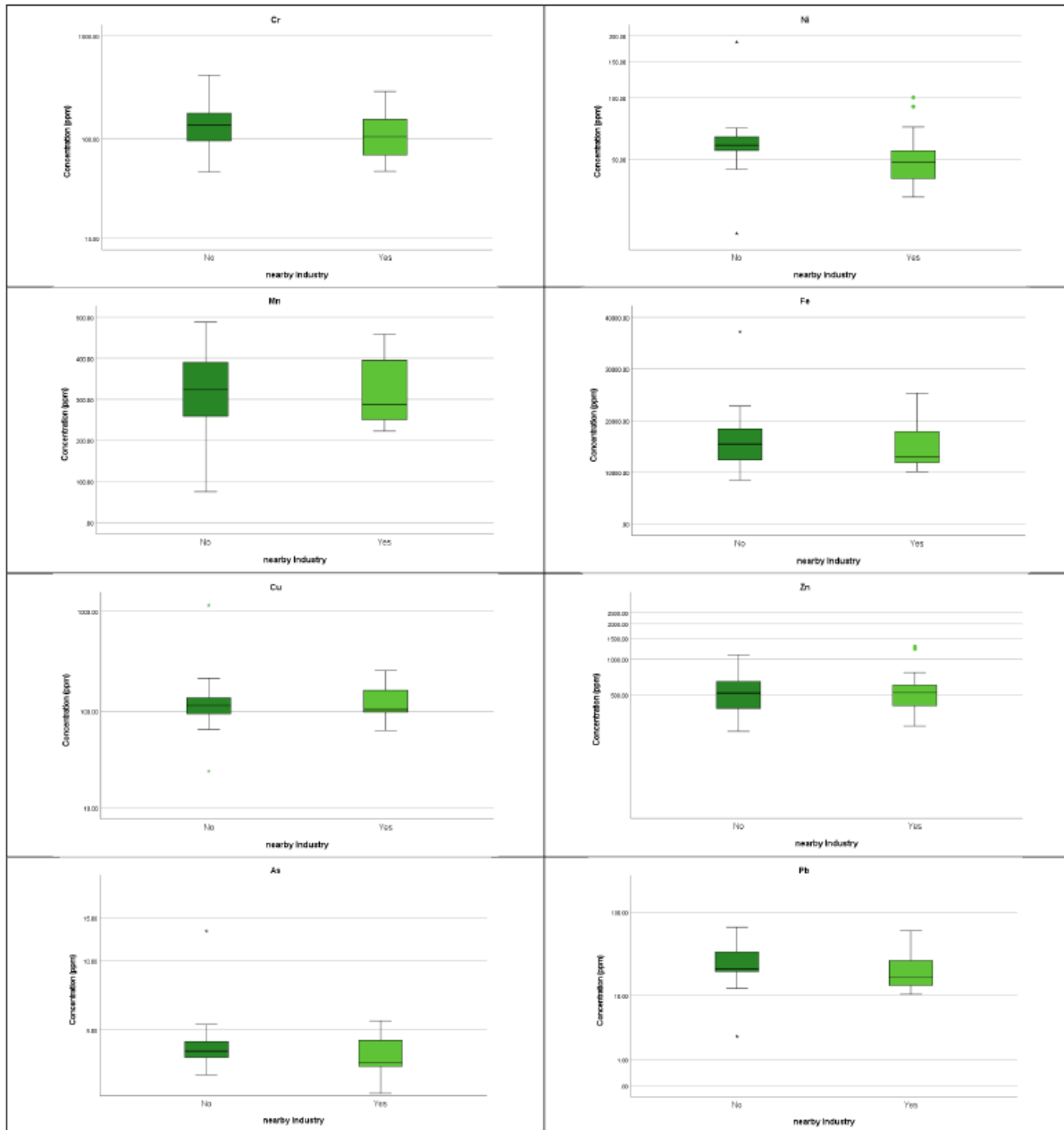


Figure 10. Box plot of elemental concentration of homes where located nearby Industry.

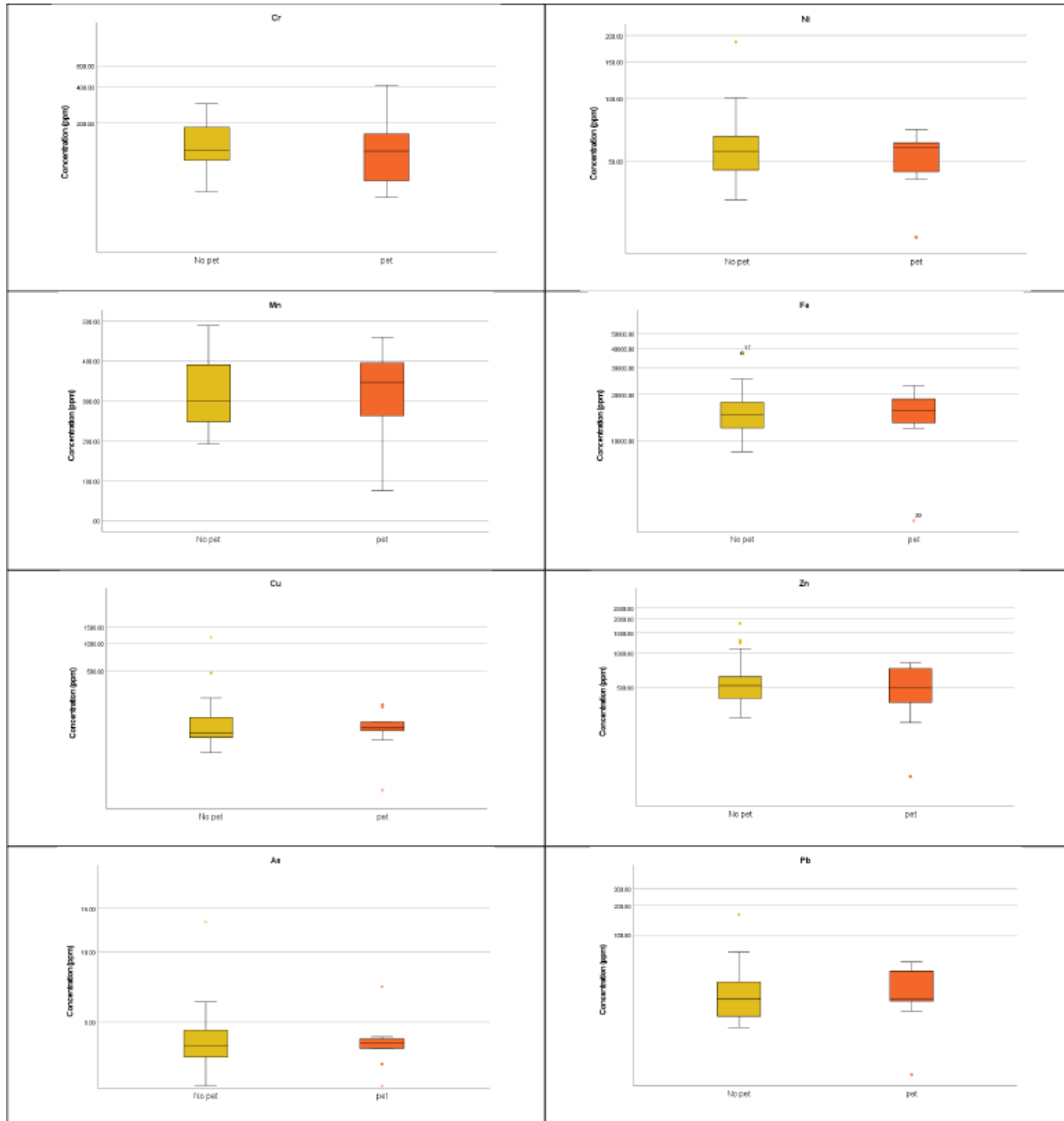


Figure 11. Box plot of elemental concentration of homes with and without pet.

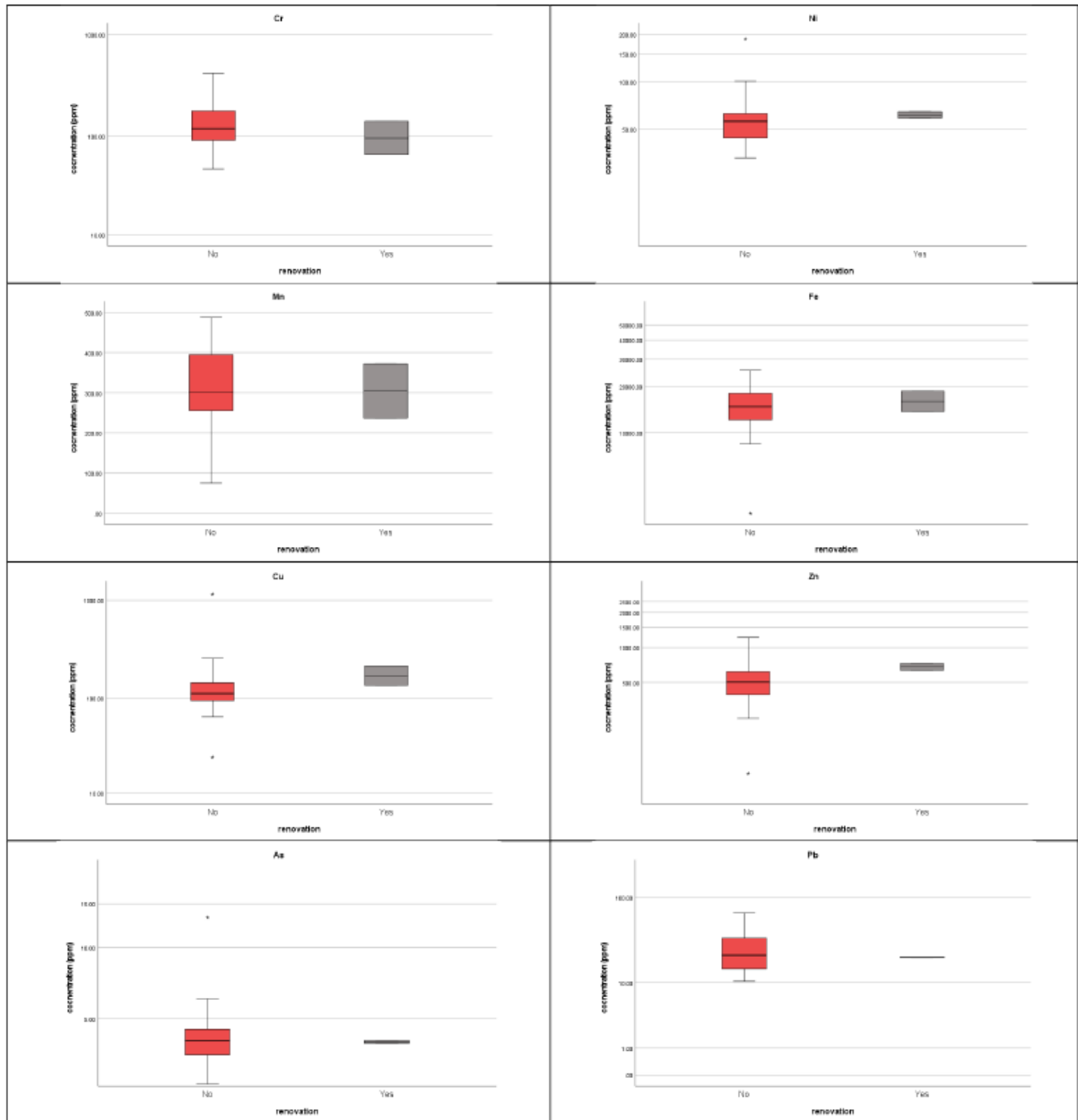


Figure 12. Box plot of elemental concentration of homes which undergoes and does not undergo renovation.

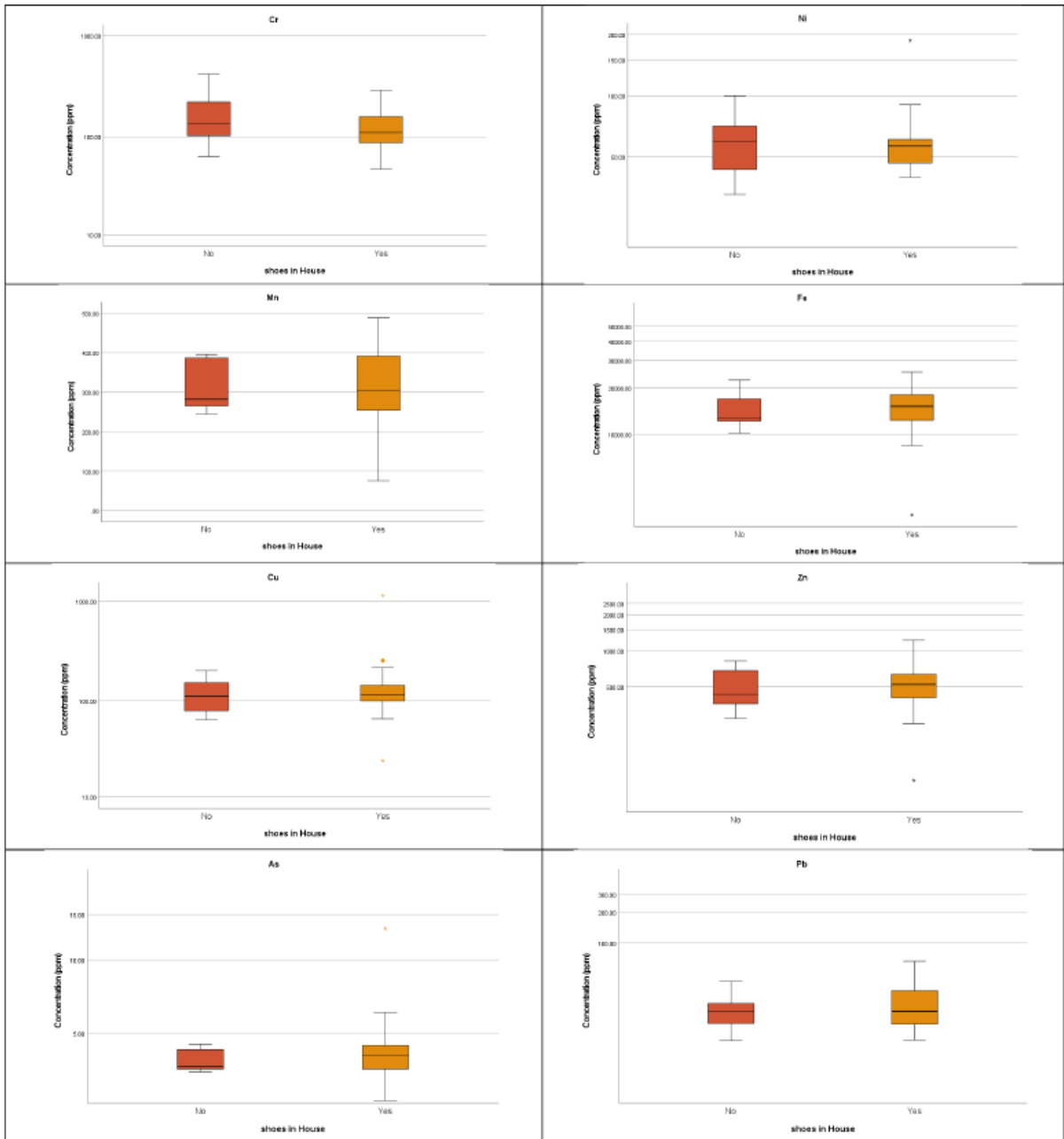


Figure 13. Box plot of elemental concentration of homes which use and does not use shoes indoors.

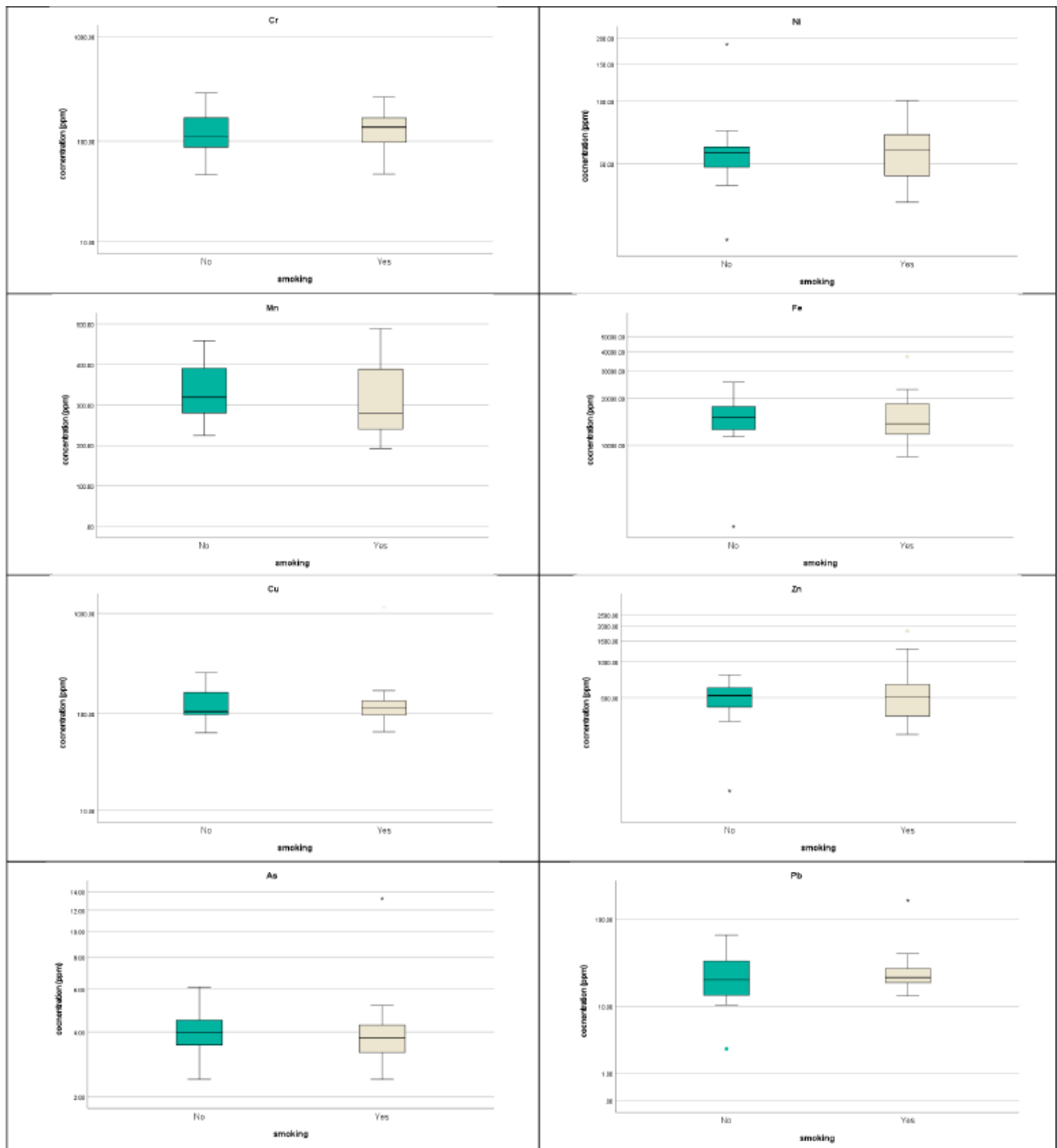


Figure 14. Box plot of elemental concentration of homes with and without smoking indoors.

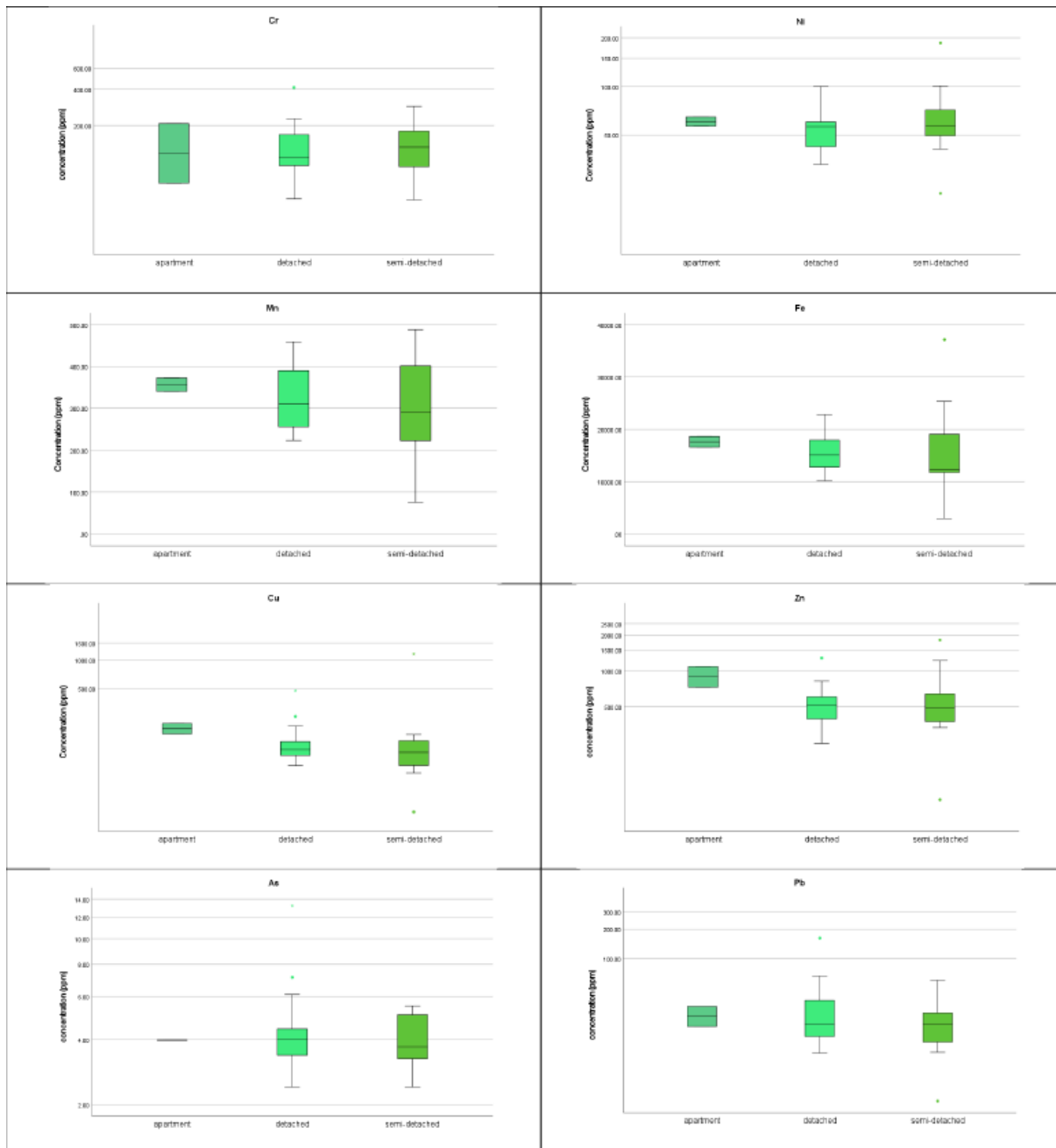
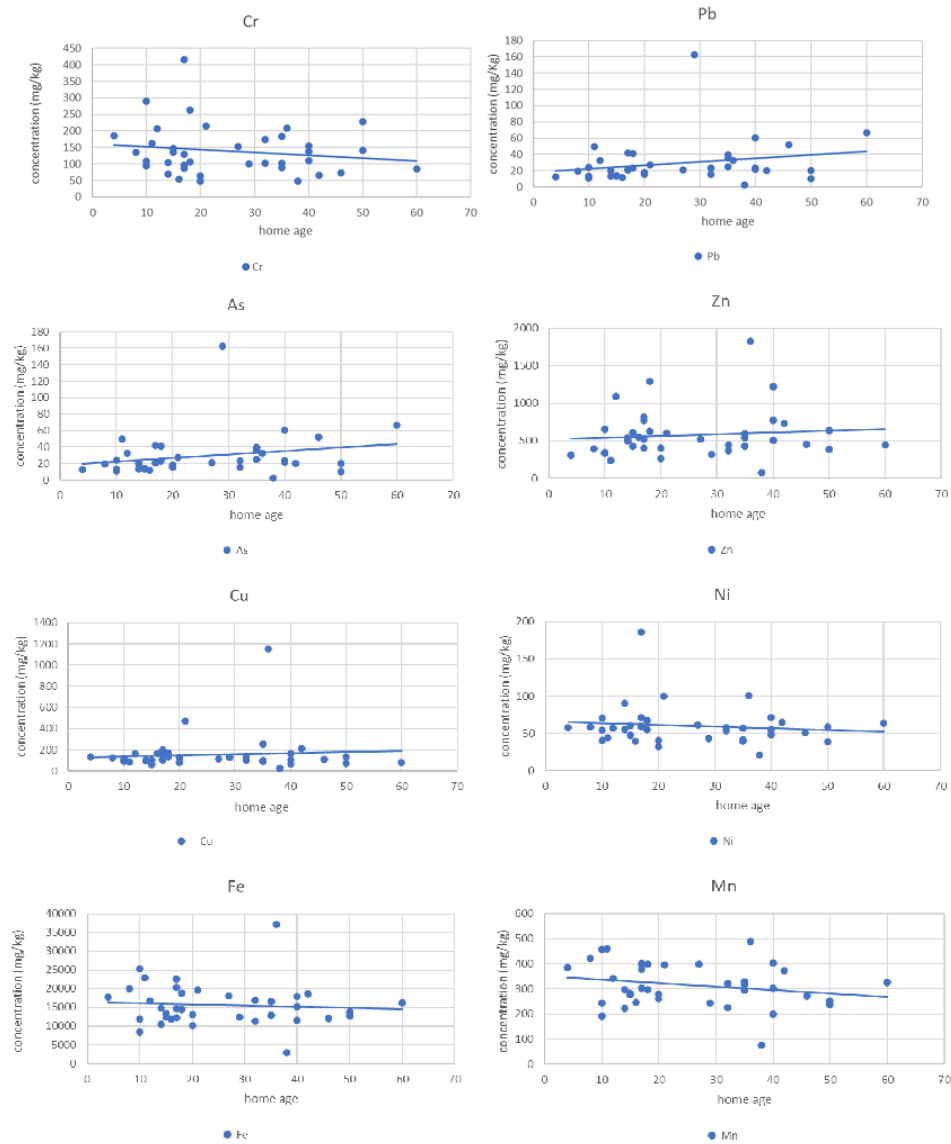


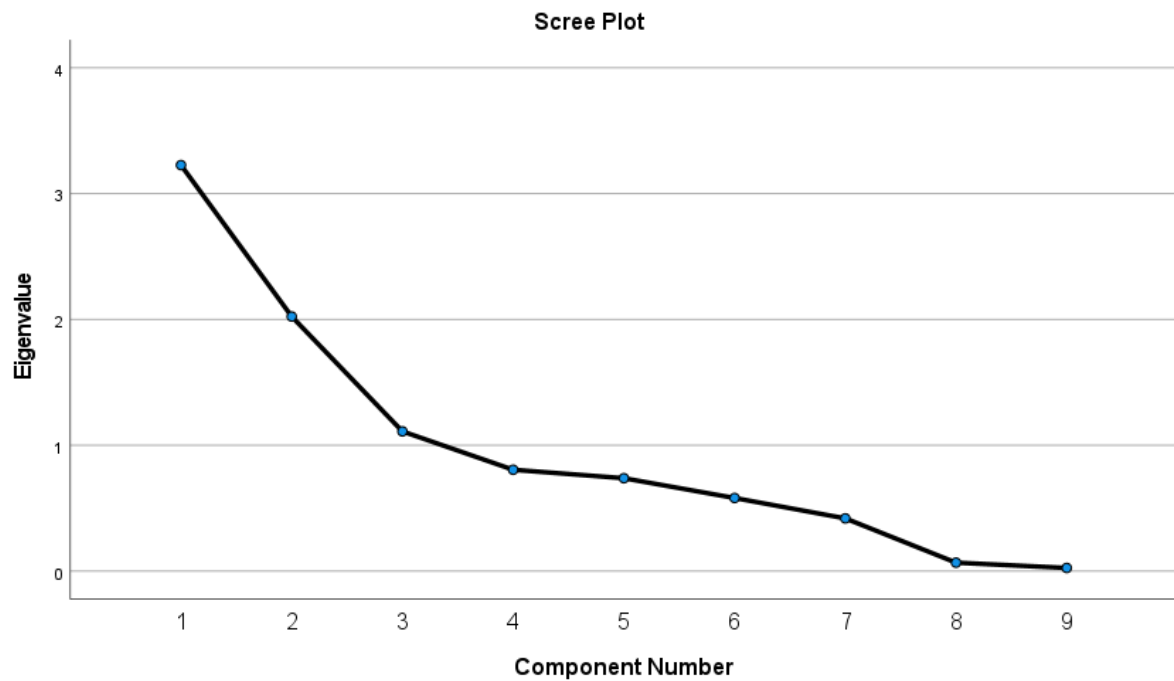
Figure 15. Box plot of elemental concentration by home type.



Trace metal	p	equation
As	0.0003	$Y=0.4326x+17.772$
Cr	0.94	$Y=-0.8746x+160.85$
Cu	<0.001	$Y=1.077x+129.31$
Fe	0.08	$Y=-32.214x+16465$
Mn	0.149	$Y=-1.3894x+350.94$
Ni	0.85	$Y=-0.225x+65.79$
Pb	<0.001	$Y=0.4326x+17.772$
Zn	0.015	$Y=2.2774x+520.78$

Figure 16. All trace metals show a trend of increasing concentration with increasing home age yet scatter in each case and Statistics for metal concentration via home age. Significant p values are shown in bold.

Appendix VII- Principal component analysis of house dust

**Rotated Component Matrix^a**

	Component		
	1	2	3
Cr	.817	-.050	-.160
Mn	.793	.087	.446
Fe	.885	.097	.337
Ni	.470	-.012	.388
Cu	.290	.060	.602
Zn	.071	-.011	.849
As	.158	.961	-.056
Pb	-.098	.959	.069

Component	% Of Variance
1	26.93
2	23.5
3	20.27

Extraction Method: Principal Component Analysis.

Rotation Method: Varimax with Kaiser Normalization.^a

a. Rotation converged in 5 iterations.

Figure 1. the results of Principal Component Analysis of Cyprus Dust (all region n=42).

Appendix VIII – Scatter plots for magnetic susceptibility and elements for household dust.

